©2016

Shuang Shuang Chen

ALL RIGHTS RESERVED

PROCESS DEVELOPMENT, OPTIMIZATION AND PRECLINICAL EVALUATION OF CALCIUM PHOSPHATE CONTAINING POLYMER SCAFFOLDS FOR BONE REGNERATION

by

SHUANG SHUANG CHEN

A dissertation submitted to the

Graduate School-New Brunswick

Rutgers, The State University of New Jersey

In partial fulfillment of the requirements

For the degree of

Doctor of Philosophy

Graduate Program in Chemical and Biochemical Engineering

Written under the direction of

Joachim Kohn

And approved by

_____

_____

_____

_____

New Brunswick, New Jersey

January, 2016

ABSTRACT OF THE DISSERTATION

PROCESS DEVELOPMENT, OPTIMIZATION AND PRECLINICAL EVALUATION OF CALCIUM PHOSPHATE CONTAINING POLYMER SCAFFOLDS FOR BONE REGNERATION

By SHUANG SHUANG CHEN

Dissertation Director:

Joachim Kohn

Large bone defects resulting from trauma, tumor resection, congenital abnormalities or reconstructive surgery remain significant clinical problems that affect millions of people. The current treatments are autologous or allogeneic bone grafts; each has drawbacks including donor site morbidity, limited available quantity, or risk of viral transmission and immunogenicity respectively. Alternatively, bone graft substitutes (BGS) have been developed as promising substrates for bone repair. However, the current BGS are often fabricated from simple laboratory processes that are never optimized or scaled-up. Most of them are only evaluated *in vitro* and if they are evaluated *in vivo*, only small animals models such as rats and rabbits are used. Therefore, none of the approaches proposed thus far have proved very effective. There remains a clinical demand for BGS that can treat large bone defects.

This dissertation supports effective and innovative solutions to this familiar problem in orthopedic surgery by (1) optimizing and scaling-up a fabrication process for scaffolds based on E1001(1k), a member of large combinatorial library of tyrosine-derived polycarbonates. (2) Enhancing the osteoconductivity of the scaffolds by adding a variety of calcium phosphates (CaP) including beta-tricalcium phosphate (β-TCP), hydroxyapatite (HA), and dicalcium phosphate dehydrate (DCPD) into the scaffolds. (3) Assessing the bone regeneration capacity of the scaffolds progressively from small animals (rabbit calvarial non-critical size defect and rat subcutaneous model) to a large animal model (goat calvarial critical size defect).

The fabrication process was optimized and scaled-up and is ready for transfer to a third party contractor under Good Manufacturing Practice. Scaffolds with homogeneous, consistent and optimized structure including unique bimodal pore size distribution, high porosity, surface area and interconnectivity were produced. *In vitro* characterization using human mesenchymal stem cells revealed that E1001(1k)-CaP scaffolds supported cell attachment, proliferation and osteogenic differentiation. *In vivo* evaluation of the scaffolds in small animal models demonstrated excellent biocompatibility and osteoconductivity. Furthermore, the preclinical evaluation in the goat calvarial critical size defects revealed performance superiority of E1001(1k)-CaP scaffolds over chronOS, a commercial BGS. Treatment with E1001(1k)-CaP scaffolds provided complete bridging of the 2 cm human size defects without supplemental osteogenic growth factor, which is of significant importance and has never been reported in the literature. These results suggest that E1001(1k)-CaP scaffold could be the next-generation synthetic bone graft substitute for large bone defect repair.

ACKNOWLEDGEMENTS

Great thank to my research advisor, Dr. Joachim Kohn for his guidance and supports in this work. In addition, special thanks to my thesis committees, Dr. Charles Roth, Dr. John Ricci and Dr. Prabhas Moghe for their time and helpful suggestions.

I would like to thank my collaborators, Sean Mcbride and Dr. Jeffery O. Hollinger at Carnegie Mellon University for doing the goat surgery. Special thanks to my service contractors: Dr. Amit Vasanji at ImageIQ, James Herrick at Mayo Clinic, Julia Katris and Dr. Timothy Bromage at New York University College of Dentistry, Dr. Michael Goedken, Dr. Marianne Polunas and Pedro Louro at Research Pathology Service, Rutgers University.

Many thanks to the staffs and scientists at the New Jersey Center for Biomaterials, Woloszyn Derek for rat implantation, Dr. Zheng Zhang for rat necropsy, Carmine Iovine and Dr. Lauren Macri for helpful discussion. As well as other lab members: Dr. Ophir Otiz, Dr. Sanjeeva Murthy, Barry Cunningham, Koustubh Dube, Dr. Yu-Kai Lee, Dr. Yong Mao, Dr. Ritu Goyal, Dr. Divya Bhatnagar, Dr. Vinod Damodaran, Onyi Freeman, Ganesan Subramanian.

Also, I would like to thank Dr. Thomas Emge for training me X-ray diffractometer, Dr. Patricia Buckendahl for training me micro-computed tomography, and Valentin Starovoytov for scanning electron microscopy assistance.

This work was supported by the Department of Defense as part of the Armed Forces Institute of Regenerative Medicine (AFIRM) effort, under Award No. W81XWH-08-2-0034.

DEDICATION

To my parents, my brother and my husband

TABLE OF CONTENTS

List of Tables

List of Figures

List of Equations

List of Abbreviations

3D	three-dimensional
ALP	alkaline phosphatase
ASP	alternate soaking process
BA	bone area
BET	Brunauer Emmett and Teller
BGS	bone graft substitutes
BV	bone volume
BV/TV	bone volume over total volume
Ca/P	calcium to phosphate ratio
CaP	calcium phosphate
CSD	critical size defect
DCPD	dicalcium phosphate dihydrate
DI	deionized
DT	desaminotyrosyl-tyrosine
DTR	desaminotyrosyl-tyrosine alkyl ester
E1001(1k)	poly(DTR-co-10% DT-co-1% PEG(1k)) carbonate
EtO	ethylene oxide
GPC	gel permeation chromatography
H&E	hematoxylin and eosin
HA	Hydroxyapatite

He	Helium
hMSC	human mesenchymal stem cells
ICDD	International Centre for Diffraction Data
ICP-OES	Inductively coupled plasma optical emission spectrometry
kDa	kilo-Dalton
LI	linear ingrowth
MicroCT	micro-computed tomography
MPa	Megapascal
MTS	mechanical testing
OCP	octacalcium phosphate
PBS	phosphate buffered saline
PEG	poly(ethylene glycol)
PGA	polyglycolic acid
PLA	polylactic acid
PLGA	polylactic-co-glycolic acid
rhBMP-2	recombinant human bone morphogenetic protein-2
ROI	region of interest
SBF	simulated body fluid
SEM	scanning electron microscope
SrOCP	strontium substituted octacalcium phosphate
TCPS	tissue culture polystyrene
TGA	thermogravimetric analysis
TV	total volume

TyrPC	tyrosine-derived polycarbonates
XRD	X-ray diffraction
β-TCP	beta-tricalcium phosphate

1

Introduction

1.1 Critical size bone defect

Bone possesses an intrinsic capacity for regeneration as part of the repair process in response to injury, as well as during skeletal development or continuous remodeling throughout adult life [1-3]. However, when the defect size exceeds the healing capacity of osteogenic tissue, the natural bone healing is impaired and surgical intervention or treatment is required. The smallest size defect that will not spontaneously heal with bone tissue over the natural lifetime of an animal is called critical size defect (CSD) [4]. Critical size bone defect can be resulted from trauma, tumor resection, congenital abnormality or reconstructive surgery. The reconstruction of critical size bone defects remains as an unsolved clinical problem that affects millions military and civilian populations [5, 6].

In the United States, approximately 1,100,000 bone-grafting procedures were performed in 2004 at an estimated total cost of more than $ 5 billion [7, 8]. The number is expect to increase due to aging world population and increasing numbers of returning soldiers whom need extensive bone repair [9, 10]. To recognize the global burden of musculoskeletal repair, the United Nations and the World Health Organization have endorsed the years 2000-2010 as the Bone and Joint Decade [10].

1.2 Standard of cares: autografts and allografts

The current ‘gold standard’ to treat critical size bone defects is autograft [11]. An autogenous bone graft is an osseous tissue harvested from the patient, usually from the iliac crest. It is known to produce the best clinical outcome because it possesses the osteogenic progenitor cells, osteoconductive matrices and osteoinductive growth factors, three components determine successful bone regeneration [5, 12]. However, the use of autologous bone has its limitations such as donor site morbidity, increased surgery time and limited available quantity [5, 13].

An alternative to autograft is allograft, which is taken from donors or cadavers [14]. The use of allografts eliminates donor site morbidity but introduces a risk of viral transmission and immunogenicity [15]. Hence, due to the limitations of autogenous and allogeneic bone grafts, there remains a clinical demand for bone graft substitutes (BGS) that can treat large critical size bone defects [15, 16].

1.3 Bone tissue engineering

Bone tissue engineering is an interdisciplinary field that applies the knowledge of engineering, material science and life science to regenerate damaged bone tissue [17, 18]. It has emerged as a promising alternative to autogenous and allogeneic bone grafts for bone regeneration. It includes gene-, cell- and cytokine-based therapies [8, 19, 20]. Gene- and cell-based therapies are attracting increasing attention recently, however the results are controversial [20-23]. In contrast, cytokine-based therapy using growth factors such as bone morphogenetic proteins (BMPs) is more advantageous in terms of feasibility and practical potential for nearest clinical application compared with gene- and cell-based

therapies [24-26]. BMP-2 and BMP-7 are now in clinical use. Regardless of gene-, cell- or cytokine-based therapies, an appropriate 3D scaffold as a substrate for cells attachment and proliferation and/or as a carrier of sustainable growth factors delivery is of paramount importance in bone regeneration. An ideal scaffold should [27, 28]:

- Be biocompatible, triggers minimal host inflammatory or immunogenic responses [29];
- Have an appropriate three-dimensional (3D) structure that supports *in vitro* cell attachment, proliferation and differentiation and *in vivo* vascularization and bone regeneration [28, 30];
- Be biodegradable at a rate that allows the scaffold to disappear in concurrence with new tissue formation [18, 31-33]. This eliminates the need for a second operation to remove the implant. The degradation products must be biocompatible as well;
- Have mechanical properties match with host bone tissue [34, 35].

1.4 Biomaterials for bone repair

Over the past several decades, many bone substitute materials, intended to replace the need for autologous or allogeneic bone, have been widely investigated. In general, they consist bioactive ceramics, bioglasses, natural or synthetic polymers, or composites of these.

1.4.1 Natural/synthetic polymers

Natural polymers commonly used in tissue engineering include collagen [36], chitosan, fibrin, elastin, glycosaminoglycan and hyaluronic acid [36-39]. They are often isolated directly from the extracellular matrix and contain surface ligands that are specific for cell adhesion and proliferation. As a result, they are biocompatible and typically degradable with non-toxic degradation products. However, natural polymers are mechanical weak that are unsuitable for high strength applications.

A number of degradable synthetic polymers [40, 41] have also been investigated for bone tissue engineering. The family of poly(alpha-hydroxy acid) polymers including polylactic acid (PLA), polyglycolic acid (PGA), and their copolymer polylactic-co-glycolic acid (PLGA) are the most widely used synthetic polymers in tissue engineering applications [42-44]. The physical and degradation properties of PLGA can be tailored by altering the monomer ratios (lactide: glycolide) to meet specific tissue engineering applications [43]. However, the major disadvantages of those poly(alpha-hydroxy acid) polymers are the release of acidic degradation by-products that can alter the pH in surrounding tissue [45]. In turn, this can cause adverse tissue and inflammatory reactions. Moreover, the synthetic polymers are neither highly osteocondutive nor are they intrinsically osteoinductive.

1.4.2 Calcium phosphates

Calcium phosphate (CaP) materials have been successfully used in cranio-maxillofacial, dental and orthopedic surgery because of their outstanding bone regeneration properties [46-48]:

- They have similar chemical composition as the bone minerals
- They are bioactive, able to form carbonated hydroxyapatite on their surface after immersing in simulated body fluid (SBF).
- They are osteoconductive, able to provide a scaffold for new bone formation and support osteoblasts adhesion and proliferation.
- They are osteointegrative, able to integrate with the host tissue and form an intimate physicochemical bond between the implant and native bone.
- In addition, calcium phosphates can be engineered to be osteoinductive by incorporating osteogenic growth factors such as recombinant human bone morphogenetic protein-2 (rhBMP-2).

Calcium phosphates (CaPs) have been used in the forms of cements [49, 50], ceramics [51] and coatings on metallic hip and dental implants [52-54]. They can be natural origin (freeze-dried or banked bone and derived coral hydroxyapatite) or synthetic origin (obtained after aqueous precipitation or after sintering) [46]. Table 1.1 summarizes the chemical name, the formula, the abbreviation, the calcium to phosphorus ratio (Ca/P) and the solubility of some synthetic calcium phosphates: hydroxyapatite, tricalcium phosphate, dicalcium phosphate dihydrate and octacalcium phosphate, used for bone tissue engineering application [55].

Hydroxyapatite (HA) is the most widely used calcium phosphate in bone tissue engineering [46]. It has been used in the repair of craniofacial osseous defects since 1970s [56] and received FDA approval in 1994. This material is highly biocompatible, bioactive and osteoconductive becuase it is the primary phase of calcium phosphate in

the human skeleton [57, 58]. Stoichiometric HA with Ca/P of 1.67 is barely soluble [46, 55]. Its resorption rate does not match the rate of bone remodeling. More recently, carbonated apatite prepared by aqueous precipitation with accelerated degradation and resorption rate have been developed [59-62].

Tricalcium phosphate (TCP) resorbs faster than sintered HA, thereby have shown to foster better bone regeneration in various *in vivo* models [63, 64]. Moreover, biphasic calcium phosphates (BCP), consist of sparely soluble HA and highly soluble tricalcium phosphate have been developed to tune degradation rate by varying the ratio of each component [65].

Octacalcium phosphate (OCP) has attracted great interest as a bone substitute material in recent years because of its potential to promote a higher volume of newly formed bone as compared to other calcium phosphates, such as HA, by acting as loci for bone induction [66-68]. In addition, OCP has been observed as a transient intermediate in the precipitation of the thermodynamically more stable HA and biological apatite [69].

Dicalcium phosphate dihydrate (DCPD or brushite) is one of the most soluble of the calcium phosphate salts because it is metastable at physiological conditions [48, 51, 69, 70]. Moreover, it plays important role in the biological mineralization process. It is believed to be one of the precursors of biological apatite in bone and tooth [71, 72]. DCPD has been used as one of the initial components as well as the end product of hydraulic calcium phosphate cements. DCPD-based materials have also been used as coating for metallic implants since 1990s [73, 74].

Table 1.1 Main biologically relevant calcium phosphates.

Calcium phosphate	Formula	Abbreviation	Ca/P	Solubility at 25°C, – log(Ka)	Solubility at 25°C, g/L
Dicalcium phosphate dihydrate	$CaHPO_4 \cdot 2H_2O$	DCPD	1.00	6.59	0.088
Octacalcium phosphate	$Ca_8(PO_4)_4(HPO_4)_2 \cdot 5H_2O$	OCP	1.33	96.6	0.0081
Tricalcium phosphate	$Ca_3(PO_4)_2$	TCP	1.5	28.9	0.0005
Hydroxyapatite	$Ca_{10}(PO_4)_6(OH)_2$	HA	1.67	116.8	0.0003

HA is the most thermodynamically stable at physiological conditions, followed by TCP, OCP and then DCPD. The dissolution of calcium phosphate and subsequently re-precipitation of an apatite layer significantly enhance implants integration with the host tissue [46, 75]. Furthermore, more studies have demonstrated that ionic dissolution products (calcium and phosphorus ions) play a significant role in driving specific molecular and cellular responses by directly activating intracellular mechanism through Ca-sensing receptors in osteoblastic cells [76-78]. Numerous studies have reported that calcium phosphate supports the *in vitro* attachment, proliferation and differentiation of

osteoblastic progenitor cells and exhibits excellent *in vivo* biocompatibility and osteoconductivity [79-81]. Despite their favorable biological properties, the clinical applications of CaP scaffolds have been limited due to their low mechanical strength and high brittleness.

1.4.3 Composites

To overcome the brittleness of calcium phosphate as well as to enhance the osteoconductivity of polymer scaffold, composites of calcium phosphate and polymer have been developed [58, 82, 83]. The composites combine the toughness of a polymer phase with the compressive strength of a calcium phosphate to generate bioactive materials with improved mechanical properties, degradation profile and biocompatibility. Moreover, bone is a composite composed of inorganic hydroxyapatite crystals deposited within an organic matrix consisting of ~ 95% type I collagen [84]. CaP-polymer composites are designed to mimic the composition as well as 3D structure of human bone.

1.5 Our solutions

Despite the advancements in designing bone graft substitutes (BGS) recent years, most of them are fabricated from simple laboratory processes that are never optimized or scaled-up. In addition, most BGS are only evaluated using some *in vitro* experiments. If there is any *in vivo* evaluation, only small animal models such as rats and rabbits are

used. Therefore, none of the approaches proposed thus far has proved very effective. There remains a clinical demand for BGS that can treat large bone defects.

To address the problems, this thesis used the research results of previous studies and tempted an interesting research into translation. Figure 1.1 shows the timeline and study design of this dissertation. First, a fabrication process of scaffolds based on E1001(1k), a member of large combinatorial library of tyrosine-derived polycarbonates (TyrPC) was optimized and scaled-up. Scaffolds with homogenous, consistent and optimized structure including unique bimodal pore size distribution, high porosity, surface area and interconnectivity were produced. To further enhance the osteoconductivity of the scaffolds, a variety of calcium phosphates (CaP) including beta-tricalcium phosphate (β-TCP), hydroxyapatite (HA), or dicalcium phosphate dihydrate (DCPD) was incorporated into the scaffolds. Second, the scaffolds were evaluated *in vitro* for cell attachment, proliferation and differentiation using human mesenchymal stem cells. Lastly, the bone regeneration capacity of the scaffolds was assessed progressively from small animal models including rabbit calvarial non-critical size defect and rat subcutaneous implantation, to clinically relevant goat calvarial critical size defect model. In the bone regeneration research, more than 90% *in vivo* studies use small animal models such as rats and rabbits. Although, they are very useful, the osteogenic results are not likely translated into clinical outcome. Goats are considered as valuable large animal models for the preclinical testing of bone graft substitutes because they have metabolic rate and bone remodeling rate similar to humans [23-25]. Goats also have a body weight comparable to humans and a body size suitable for the implantation of large human-sized implants and prostheses [25]. Moreover, the osteogenic results can be used to predict the

likely outcomes in clinical conditions. However, only a handful of bone regeneration researches have used large animal models due to the high cost of the studies.

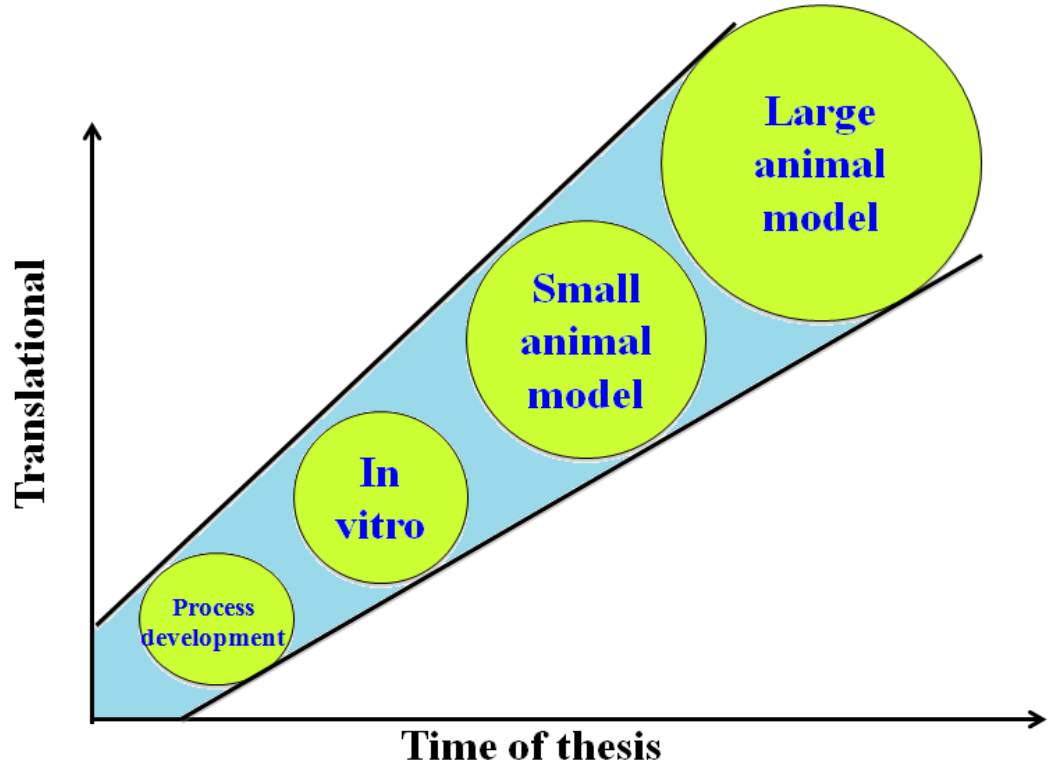

Figure 1.1 Thesis timeline and progressional approaches from small animal models to a large animal.

Tyrosine-derived polycarbonates (TyrPC) are a class of novel and proprietary polymers invented in the Kohn laboratory at the New Jersey Center for Biomaterials [85-88]. These polymers are synthesized from tyrosine-derived monomers: desaminotyrosyl-tyrosine alkyl esters (DTR) or desaminotyrosyl-tyrosine (DT), and/or low molecular weight blocks of poly(ethylene glycol) (PEG). The general chemical structure is shown in Figure 1.2 [89]. DTR is responsible of the mechanical strength of the polymer, DT for hydrolytic degradation profile and PEG for cellular behavior. They have been

polymerized into homopolymers of DTR, copolymers of DTR and DT and copolymer of DTR and PEG and terpolymers of DTR, DT and PEG. By tuning each monomer, the physical, chemical, biomechanical and biological properties of the polymers can be precisely controlled [87, 90].

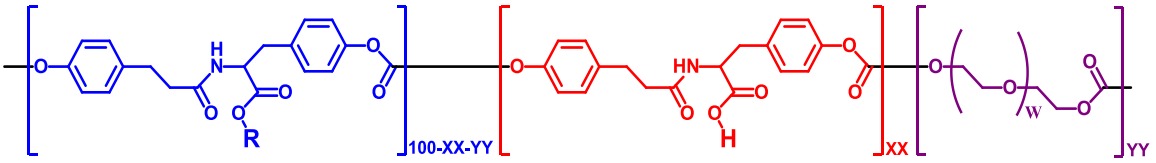

Figure 1.2 Chemical structure of poly(DTR-*co*-xx% DT-*co*-yy% PEG(x)) carbonate. Where " R" is the alkyl pendent chain, "xx" is the mole percent of DT, "yy" is the mole percent of PEG, "100-xx-yy" is mole percent of DTR, and "w" is the weight average molecular weight of PEG.

A member of TyrPC, poly(DTE-*co*-10 mol% DT-*co*-01 mol% PEG_{1k} carbonate), abbreviated as E1001(1k), containing 89 mol% DTE, 10 mol% of DT and 1 mol% of PEG with molecular weight of 1kDa, has been identified as a promising substrate for bone regeneration [89,97-100]. 3D porous E1001(1k) scaffold prepared by a combination of porogen leaching and freeze-drying methods, has been evaluated extensively in rabbit calvarial and radius defect models and demonstrated to support bone regeneration [89, 97-101]. The scaffold has matched rate of degradation and resorption with bone remodeling [98]. It promotes *in vitro* cells attachment, proliferation and osteogenic differentiation [99]. It also demonstrates excellent *in vivo* bone biocompatibility and osteoconductivity [97, 98, 100, 101].

However, a large variation in bone regeneration outcome was observed in previous animal studies [97, 98, 100], likely due to inconsistency in scaffold morphology and structure such as porosity, pore size and pore size distribution, surface area and pore interconnectivity as those parameters have a significant effect on cellular responses. Therefore, it is necessary to optimize and control the scaffold fabrication process in order to produce scaffolds with homogenous and consistent structure. Moreover, the fabrication process needs to be scaled-up to produce human-sized scaffolds for translational research.

To further enhance the osteoconductivity of E1001(1k) scaffolds, calcium phosphate has been incorporated into scaffolds. However, not much significantly improved bone formation was observed in previous animal studies and bone formation was very limited to the margin of the defect. Thus, despite the testing of E1001(1k)-based scaffolds in more than 300 rabbits, nothing really stands out that can out-perform the commercial products.

Therefore, in this dissertation, in addition to the commonly used HA and β-TCP, for the first time in the literature, highly soluble DCPD was combined with a polymer as a composite scaffold and was evaluated *in vitro* as well as *in vivo* for bone regeneration. The rational of choosing DCPD because it is one of the precursors of biological apatite and its high resorption rate may enhance bone healing. Moreover, as opposed to the traditional used bulk composite method, a new approach of depositing CaP as a coating on the preformed polymer scaffolds was used. In the bulk composite method, calcium phosphate minerals are often blended with polymer powder or solution as fillers during fabrication process. Although, most frequently used, it is suspected that embedding of CaP within the polymer may lead to the masking of its bioactivity due to the formation of

polymer skin covering the inorganic particles [60, 62, 108]. Indeed, all the commercial products of calcium phosphate with natural or synthetic polymers were prepared as bulk composites. Currently, there is no product where CaP is deposited as a coating on pre-formed scaffolds. It is suspected that CaP coating can provide favorable osteogenic surface topography for cell attachment, differentiation and *in vivo* osteogenesis.

Calcium phosphate coating has been used on metallic implants since 1990s in the purpose of enhancing osteointegration of the implants with host tissue [52]. More recently, this strategy has been applied to pre-formed 3D biomaterials as a powerful technique to enhance polymer osteoconductivity. Biomimetic coating method and alternate soaking process (ASP) are often used to deposit CaP coating on polymeric biomaterials, however, both have drawbacks. Biomimetic coating method is based on the immersion of implants in simulated body fluid (SBF) [109-111]. Alternate soaking process [112-114] mineralizes a biomaterial by alternatively soaking it in cycles of calcium-ions and phosphate-ions containing solutions. Both methods take a long time (days and weeks) for a stable apatite deposition on scaffold [107, 115], thus lead to biodegration of the polymers prior to their tissue engineering application. Furthermore, CaP minerals are likely to aggregate on the outer region of geometrically complex 3D porous scaffold, resulting in the formation of a non-uniform layer of calcium phosphate materials with increased thickness at the scaffold surface and interfere with the porous structure and lead to the hindrance of cell in-growth. To overcome the limitations associated with the current calcium phosphate mineralization methods, a straightforward, fast and versatile modified alternate soaking process was developed. Calcium phosphate mineralized scaffolds prepared by this method were evaluated.

1.6 Overall goal and specific aims

The **overall goal** for this dissertation is to produce therapeutics based on composite 3D porous scaffold of tyrosine-derived polycarbonate and calcium phosphates to regenerate large critical size bone defects. The **Specific Aims** of this dissertation are:

- Develop, and optimize the scaffold fabrication process to produce scaffolds with uniform and consistent structure and morphology, and scale-up the process to produce large human-sized implants for translational research.
- Mineralize E1001(1k) scaffold with calcium phosphate to further enhance its osteoconductivity. This includes designing a straightforward, fast and versatile calcium phosphate mineralization method with tunable surface topography and chemical composition.
- Characterize the 3D porous scaffolds with an array of different techniques, assess the pros and cons of each technique and optimize scaffold properties include chemical composition, 3D structure, degradation properties and mechanical properties.
- Assess the biocompatibility, safety and efficacy of E1001(1k)/CaP scaffolds in a rabbit calvarial noncritical size defect model, and screen the optimal composite scaffold platform for bone regeneration.
- Evaluate the effect of E1001(1k)/CaP scaffolds on *in vitro* human mesenchymal stem cells (hMSCs) attachment, proliferation and osteogenic differentiation and *in vivo* biocompatibility and bone induction capability with or with human recombinant bone morphogenic protein-2 (rhBMP-2) in rat subcutaneous implantation.

- Evaluate the safety and efficacy of E1001(1k)/CaP scaffolds using a clinically relevant goat calvarial critical size defect model, and compare the osteogenic outcome with a commercial bone graft substitute.

1.7 Thesis Organization

This dissertation is organized into seven chapters. In **Chapter 1**, a literature overview of the clinical need of large critical size defect repair, the current state of art and the proposed approaches of addressing the demand are presented. In **Chapter 2**, the optimization and scale-up of the scaffold fabrication process are described. In **Chapter 3**, a straightforward, fast and versatile modified alternate soaking process is introduced to mineralize the polymeric scaffold and further enhance scaffold osteoconductivity. **Chapter 4** describes a comparative study on bone regeneration by octacalcium phosphate, beta-tricalcium phosphate and strontium in tyrosine-derived polycarbonate scaffolds using rabbit calvarial non-critical size defect model**. In Chapter 5,** the effect of calcium phosphate and rhBMP-2 on *in vitro* human mesenchymal stem cells (hMSCs) attachment, proliferation and differentiation and in *vivo* biocompatible and bone induction capability in rat subcutaneous implantation are reported. **Chapter 6** describes the safety and efficacy of the composite scaffolds in a large animal model: goat calvarial critical size defect model. A novel tyrosine-derived polycarbonate / dicalcium phosphate dihydrate composite scaffold with significantly better bone regeneration capacity over chornO, a commercial bone graft substitute is reported. Finally, **Chapter 7** summarizes significant finding from the dissertation and significance of the studies.

Reference

[1] Kon E, Filardo G, Roffi A, Di Martino A, Hamdan M, De Pasqual L, et al. Bone regeneration with mesenchymal stem cells. Clin Cases Miner Bone Metab 2012;9:24-7.

[2] Dimitriou R, Jones E, McGonagle D, Giannoudis P. Bone regeneration: current concepts and future directions. BMC Medicine 2011;9:1-10.

[3] Einhorn TA. The cell and molecular biology of fracture healing. Clin Orthop Relat Res 1998;355:S7-21.

[4] Spicer PP, Kretlow JD, Young S, Jansen JA, Kasper FK, Mikos AG. Evaluation of bone regeneration using the rat critical size calvarial defect. Nat Protocols 2012;7:1918-29.

[5] De Long WG, Jr., Einhorn TA, Koval K, McKee M, Smith W, Sanders R, et al. Bone grafts and bone graft substitutes in orthopaedic trauma surgery. A critical analysis. J Bone Joint Surg Am 2007;89:649-58.

[6] Amini AR, Laurencin CT, Nukavarapu SP. Bone tissue engineering: recent advances and challenges. Crit Rev Biomed Eng 2012;40:363-408.

[7] Kretlow JD, Mikos AG. Review: mineralization of synthetic polymer scaffolds for bone tissue engineering. Tissue Eng 2007;13:927-38.

[8] Liu Y, Wu G, de Groot K. Biomimetic coatings for bone tissue engineering of critical-sized defects. J R Soc Interface 2010;6:19.

[9] Manring MM, Hawk A, Calhoun JH, Andersen RC. Treatment of War Wounds: A Historical Review. Clinical Orthopaedics and Related Research 2009;467:2168-91.

[10] Woolf AD, Pfleger B. Burden of major musculoskeletal conditions. Bull World Health Organ 2003;81:646-56.

[11] Myeroff C, Archdeacon M. Autogenous Bone Graft: Donor Sites and Techniques. The Journal of Bone & Joint Surgery 2011;93:2227-36.

[12] Gazdag A, Lane J, Glaser D, Forster R. Alternatives to Autogenous Bone Graft: Efficacy and Indications. Journal of the American Academy of Orthopaedic Surgeons 1995;3:1-8.

[13] Nandi S, Roy S, Mukherjee P, Kundu B, De D, Basu D. Orthopaedic applications of bone graft & graft substitutes : a review2010.

[14] Nandi SK, Roy S, Mukherjee P, Kundu B, De DK, Basu D. Orthopaedic applications of bone graft & graft substitutes: a review. Indian J Med Res 2010;132:15-30.

[15] Damien CJ, Parsons JR. Bone graft and bone graft substitutes: A review of current technology and applications. Journal of Applied Biomaterials 1991;2:187-208.

[16] Laurencin C, Khan Y, El-Amin SF. Bone graft substitutes. Expert Rev Med Devices 2006;3:49-57.

[17] Howard D, Buttery LD, Shakesheff KM, Roberts SJ. Tissue engineering: strategies, stem cells and scaffolds. Journal of Anatomy 2008;213:66-72.

[18] Langer R, Vacanti JP. Tissue engineering. Science 1993;260:920-6.

[19] Amini AR, Laurencin CT, Nukavarapu SP. Bone Tissue Engineering: Recent Advances and Challenges. Critical reviews in biomedical engineering 2012;40:363-408.

[20] Sundelacruz S, Kaplan DL. Stem cell- and scaffold-based tissue engineering approaches to osteochondral regenerative medicine. Seminars in cell & developmental biology 2009;20:646-55.

[21] Chung IH, Yamaza T, Zhao H, Choung PH, Shi S, Chai Y. Stem cell property of postmigratory cranial neural crest cells and their utility in alveolar bone regeneration and tooth development. Stem Cells 2009;27:866-77.

[22] Kawai M, Maruyama H, Bessho K, Yamamoto H, Miyazaki J, Yamamoto T. Simple strategy for bone regeneration with a BMP-2/7 gene expression cassette vector. Biochem Biophys Res Commun 2009;390:1012-7.

[23] Park J, Ries J, Gelse K, Kloss F, von der Mark K, Wiltfang J, et al. Bone regeneration in critical size defects by cell-mediated BMP-2 gene transfer: a comparison of adenoviral vectors and liposomes. Gene Ther 2003;10:1089-98.

[24] Lee SS, Huang BJ, Kaltz SR, Sur S, Newcomb CJ, Stock SR, et al. Bone regeneration with low dose BMP-2 amplified by biomimetic supramolecular nanofibers within collagen scaffolds. Biomaterials 2013;34:452-9.

[25] Fu Y-C, Nie H, Ho M-L, Wang C-K, Wang C-H. Optimized bone regeneration based on sustained release from three-dimensional fibrous PLGA/HAp composite scaffolds loaded with BMP-2. Biotechnology and Bioengineering 2008;99:996-1006.

[26] Chen D, Zhao M, Mundy GR. Bone morphogenetic proteins. Growth Factors 2004;22:233-41.

[27] Bose S, Roy M, Bandyopadhyay A. Recent advances in bone tissue engineering scaffolds. Trends in biotechnology 2012;30:546-54.

[28] Polo-Corrales L, Latorre-Esteves M, Ramirez-Vick JE. Scaffold Design for Bone Regeneration. Journal of nanoscience and nanotechnology 2014;14:15-56.

[29] Onuki Y, Bhardwaj U, Papadimitrakopoulos F, Burgess DJ. A Review of the Biocompatibility of Implantable Devices: Current Challenges to Overcome Foreign Body Response. Journal of Diabetes Science and Technology 2008;2:1003-15.

[30] Karageorgiou V, Kaplan D. Porosity of 3D biomaterial scaffolds and osteogenesis. Biomaterials 2005;26:5474-91.

[31] Middleton JC, Tipton AJ. Synthetic biodegradable polymers as orthopedic devices. Biomaterials 2000;21:2335-46.

[32] Ye WP, Du FS, Jin WH, Yang JY, Xu Y. In vitro degradation of poly (caprolactone), poly (lactide) and their block copolymers: Influence of composition, temperature and morphology. Reactive and Functional Polymers 1997;32:161-8.

[33] Burkersroda Fv, Schedl L, Göpferich A. Why degradable polymers undergo surface erosion or bulk erosion. Biomaterials 2002;23:4221-31.

[34] Woodard JR, Hilldore AJ, Lan SK, Park CJ, Morgan AW, Eurell JAC, et al. The mechanical properties and osteoconductivity of hydroxyapatite bone scaffolds with multi-scale porosity. Biomaterials 2007;28:45-54.

[35] Howk D, Chu TM. Design variables for mechanical properties of bone tissue scaffolds. Biomed Sci Instrum 2006;42:278-83.

[36] Cheema U, Ananta M, Mudera V. Collagen: Applications of a Natural Polymer in Regenerative Medicine. Regenerative Medicine and Tissue Engineering - Cells and Biomaterials 2011;ISBN: 978-953-307-663-8.

[37] Swetha M, Sahithi K, Moorthi A, Srinivasan N, Ramasamy K, Selvamurugan N. Biocomposites containing natural polymers and hydroxyapatite for bone tissue engineering. International Journal of Biological Macromolecules 2010;47:1-4.

[38] Sell SA, Wolfe PS, Garg K, McCool JM, Rodriguez IA, Bowlin GL. The Use of Natural Polymers in Tissue Engineering: A Focus on Electrospun Extracellular Matrix Analogues. Polymers 2010;2:522.

[39] Monzack E, Rodriguez K, McCoy C, Gu X, Masters K. Natural Materials in Tissue Engineering Applications. In: Burdick J, Mauck R, editors. Biomaterials for Tissue Engineering Applications: Springer Vienna; 2011. p. 209-41.

[40] Gunatillake PA, Adhikari R. Biodegradable synthetic polymers for tissue engineering. Eur Cell Mater 2003;5:1-16.

[41] Dhandayuthapani B, Yoshida Y, Maekawa T, Kumar S. Polymeric Scaffolds in Tissue Engineering Application: A Review. International Journal of Polymer Science 2011;2011.

[42] Anderson JM, Shive MS. Biodegradation and biocompatibility of PLA and PLGA microspheres. Advanced Drug Delivery Reviews 1997;28:5-24.

[43] Makadia HK, Siegel SJ. Poly Lactic-co-Glycolic Acid (PLGA) as Biodegradable Controlled Drug Delivery Carrier. Polymers 2011;3:1377-97.

[44] Gentile P, Chiono V, Carmagnola I, Hatton PV. An Overview of Poly(lactic-co-glycolic) Acid (PLGA)-Based Biomaterials for Bone Tissue Engineering. International Journal of Molecular Sciences 2014;15:3640-59.

[45] Fu K, Pack D, Klibanov A, Langer R. Visual Evidence of Acidic Environment Within Degrading Poly(lactic-co-glycolic acid) (PLGA) Microspheres. Pharm Res 2000;17:100-6.

[46] Barrère F, van Blitterswijk CA, de Groot K. Bone regeneration: molecular and cellular interactions with calcium phosphate ceramics. International Journal of Nanomedicine 2006;1:317-32.

[47] LeGeros RZ. Calcium phosphate-based osteoinductive materials. Chem Rev 2008;108:4742-53.

[48] LeGeros RZ. Properties of osteoconductive biomaterials: calcium phosphates. Clin Orthop Relat Res 2002;395:81-98.

[49] Ambard AJ, Mueninghoff L. Calcium phosphate cement: review of mechanical and biological properties. J Prosthodont 2006;15:321-8.

[50] Sugawara A, Asaoka K, Ding S-J. Calcium phosphate-based cements: clinical needs and recent progress. Journal of Materials Chemistry B 2013;1:1081-9.

[51] Bohner M. Calcium orthophosphates in medicine: from ceramics to calcium phosphate cements. Injury 2000;31, Supplement 4:D37-D47.

[52] Narayanan R, Seshadri SK, Kwon TY, Kim KH. Calcium phosphate-based coatings on titanium and its alloys. J Biomed Mater Res B Appl Biomater 2008;85:279-99.

[53] Barrere F, van der Valk CM, Dalmeijer RA, Meijer G, van Blitterswijk CA, de Groot K, et al. Osteogenecity of octacalcium phosphate coatings applied on porous metal implants. J Biomed Mater Res A 2003;66:779-88.

[54] de Groot K, Wolke JG, Jansen JA. Calcium phosphate coatings for medical implants. Proc Inst Mech Eng H 1998;212:137-47.

[55] Dorozhkin SV. Amorphous calcium orthophosphates: nature, chemistry and biomedical applications. Int J Mater Chem 2012;2:19-46.

[56] Rah DK. Art of replacing craniofacial bone defects. Yonsei Med J 2000;41:756-65.

[57] Kim S-S, Sun Park M, Jeon O, Yong Choi C, Kim B-S. Poly(lactide-co-glycolide)/hydroxyapatite composite scaffolds for bone tissue engineering. Biomaterials 2006;27:1399-409.

[58] Wei G, Ma PX. Structure and properties of nano-hydroxyapatite/polymer composite scaffolds for bone tissue engineering. Biomaterials 2004;25:4749-57.

[59] Yang F, Wolke J, Jansen J. Biomimetic calcium phosphate coating on electrospun poly (ε-caprolactone) scaffolds for bone tissue engineering. Chemical Engineering Journal 2008;137:154-61.

[60] Nandakumar A, Yang L, Habibovic P, van Blitterswijk C. Calcium Phosphate Coated Electrospun Fiber Matrices as Scaffolds for Bone Tissue Engineering. Langmuir 2010;26:7380-7.

[61] Holzwarth JM, Ma PX. Biomimetic nanofibrous scaffolds for bone tissue engineering. Biomaterials 2011;32:9622-9.

[62] Seyedjafari E, Soleimani M, Ghaemi N, Shabani I. Nanohydroxyapatite-coated electrospun poly(l-lactide) nanofibers enhance osteogenic differentiation of stem cells and induce ectopic bone formation. Biomacromolecules 2010;11:3118-25.

[63] Cao H, Kuboyama N. A biodegradable porous composite scaffold of PGA/β-TCP for bone tissue engineering. Bone 2010;46:386-95.

[64] Ogose A, Hotta T, Kawashima H, Kondo N, Gu W, Kamura T, et al. Comparison of hydroxyapatite and beta tricalcium phosphate as bone substitutes after excision of bone tumors. J Biomed Mater Res B Appl Biomater 2005;72:94-101.

[65] LeGeros RZ, Lin S, Rohanizadeh R, Mijares D, LeGeros JP. Biphasic calcium phosphate bioceramics: preparation, properties and applications. J Mater Sci Mater Med 2003;14:201-9.

[66] Suzuki O, Imaizumi H, Kamakura S, Katagiri T. Bone regeneration by synthetic octacalcium phosphate and its role in biological mineralization. Curr Med Chem 2008;15:305-13.

[67] Kamakura S, Sasaki K, Honda Y, Anada T, Suzuki O. Octacalcium phosphate combined with collagen orthotopically enhances bone regeneration. J Biomed Mater Res B Appl Biomater 2006;79:210-7.

[68] Kawai T, Anada T, Honda Y, Kamakura S, Matsui K, Matsui A, et al. Synthetic octacalcium phosphate augments bone regeneration correlated with its content in collagen scaffold. Tissue Eng Part A 2009;15:23-32.

[69] Wang L, Nancollas GH. Calcium Orthophosphates: Crystallization and Dissolution. Chemical reviews 2008;108:4628-69.

[70] Lc C. Next generation calcium phosphate-based biomaterials. Dental materials journal 2009;28:1-10.

[71] Johnsson MS, Nancollas GH. The role of brushite and octacalcium phosphate in apatite formation. Crit Rev Oral Biol Med 1992;3:61-82.

[72] Kanzaki N, Onuma K, Treboux G, Ito A. Dissolution kinetics of dicalcium phosphate dihydrate under pseudophysiological conditions. Journal of Crystal Growth 2002;235:465-70.

[73] Apelt D, Theiss F, El-Warrak AO, Zlinszky K, Bettschart-Wolfisberger R, Bohner M, et al. In vivo behavior of three different injectable hydraulic calcium phosphate cements. Biomaterials 2004;25:1439-51.

[74] Theiss F, Apelt D, Brand B, Kutter A, Zlinszky K, Bohner M, et al. Biocompatibility and resorption of a brushite calcium phosphate cement. Biomaterials 2005;26:4383-94.

[75] Hoppe A, Güldal NS, Boccaccini AR. A review of the biological response to ionic dissolution products from bioactive glasses and glass-ceramics. Biomaterials 2011;32:2757-74.

[76] Barradas AM, Fernandes HA, Groen N, Chai YC, Schrooten J, van de Peppel J, et al. A calcium-induced signaling cascade leading to osteogenic differentiation of human bone marrow-derived mesenchymal stromal cells. Biomaterials 2012;33:3205-15.

[77] Barradas AM, Monticone V, Hulsman M, Danoux C, Fernandes H, Tahmasebi Birgani Z, et al. Molecular mechanisms of biomaterial-driven osteogenic differentiation in human mesenchymal stromal cells. Integr Biol 2013;5:920-31.

[78] Marie PJ. The calcium-sensing receptor in bone cells: a potential therapeutic target in osteoporosis. Bone 2010;46:571-6.

[79] Metsger DS, Driskell TD, Paulsrud JR. Tricalcium phosphate ceramic--a resorbable bone implant: review and current status. J Am Dent Assoc 1982;105:1035-8.

[80] Horch HH, Sader R, Pautke C, Neff A, Deppe H, Kolk A. Synthetic, pure-phase beta-tricalcium phosphate ceramic granules (Cerasorb®) for bone regeneration in the reconstructive surgery of the jaws. International Journal of Oral and Maxillofacial Surgery 2006;35:708-13.

[81] Neamat A, Gawish A, Gamal-Eldeen AM. beta-Tricalcium phosphate promotes cell proliferation, osteogenesis and bone regeneration in intrabony defects in dogs. Arch Oral Biol 2009;54:1083-90.

[82] Rezwan K, Chen QZ, Blaker JJ, Boccaccini AR. Biodegradable and bioactive porous polymer/inorganic composite scaffolds for bone tissue engineering. Biomaterials 2006;27:3413-31.

[83] Zhang Y, Zhang M. Synthesis and characterization of macroporous chitosan/calcium phosphate composite scaffolds for tissue engineering. Journal of biomedical materials research 2001;55:304-12.

[84] Salgado AJ, Coutinho OP, Reis RL. Bone tissue engineering: state of the art and future trends. Macromol Biosci 2004;4:743-65.

[85] Ertel SI, Kohn J. Evaluation of a series of tyrosine-derived polycarbonates as degradable biomaterials. Journal of biomedical materials research 1994;28:919-30.

[86] Choueka J, Charvet JL, Koval KJ, Alexander H, James KS, Hooper KA, et al. Canine bone response to tyrosine-derived polycarbonates and poly (L-lactic acid). Journal of biomedical materials research 1996;31:35-41.

[87] James K, Levene H, Parsons JR, Kohn J. Small changes in polymer chemistry have a large effect on the bone–implant interface:: evaluation of a series of degradable tyrosine-derived polycarbonates in bone defects. Biomaterials 1999;20:2203-12.

[88] Kohn J. An Overview of the Use of Polymers in Medical Applications as Illustrated by the Design, Characterization, and Application of Tyrosine-Derived Polymers. Medical plastics: degradation resistance & failure analysis 1998:1.

[89] Magno MHR, Kim J, Srinivasan A, McBride S, Bolikal D, Darr A, et al. Synthesis, degradation and biocompatibility of tyrosine-derived polycarbonate scaffolds. Journal of Materials Chemistry 2010;20:8885-93.

[90] Yu C, Kohn J. Tyrosine–PEG-derived poly (ether carbonate) s as new biomaterials: part I: synthesis and evaluation. Biomaterials 1999;20:253-64.

[91] Tangpasuthadol V, Pendharkar SM, Kohn J. Hydrolytic degradation of tyrosine-derived polycarbonates, a class of new biomaterials. Part I: Study of model compounds. Biomaterials 2000;21:2371-8.

[92] Tangpasuthadol V, Pendharkar SM, Peterson RC, Kohn J. Hydrolytic degradation of tyrosine-derived polycarbonates, a class of new biomaterials. Part II: 3-yr study of polymeric devices. Biomaterials 2000;21:2379-87.

[93] Meechaisue C, Dubin R, Supaphol P, Hoven VP, Kohn J. Electrospun mat of tyrosine-derived polycarbonate fibers for potential use as tissue scaffolding material. Journal of Biomaterials Science, Polymer Edition 2006;17:1039-56.

[94] Ezra MI. Fabrication and evaluation of a tyrosine-derived polycarbonate conduit to enhance functional recovery of a 5 mm peripheral nerve gap in a mouse femoral nerve model: Rutgers University-Graduate School-New Brunswick; 2012.

[95] Sheihet L, Chandra P, Batheja P, Devore D, Kohn J, Michniak B. Tyrosine-derived nanospheres for enhanced topical skin penetration. International journal of pharmaceutics 2008;350:312-9.

[96] Sheihet L, Garbuzenko OB, Bushman J, Gounder MK, Minko T, Kohn J. Paclitaxel in tyrosine-derived nanospheres as a potential anti-cancer agent: in vivo evaluation of toxicity and efficacy in comparison with paclitaxel in Cremophor. European Journal of Pharmaceutical Sciences 2012;45:320-9.

[97] Kim J, McBride S, Donovan A, Darr A, Magno MH, Hollinger JO. Tyrosine-derived polycarbonate scaffolds for bone regeneration in a rabbit radius critical-size defect model. Biomed Mater 2015;10:1748-6041.

[98] Kim J, Magno MH, Waters H, Doll BA, McBride S, Alvarez P, et al. Bone regeneration in a rabbit critical-sized calvarial model using tyrosine-derived polycarbonate scaffolds. Tissue Eng Part A 2012;18:1132-9.

[99] Kim J, Magno MH, Alvarez P, Darr A, Kohn J, Hollinger JO. Osteogenic differentiation of pre-osteoblasts on biomimetic tyrosine-derived polycarbonate scaffolds. Biomacromolecules 2011;12:3520-7.

[100] Kim J, Magno MHR, Ortiz O, McBride S, Darr A, Kohn J, et al. Next-generation resorbable polymer scaffolds with surface-precipitated calcium phosphate coatings. Regenerative Biomaterials 2015.

[101] Luangphakdy V, Walker E, Shinohara K, Pan H, Hefferan T, Bauer TW, et al. Evaluation of Osteoconductive Scaffolds in the Canine Femoral Multi-Defect Model. Tissue Engineering Part A 2013;19:634-48.

[102] Haaparanta AM, Haimi S, Ella V, Hopper N, Miettinen S, Suuronen R, et al. Porous polylactide/beta-tricalcium phosphate composite scaffolds for tissue engineering applications. J Tissue Eng Regen Med 2010;4:366-73.

[103] Cao L, Duan PG, Wang HR, Li XL, Yuan FL, Fan ZY, et al. Degradation and osteogenic potential of a novel poly(lactic acid)/nano-sized beta-tricalcium phosphate scaffold. Int J Nanomedicine 2012;7:5881-8.

[104] Andiappan M, Sundaramoorthy S, Panda N, Meiyazhaban G, Winfred S, Venkataraman G, et al. Electrospun eri silk fibroin scaffold coated with hydroxyapatite for bone tissue engineering applications. Prog Biomater 2013;2:1-11.

[105] Surmenev RA, Surmeneva MA, Ivanova AA. Significance of calcium phosphate coatings for the enhancement of new bone osteogenesis – A review. Acta Biomaterialia 2014;10:557-79.

[106] Li J, Baker BA, Mou X, Ren N, Qiu J, Boughton RI, et al. Biopolymer/Calcium phosphate scaffolds for bone tissue engineering. Adv Healthc Mater 2014;3:469-84.

[107] Seyedjafari E, Soleimani M, Ghaemi N, Shabani I. Nanohydroxyapatite-Coated Electrospun Poly(l-lactide) Nanofibers Enhance Osteogenic Differentiation of Stem Cells and Induce Ectopic Bone Formation. Biomacromolecules 2010;11:3118-25.

[108] Vaquette C, Ivanovski S, Hamlet SM, Hutmacher DW. Effect of culture conditions and calcium phosphate coating on ectopic bone formation. Biomaterials 2013;34:5538-51.

[109] Lu X, Leng Y. Theoretical analysis of calcium phosphate precipitation in simulated body fluid. Biomaterials 2005;26:1097-108.

[110] Kokubo T, Takadama H. How useful is SBF in predicting in vivo bone bioactivity? Biomaterials 2006;27:2907-15.

[111] Yang F, Wolke JGC, Jansen JA. Biomimetic calcium phosphate coating on electrospun poly(ε-caprolactone) scaffolds for bone tissue engineering. Chemical Engineering Journal 2008;137:154-61.

[112] Strange DGT, Oyen ML. Biomimetic bone-like composites fabricated through an automated alternate soaking process. Acta Biomaterialia 2011;7:3586-94.

[113] Furuzono T, Taguchi T, Kishida A, Akashi M, Tamada Y. Preparation and characterization of apatite deposited on silk fabric using an alternate soaking process. Journal of biomedical materials research 2000;50:344-52.

[114] Zhao J, Zhang Z, Wang S, Sun X, Zhang X, Chen J, et al. Apatite-coated Silk Fibroin Scaffolds to Healing Mandibular Border Defects in Canines. Bone 2009;45:517-27.

[115] He C, Xiao G, Jin X, Sun C, Ma PX. Electrodeposition on nanofibrous polymer scaffolds: Rapid mineralization, tunable calcium phosphate composition and topography. Advanced functional materials 2010;20:3568-76.

2

Scaffold Fabrication Process Optimization and Scale-Up

2.1 Introduction

Porous scaffolds are widely used in tissue engineering to provide a three-dimensional (3D) structure for both *in vitro* studies of cell-scaffold interactions and *in vivo* studies of tissue regeneration [1, 2]. Regardless of the application, the scaffold materials, as well as the 3D structure of the scaffold, have a significant effect on cellular responses. An ideal scaffold should be biocompatible, therefore does not trigger adverse tissue responses. In addition, it should degrade in the body at a rate in concurrence with new tissue growth [3] and the degradation products are harmless. Moreover, the scaffold must have a high pore volume fraction or porosity that allows the migration and proliferation of cells [4]. The pore size should be designed to be large enough for cell migration but also small enough to retain cells inside the scaffold [4, 5]. In addition, to allow for transportation of cells and metabolites, the scaffold must have a high specific surface area as well as an interconnected pore network [6, 7].

In the Kohn laboratory, a promising bone regeneration scaffold fabricated from E1001(1k), a tyrosine-derived polycarbonate has been developed [8-12]. This scaffold features favorable porosity and interconnectivity that permitting *in vivo* angiogenesis and osteogenesis. Significantly better osteogenic outcome was observed in the canine femoral

multi-defects model [13] over poly(L-lactide-co-glycolide) (PLGA) and poly(L-lactide-co-ε-caprolactone) (PLCL) scaffolds. Porous E1001(1k) scaffolds have been manufactured using a combination of porogen leaching and freeze-drying technique [9]. Using this technique, a mixture of E1001(1k) solution and porogen was quenched in liquid nitrogen and followed by a freeze-drying process. The sublimation of solvents leads to formation of micropores on the wall of scaffold. The subsequent leaching of the porogen leads to the formation of macropores replicating the size of porogen. Previous studies have shown large variation of *in vivo* bone regeneration outcome in rabbit calvarial critical size defects, likely due to variation in scaffold structure [8, 12]. Varied batch-to-batch polymer molecular weight and insufficient mixing of polymer solution-salt particles-calcium phosphate may contribute to variation in scaffold structure. Moreover, the rapid and uncontrolled quenching in liquid nitrogen typically used in fabricating porous scaffolds via freeze-drying results in temporal and spatial variation in heat transfer through the mixture, leading to non-uniformly nucleation and growth of solvents crystals and ultimately, scaffold heterogeneity [1]. Therefore, the production of scaffolds requires precise control over the processing parameters to achieve a scaffold structure that is both specific and consistent throughout the materials.

The objective here was to optimize and scale-up the E1001(1k) scaffold fabrication process in order to produce scaffolds with uniform structure and consistent batch-to-batch variation. To this end, the conventional technique of fabricating E1001(1k) scaffolds was modified in four specific ways. (1) The polymer concentration and molecular weight range that produce optimal scaffold structure was defined. (2) Homogeneous mixing of polymer solution, salt particles and/ or calcium phosphate

minerals was achieved using an overhead mixer and elevated mixing temperature. (3) A controlled freezing process was established to minimize variation in heat transfer. (4) Custom-design cutting tools were used to produce scaffolds with consistent shapes and sizes.

2.2 Materials and methods

2.2.1 Materials

Sodium chloride (NaCl) was purchased from Sigma-Aldrich Chemical Co. (St. Louis, MO). The NaCl particles were sieved to obtain sizes between 212-425 μm and used as a porogen during scaffold fabrication. 1,4-Dioxane was obtained from Fischer Scientific (Pittsburgh, PA). Teflon molds (50 mm in diameter ×10 mm in height) were purchased from Saint-Gobain Performance Plastics (Valley Forge, PA).

2.2.2 Scaffold fabrication

3D porous scaffolds were fabricated from E1001(1k) using a combination of salt leaching and freeze-drying methods. Briefly, the polymer was first dissolved in deionized (DI) water and 1,4-dioxane overnight. The polymer solution was mixed uniformly with salt particles. The mixture was then casted into a Teflon mold (50 mm in diameter × 10 mm in height, LabPure Laboratory Products), quenched at desired temperature and freeze-dried for 2 days. Disk-shaped scaffolds (15.5 mm diameter × 2.4 mm thick) were punched out from the mold using a custom-designed cutting tool. Salt particles were

leached out in distill water, and the nonporous skin was sliced off. Finally, the scaffolds were dried in a lyophilizer for 1 day.

2.2.3 Polymer concentration and molecular weight optimization

In order to develop a strategy to accommodate the varying polymer molecular weight, the effect of polymer concentration (15% and 20%) and molecular weight (280, 320, 390 kDa) on scaffold properties were investigated (Table 2.1). The scaffolds were fabricated according to procedure in the Section 2.2.2. The % polymer means the weight % of polymer as respect to the volume of 1, 4-dioxane and DI water. For example, 15% means 15 g of polymer in 100 ml of 1, 4-dioxane and DI water. The 1, 4-dioxane: DI water ratio was kept at 86: 14, which means in 100 ml of solvents, there are 86 ml 1, 4-dioxane and 14 ml DI water. The amount of salt particles was also kept the same for each group at 90% in respect to the total weight of salt and polymer.

Table 2.1 Scaffold fabrication conditions: varying polymer concentration and molecular weight.

Formula	Molecular Weight, kDa	% Polymer	Dioxane : DI water	% Porogen
1	280	20	86: 14	90
2	320	15	86: 14	90
3	320	20	86: 14	90
4	390	15	86: 14	90
5	390	20	86: 14	90

2.2.4 Uniform mixing

To achieve a uniform mixing of polymer solution, salt particles and calcium phosphate minerals, an overhead mixer (EuroStar Power Contro Visc IKA®WERKE, Wilmington, NC) was used. The scaffolds were fabricated according to the procedure in Section 2.2.2 with small modification. The mixing speed and time were 100 rpm and 30 min respectively. Two mixing temperature, room temperature and 50°C were investigated. The size of the mold was 75 mm in diameter × 50 mm in height. The scaffold thickness was 30 mm. Samples were taken from bottom, middle and top segments of the scaffolds (Fig. 2.1) for SEM and thermogravimetric analyses (TGA). TGA was performed at a heating rate of 10°C/ min from 25 to 800°C under flowing nitrogen.

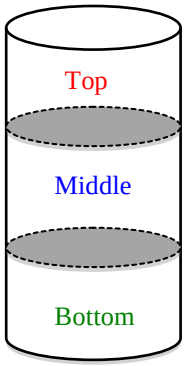

Figure 2.1 Samples were taken from the bottom, middle, and top segments of a 30 mm scaffolds for scanning electroscope (SEM) and thermogravimetric analyses (TGA).

2.2.5 Controlled freeze rate and freeze temperature

To investigate the effect of freeze rate and freeze temperature on scaffold properties, scaffolds were fabricated according to the procedure in Section 2.2.2 with

modification in freezing condition. The salt particles-polymer solution mixture was frozen to -10˚C, -30˚C or -50˚C at -1 ˚C/min or quenched at -50 ˚C using Laboratory Series Freeze Dryer LD85 (MillRock Technology, Kingston, NY). One polymer formulation (366 kDa, 20 wt%, 86:14 dioxane: water ratio) was used. Only freezing condition was varied. Primary drying and secondary drying conditions were kept the same. Primary drying: 0˚C and 50 mTorr for 24 hours. Secondary drying: 20˚C and 50 mTorr for 24 hours. The freeze dryer has build-in software to control the freeze temperature and freeze rate. One thermocouple was used to monitor the shelf temperature; two were inserted at the opposite edges of the mold, and one in the center of the mold to monitor the temperature of the salt particles-polymer solution mixture. The temperature was recorded using the system software for every minute. For scaffold fabrication condition of "quench at − 50°C", the freeze dryer shelf temperature was preset and stabilized at − 50°C before placing the samples in the shelf. During the installation of thermocouples, the samples already started to freeze and thus the initial temperature profile was not captured.

2.2.6 Cutting tools design

In order to produce scaffolds with consistent shapes and sizes, custom-designed cutting tools were built (Fig. 2.2). The cutting system consists of stainless steel punchers of various sizes (Fig.2.2a), a modified arbor pressure (Fig.2.2b) and cutting molds (Fig.2.2c). The arbor press was purchased from Harbor Freight Tools (Item # 3552, East Brunswick, NJ) and was modified so that the cutting puncher can be mounted in.

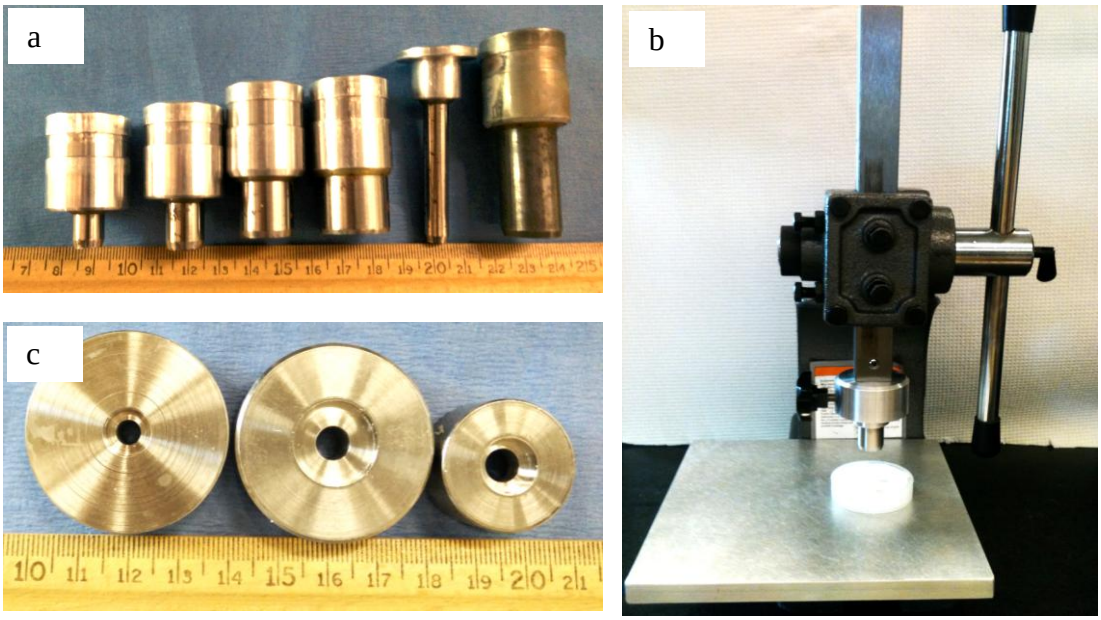

Figure 2.2 Custom-designed scaffold cutting tool consist of (a) stainless steel punchers of various sizes, (b) a modified arbor press, (c) cutting molds of various sizes.

2.2.7 Scaffold characterization

The scaffolds fabricated in Section 2.2.3-2.2.5 were characterized using the following techniques.

The porosity (ε) of porous scaffold was determined as follow:

$$\varepsilon = 1 - \frac{m}{\rho_s * V}$$

Where m is the mass of the scaffold measured using a Mettler Toledo balance. ρ_s is the solid density of the bulk polymer, which is 1.2 g/ml. V is the volume of the scaffold determined by measuring the dimension of scaffolds (diameter and thickness).

The internal pore structure of the scaffolds was assessed using scanning electron microscopy (SEM, Amray 1830I, 20 kV). Scaffold cross-sections were cut carefully

using a razor blade and were sputter coated with gold/palladium at 30 mA for 120 sec prior to SEM examination.

The compressive mechanical properties of the scaffolds were evaluated at room temperature using ReNew MTS System 4. The cross-head speed was 0.5 mm/min and load cell was 100 N. 4-6 samples were tested for each fabrication condition. The Young's Modulus was calculated as initial slope of the linear elastic region. The compressive strength was the stress level at 10% strain according to ISO 844-2004 for determination of compressive properties of rigid cellular plastics.

The scaffolds were also characterized using X-ray micro-computed tomography (microCT). The scans were performed in a microCT scanner (Skyscan 1172, Bruker-microCT, Belgium) at a resolution of 10 μm, a voltage of 60 kVp, a current of 170 mA, and with a 0.5 mm Aluminum filter. The reconstruction of projection images was performed using Skyscan system software package. The distribution of calcium phosphate minerals was assessed qualitatively using the projection images.

2.3 Results

2.3.1 The effect of polymer concentration and molecular weight

Using the combination of porogen leaching and freeze-drying, highly porous 3D scaffolds were fabricated. Fig. 2.3 shows the effect of polymer concentration (15% and 20%) and polymer molecular weight (280, 320 and 390 kDa) on scaffold architecture. Images at low magnification show highly porous and interconnected macroscopic pores between 200 to 400 μm for all scaffolds in the range of polymer concentration and

molecular weight studied except for the scaffold fabricated from the condition of 390 kDa and 20%. This scaffold had cuboidal pores that were less open or interconnected. This is likely due to the high polymer solution viscosity that contributes to the difficulty of achieving uniform mixing between polymer solution and salt particles, and thus less open pore architecture. Images at high magnification showing the microscopic structure of scaffold pore wall revealed a significant effect of polymer concentration and molecular weight on micropores size. It was observed that the size of micropores decreased as the concentration of the E1001(1k) solution increased from 15 % to 20% or as the polymer molecular increased from 280 to 390 kDa.

The effect of polymer concentration and molecular weight on scaffold porosity and compressive elastic modulus was summarized in Table 2.2**.** All scaffolds exhibited porosity greater than 90 % regardless of fabrication conditions. As the polymer concentration increased, the compressive elastic modulus increased at the expense of decreased scaffold porosity. No significant difference in scaffold porosity or compressive elastic modulus was observed by varying the polymer molecular weight indicated that the effect of polymer molecular weight was minimal.

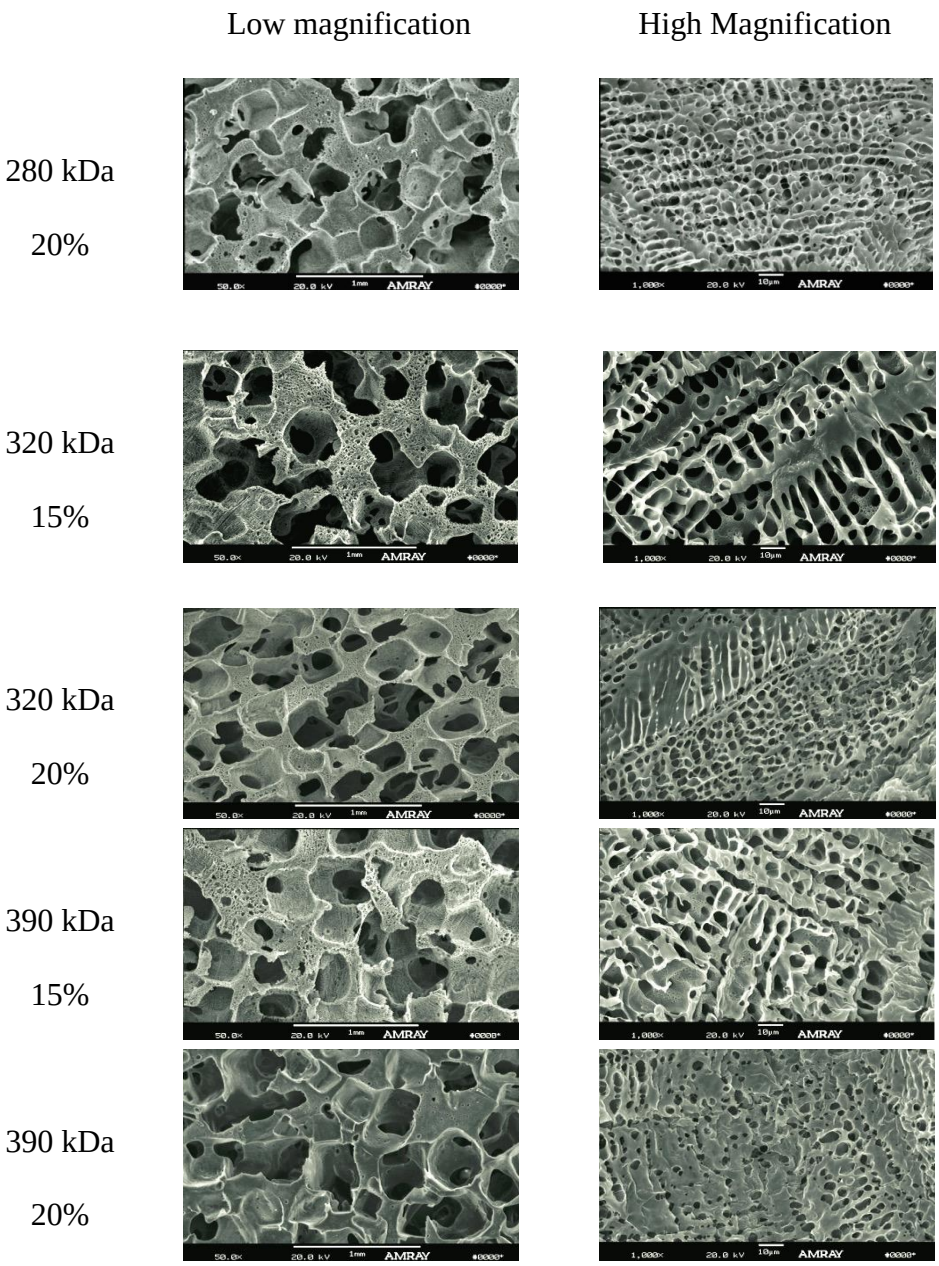

Figure 2.3 Scanning electron microscope images of scaffolds fabricated from polymer of different molecular weight (280, 320 and 390 kDa) and concentration (15% and 20%). Images on the left panel were taken at 50X and the scale bar is 1 mm. Images on the right panel were taken at 1000X and the scale bar is 10 μm.

Table 2.2 Scaffold porosity and compressive elastic modulus: the effect of polymer concentration and molecular weight

Formula	Mw, kDa	% Polymer	Mean porosity ± SD	Modulus ± SD, MPa
1	280	20	92.4 ± (0.3)	1.83 ± (0.51)
2	320	15	92.9 ± (0.2)	1.38± (0.19)
3	320	20	92.0 ± (0.6)	1.51± (0.51)
4	390	15	93.6 ± (0.1)	1.40 ± (0.30)
5	390	20	91.7 ± (0.7)	2.24 ± (0.27)

2.3.2 The effect of freeze temperature and freeze rate

To investigate the effect of freeze temperature and freeze rate on scaffold properties, four freeze-drying conditions were used to fabricate the scaffolds: freeze to − 10°C, − 30°C and − 50°C at − 1°C/min, and quenched at − 50°C. Fig. 2.4 shows the temperature-time profile of the polymer solution-salt mixture at the center of the mold using freezing conditions of − 10°C, − 30°C or − 50°C at − 1°C/min. Distinctive phase transitions at 2°C and − 3°C were observed, which may correspond to the depressed freezing points of dioxane and water respectively. Dioxane has higher freezing point than water (11°C vs. 0°C), therefore, it is speculated to freeze first. For − 50°C, there was an additional transition at − 34°C, which is speculated to be the wet glass transition point of E1001(1k) solution. Fig. 2.5 shows the average temperature of the polymer solution-salt mixture during freezing for the quenching and constant cooling rate techniques. A large difference in temperature (larger error bar) was observed between measurement locations

during the freeze process for the quenching condition as compared for the constant rate cooling technique.

Fig. 2.6 shows the SEM images of scaffolds. Characteristic bimodal pore size distribution of highly interconnected macropores and micropores were obtained for all conditions. For scaffolds fabricated via − 10°C, − 30°C and − 50°C at − 1°C/min, no significant difference in scaffold macroporous or microporous structure was observed. The micropores (< 50 μm) were random distributed throughout the wall of scaffold. For scaffold fabricated via ‘ quench at − 50°C’, similar macroporous structure was observed. However, the micropores were highly aliened. For all conditions, the porosity of scaffold was about 94% and similar compressive elastic modulus was measured (≈ 1 MPa) (Table 2.3).

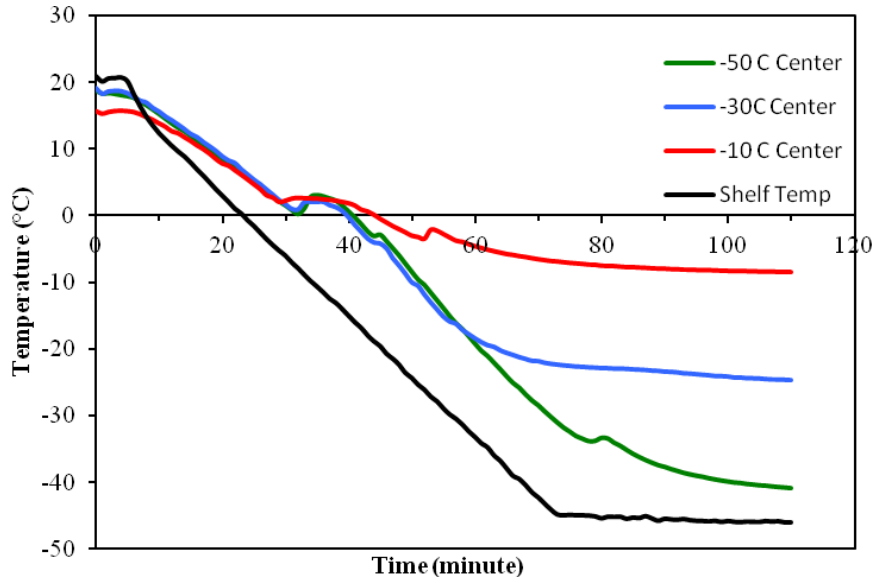

Figure 2.4 Temperature-time profile of freezing conditions of -10°C, -30°C and -50°C at -1°C/min, distinctive dioxane and water solidification and glass transition of polymer solution were observed. The shelf temperature as a function of time is also show as a control

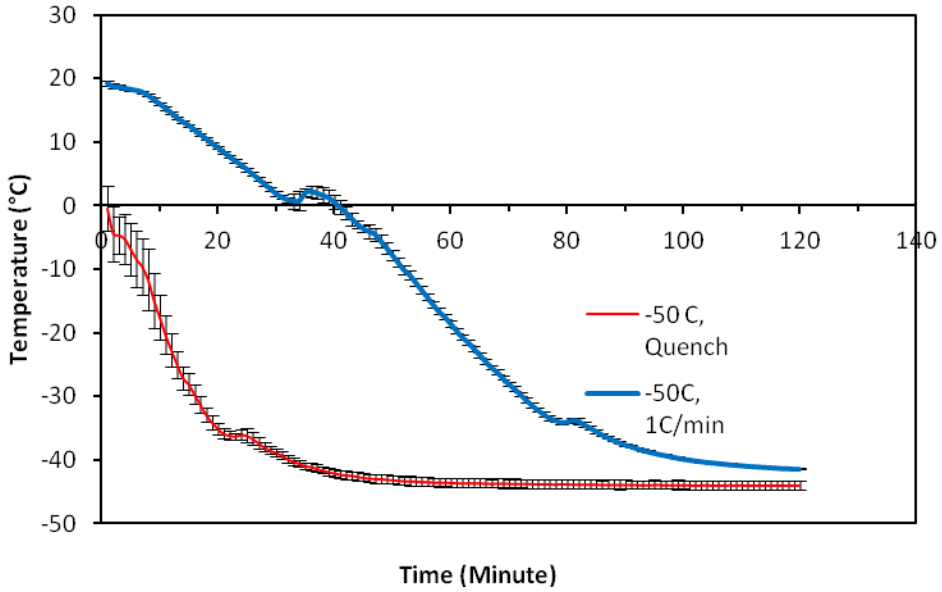

Figure 2.5 Average temperature-time profile of freezing condition of freeze to −50°C at −1°C/min and quench at −50°C

Freeze to − 10°C @ −1°C/min

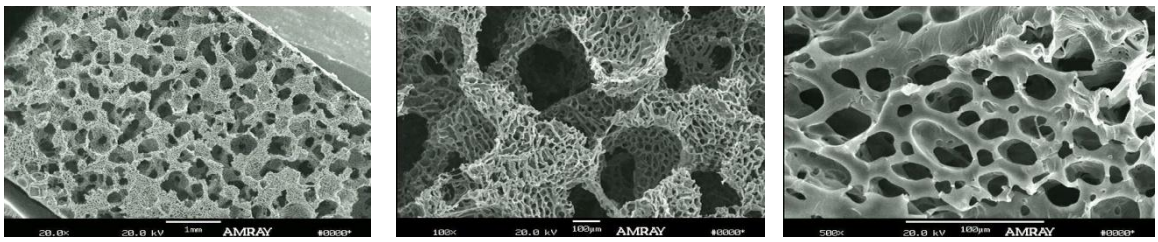

Freeze to − 30°C @ −1°C/min

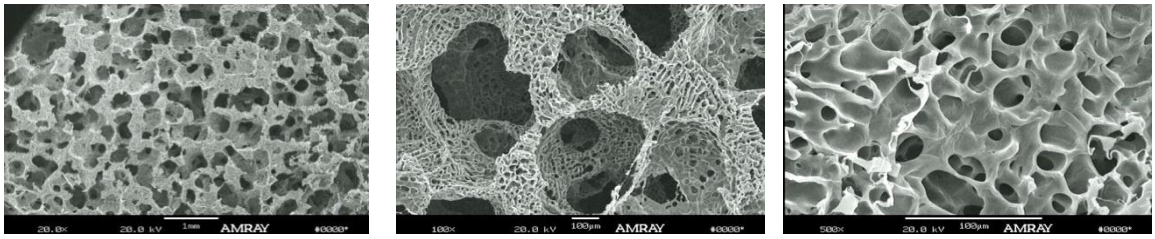

Freeze to − 50°C @ −1°C/min

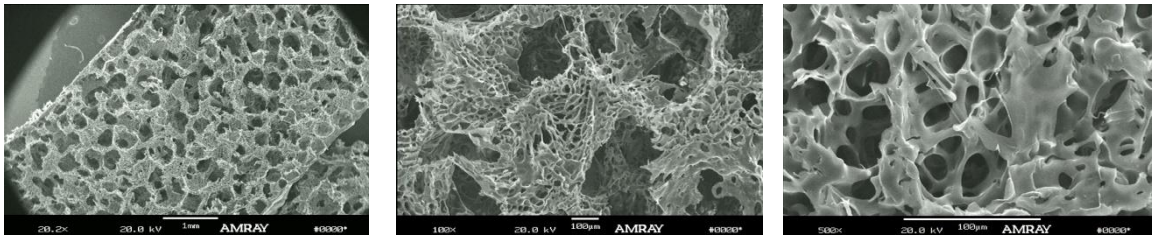

Quench at − 50°C

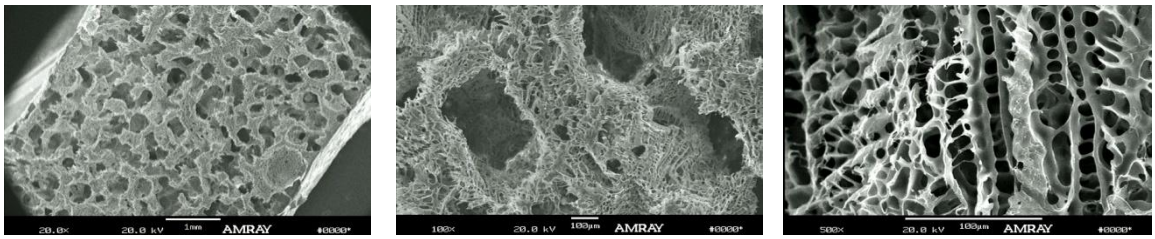

Figure 2.6 Scanning electron microscope images of scaffolds fabricated using different freezing conditions.

Table 2.3 Porosity and compressive elastic modulus of scaffolds prepared via different freezing temperature and rate.

Freezing Conditions	Porosity by helium pyconometry	Porosity by gravimetric method	n	Compressive elastic modulus (Mpa)	n
-50˚C at -1˚C/min	93.7 ± 0.2	94.0 ± 0.2	6	0.89 ± 0.05	4
-30˚C at -1˚C/min	94.1 ± 0.1	94.0 ± 0.1	6	1.15 ± 0.26	4
-10˚C at -1˚C/min	93.7 ± 0.2	93.6 ± 0.2	6	1.27 ± 0.20	4
Quenched at -50˚C	92.9 ± 0.2	93.5 ± 0.2	6	1.37 ± 0.19	4

2.3.3 The effect of mixing conditions

The SEM images showed similar scaffold morphology in each segment along the height of scaffolds (data not shown). There was no significant difference in the amount of calcium phosphate in the samples taken from the bottom, middle and top segments (Fig. 2.7) at both mixing temperatures, indicating uniform distribution of calcium phosphate throughout the scaffold matrix. The amount of calcium phosphate was about 26%, which was slightly less than the theoretically amount (30%) because loosely bound particles were washed away during the leaching process. Using mixing condition at room temperature, small amount of air bubble entrapped inside the scaffolds was observed using microCT (Fig. 2.8a). The air bubbles were removed by mixing at elevated temperature at 50°C, (Fig. 2.8b).

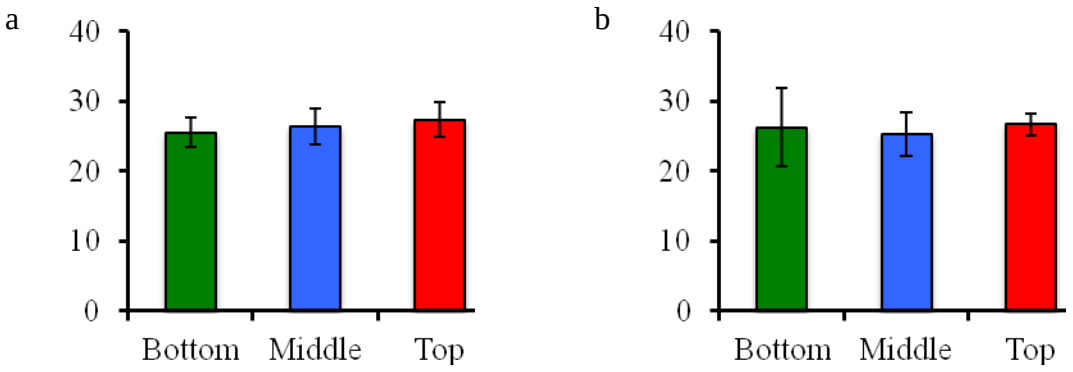

Figure 2.7 The amount of calcium phosphate in the polymer matrix for samples taken from the bottom, middle, and top segments along the height of 30 mm thick scaffolds prepared using mixing temperature of (a) room temperature, and (b) 50°C.

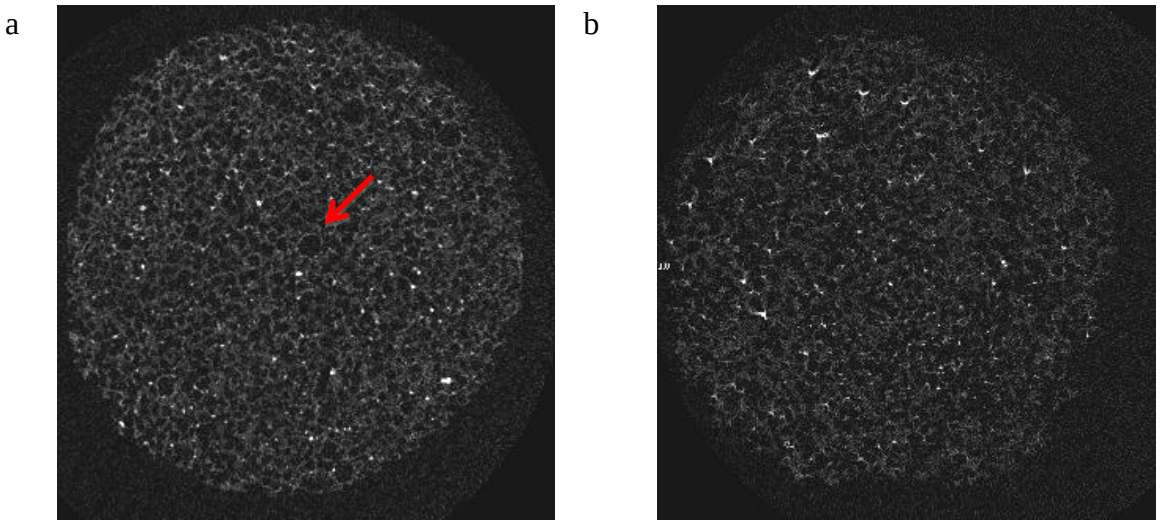

Figure 2.8 2D microCT transverse images of scaffolds prepared using mixing temperature of (a) room temperature, and (b) 50°C. Red arrow indicates air bubbles, which were removed using mixing temperature of 50°C.

2.3.4 Consistent scaffold shape and size

Using custom-designed cutting tools, scaffolds with various sizes were fabricated (Fig.2.9). Table 2.4 shows the diameter, thickness and applications of scaffolds that have been fabricated. The scaffolds mass deviation within a batch was about 4% implying small variation in scaffold structure.

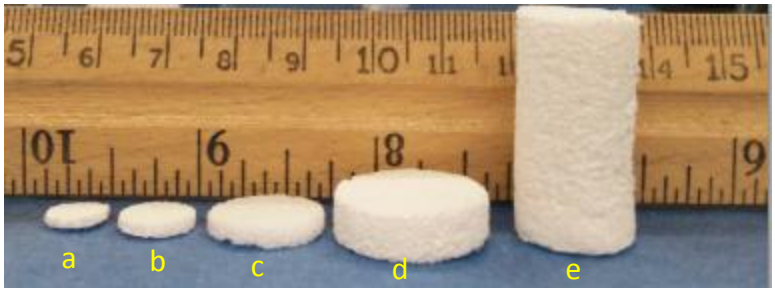

Figure 2.9 E1001(1k)-based scaffolds with various sizes. The dimension of scaffolds were summarized in Table 2.4

Table 2.4 Scaffolds dimensions and their applications.

Images	Diameter, mm	Thickness, mm	Applications
a	8	2.5	1. Rat subcutaneous implantation 2. Rabbit non-critical size calvarial defect
b	10	2	*In vitro* cell culture in 48-well plate
c	15	2.5	Rabbit calvarial critical size defect
d	20	6	Goat calvarial critical size defect
e	15	30	Sheep tibia segmental defect

2.4 Discussion

The 3D structure of a scaffold significantly affects cellular responses [4, 5]. Small variation in scaffold structure may lead to a significant difference in bone regeneration outcome *in vivo*. Therefore, the production of scaffolds requires precise control over the processing parameters to achieve a scaffold structure that is both specific and consistent throughout the materials [14]. In this study, the process to fabricate E1001(1k) scaffold using a combination of porogen leaching and freeze drying was optimized and scaffolds with homogeneous structure were produced. The fabrication process is ready for transfer to a third party contractor under Good Manufacturing Practice (GMP).

Using combined porogen leaching and freeze-drying, scaffolds with bimodal pore size distribution (macropores 200 – 400 μm and micropores < 20 μm) were fabricated. The large open macropores are for the penetration and in-growth of cells and blood vessel. The macroporous structure greatly depends on the properties of the porogen including its type, size, shape and amount [15]. Sugars [16], salts [17-19], gelatin [20], and many more have been used as porogen. In addition, scaffold porosity and pore size were determined by the amount and size of porogen respectively. Porosity of 90% and pore size range from 200 to 400 μm are well-reported optimal characteristics for osteoblasts infiltration and bone regeneration [4, 21]. Furthermore, a uniform mixing of polymer solution and porogen is equally important in determining scaffold structure uniformity. In this study, we achieved homogenous mixing using an overhead mixer and elevated mixing temperature. A large dimension (15 mm in diameter x 30 mm in height) scaffold with uniform structure was produced. Moreover, using this mixing technique, calcium phosphate was uniformly distributed throughout the depth of scaffolds. Uniform

mixing and entrapped air bubbles are tissues often ignored in the laboratory scaffold fabrication processes [22]. Entrapped air bubbles can generate closed pore, thus, block cellular infiltration. Those two issues were successfully addressed in this study in order to produce scaffolds with homogenous structure.

On the other hand, it is often necessary to manufacture microstructure with pore diameter less than 100 μm along with macropores for optimal transportation of nutrients to the cells [6]. Studies have reported that the presence of micropores significantly increases scaffold surface area, which benefits angiogenesis and osteogenesis by enhancing endogenous protein adsorption, nutrition and osteogenic factors transportation, as well as ion exchange and bone-like apatite formation by dissolution and precipitation [4, 6, 23]. The microporous structure is mainly determined by the solvent crystals, which are affected by the freezing condition [24]. The rapid and uncontrolled quenching in liquid nitrogen typically used in fabricating porous scaffolds via freeze-drying results in temporal and spatial variation in heat transfer through the mixture [1]. A large difference in temperature was observed among measurement locations during freezing for the 'quench at −50°C' condition. The variation in temperature distribution is believed to lead to non-uniform nucleation and growth of solvents crystals and ultimately, scaffold heterogeneity. Moreover, using rapid quenching condition, solvents solidify quickly along the direction of freezing front resulting aligned small micropores [14, 25, 26]. Furthermore, surface cracks are often found after the release of thermal stress during freeze-drying, which significantly reduce the production yield. Using constant cooling, no crack was found in this study. A significant less variation in temperature was observed for constant cooling conditions of −1°C/min, indicating uniform temperature distribution,

which positively influence structure uniformity [27]. At a slow freezing rate, solvent crystals have time to coarsen, and the resulting micropores are often larger than micropores formed using rapid quenching [28].

The molecular weight of E1001(1k) polymer used as the starting material for the 3D scaffold can be varied from 280 to 390 kDa. We observed that the molecular weight did not affect scaffold porosity and mechanical properties very much, but significantly on scaffolds microstructure. As the molecular weight increased, the micropore size become smaller, likely due to increased solution viscosity [28]. Therefore, to accommodate the structural variation caused by molecular weight, we investigated the effect of polymer molecular weight and concentration on scaffold structure, porosity and mechanical properties. Scaffold fabricated from 390 kDa and 20% revealed a less open and interconnected structure. Therefore, we concluded that for high molecular weight like 390 kDa, a lower polymer concentration should be used. Indeed, scaffold fabricated at 390 kDa and 15% had similar morphology as scaffolds fabricated at 280 or 320 kDa and 20 %. To be even more precisely, the viscosity of polymer solution should be kept the same to minimize batch-to-batch variation [28].

It is important for bone regeneration scaffolds to have reproducible shape and size [29]. For example, for *in vivo* studies, scaffolds need to have dimensions that can be fitted snuggly into defects to ensure a good contact between scaffold and native bone, a small gap between them may lead to significant variation in bone regeneration outcome. For *in vitro* experiments, consistent and reproducible samples must be used to perform controlled experiments. The cutting tools developed here allow us to punch out scaffold efficiently and accurately with scaffold mass deviation about 4%.

2.5 Conclusion

The process to fabricate E1001(1k) scaffolds using a combination of porogen leaching and freeze drying was optimized and scaled-up. Scaffolds with homogeneous structure and minimal batch-to-batch variation were produced. Also, human-sized scaffolds were also produced. The fabrication process is ready for transfer to a third party contractor under Good Manufacturing Practice (GMP).

Reference

[1] O'Brien FJ, Harley BA, Yannas IV, Gibson L. Influence of freezing rate on pore structure in freeze-dried collagen-GAG scaffolds. Biomaterials 2004;25:1077-86.

[2] Sastry KS, Patel RD. Temperature dependence of solution viscosity of polymers in solvent-nonsolvent systems. Die Makromolekulare Chemie 1969;128:166-75.

[3] Sung H-J, Meredith C, Johnson C, Galis ZS. The effect of scaffold degradation rate on three-dimensional cell growth and angiogenesis. Biomaterials 2004;25:5735-42.

[4] Karageorgiou V, Kaplan D. Porosity of 3D biomaterial scaffolds and osteogenesis. Biomaterials 2005;26:5474-91.

[5] Murphy CM, Haugh MG, O'Brien FJ. The effect of mean pore size on cell attachment, proliferation and migration in collagen-glycosaminoglycan scaffolds for bone tissue engineering. Biomaterials 2010;31:461-6.

[6] Wei J, Jia J, Wu F, Wei S, Zhou H, Zhang H, et al. Hierarchically microporous/macroporous scaffold of magnesium-calcium phosphate for bone tissue regeneration. Biomaterials 2010;31:1260-9.

[7] Polo-Corrales L, Latorre-Esteves M, Ramirez-Vick JE. Scaffold Design for Bone Regeneration. Journal of nanoscience and nanotechnology 2014;14:15-56.

[8] Kim J, Magno MH, Waters H, Doll BA, McBride S, Alvarez P, et al. Bone regeneration in a rabbit critical-sized calvarial model using tyrosine-derived polycarbonate scaffolds. Tissue Eng Part A 2012;18:1132-9.

[9] Magno MHR, Kim J, Srinivasan A, McBride S, Bolikal D, Darr A, et al. Synthesis, degradation and biocompatibility of tyrosine-derived polycarbonate scaffolds. Journal of Materials Chemistry 2010;20:8885-93.

[10] Jinku K, Sean M, Amy D, Aniq D, Maria Hanshella RM, Jeffrey OH. Tyrosine-derived polycarbonate scaffolds for bone regeneration in a rabbit radius critical-size defect model. Biomedical Materials 2015;10:035001.

[11] Kim J, Magno MH, Alvarez P, Darr A, Kohn J, Hollinger JO. Osteogenic differentiation of pre-osteoblasts on biomimetic tyrosine-derived polycarbonate scaffolds. Biomacromolecules 2011;12:3520-7.

[12] Kim J, Magno MHR, Ortiz O, McBride S, Darr A, Kohn J, et al. Next-generation resorbable polymer scaffolds with surface-precipitated calcium phosphate coatings. Regenerative Biomaterials 2015.

[13] Luangphakdy V, Walker E, Shinohara K, Pan H, Hefferan T, Bauer TW, et al. Evaluation of osteoconductive scaffolds in the canine femoral multi-defect model. Tissue Eng Part A 2013;19:634-48.

[14] Akbarzadeh R, Yousefi AM. Effects of processing parameters in thermally induced phase separation technique on porous architecture of scaffolds for bone tissue engineering. J Biomed Mater Res B Appl Biomater 2014;102:1304-15.

[15] Murphy WL, Dennis RG, Kileny JL, Mooney DJ. Salt fusion: an approach to improve pore interconnectivity within tissue engineering scaffolds. Tissue Eng 2002;8:43-52.

[16] Capes JS, Ando HY, Cameron RE. Fabrication of polymeric scaffolds with a controlled distribution of pores. J Mater Sci Mater Med 2005;16:1069-75.

[17] Nam YS, Yoon JJ, Park TG. A novel fabrication method of macroporous biodegradable polymer scaffolds using gas foaming salt as a porogen additive. J Biomed Mater Res 2000;53:1-7.

[18] Tran RT, Naseri E, Kolasnikov A, Bai X, Yang J. A new generation of sodium chloride porogen for tissue engineering. Biotechnol Appl Biochem 2011;58:335-44.

[19] Lin HR, Kuo CJ, Yang CY, Shaw SY, Wu YJ. Preparation of macroporous biodegradable PLGA scaffolds for cell attachment with the use of mixed salts as porogen additives. J Biomed Mater Res 2002;63:271-9.

[20] Kang H-W, Tabata Y, Ikada Y. Fabrication of porous gelatin scaffolds for tissue engineering. Biomaterials 1999;20:1339-44.

[21] Bose S, Roy M, Bandyopadhyay A. Recent advances in bone tissue engineering scaffolds. Trends in biotechnology 2012;30:546-54.

[22] Choi S-W, Zhang Y, Xia Y. Three-Dimensional Scaffolds for Tissue Engineering: The Importance of Uniformity in Pore Size and Structure. Langmuir 2010;26:19001-6.

[23] Lan Levengood SK, Polak SJ, Wheeler MB, Maki AJ, Clark SG, Jamison RD, et al. Multiscale osteointegration as a new paradigm for the design of calcium phosphate scaffolds for bone regeneration. Biomaterials 2010;31:3552-63.

[24] van de Witte P, Dijkstra PJ, van den Berg JWA, Feijen J. Phase separation processes in polymer solutions in relation to membrane formation. Journal of Membrane Science 1996;117:1-31.

[25] Tsai FJ, Torkelson JM. The roles of phase separation mechanism and coarsening in the formation of poly(methyl methacrylate) asymmetric membranes. Macromolecules 1990;23:775-84.

[26] Chen J-S, Tu S-L, Tsay R-Y. A morphological study of porous polylactide scaffolds prepared by thermally induced phase separation. Journal of the Taiwan Institute of Chemical Engineers 2010;41:229-38.

[27] Liu X, Ma PX. Phase separation, pore structure, and properties of nanofibrous gelatin scaffolds. Biomaterials 2009;30:4094-103.

[28] Huang YX, Ren J, Chen C, Ren TB, Zhou XY. Preparation and properties of poly(lactide-co-glycolide) (PLGA)/ nano-hydroxyapatite (NHA) scaffolds by thermally induced phase separation and rabbit MSCs culture on scaffolds. J Biomater Appl 2008;22:409-32.

[29] Karp JM, Rzeszutek K, Shoichet MS, Davies JE. Fabrication of precise cylindrical three-dimensional tissue engineering scaffolds for in vitro and in vivo bone engineering applications. J Craniofac Surg 2003;14:317-23.

3

Modified Alternate Soaking Process: Rapid Mineralization on 3D Porous Polymer Scaffolds with Tunable Calcium Phosphate Composition and Topography

3.1 Introduction

Despite the current development in bone tissue engineering, the reconstruction of critical size bone defects resulting from trauma, tumor resection, congenital abnormalities or reconstructive surgery remains a significant clinical problem [1, 2]. The global demand for bone graft substitutes (BGS) that can treat large critical size bone defects is expected to grow. Bone is a structure composed of inorganic hydroxyapatite crystals deposited within an organic matrix consisting of ~ 95% type I collagen [3, 4]. Inspired by the nature of bone, BGS made from synthetic or natural polymer and calcium phosphate (CaP), mimicking the composition as well as the structure of bone, have been well studied [5-9]. The composite is more advantageous over polymer or CaP alone scaffold because it combines the flexibility, processability, and biodegradability of polymer with the osteoconductivity of CaP.

Polymer-CaP composites have been fabricated in a number of ways that can be generalized into two categories: by forming bulk composite scaffolds [9-11] or by coating

the polymer surface with a calcium phosphate layer [6, 12-15], which both have drawbacks. In the bulk composite method, CaP particles are blended with polymer matrix as fillers. Although it is the most often used, embedding of CaP within the polymer often resulting the formation of a thin layer of polymer skin covering the inorganic particles that may lead to the masking of its bioactivity [14-16]. Calcium phosphate coating has been used on metallic implants since 1990s for the purpose of increasing the osteointegration of the implant with the host tissue [17]. Plasma spraying [18] is the classical coating method that has led to excellent clinical outcome. However, its uses is associated with several limitations including high processing temperature that is not suitable for polymers and inability to coat geometrically complex and porous structures [14]. More recently, biomimetic coating and alternate soaking process, for porous polymer scaffolds have been developed. Biomimetic deposition, initially developed by Kokubo and co-workers in the early 1990s, forms a layer of calcium phosphate by soaking biomaterials in Simulated Body Fluid (SBF) solution [19-22]. Alternate soaking process (ASP), initially developed by Taguchi and co-workers in 1998 [23-26], produces a calcium phosphate coating on biomaterials by alternately soaking the materials in Ca^{2+} and $PO4^{3-}$ containing solutions [27-30]. Both techniques have been utilized as powerful methods to increase the osteoconductivity or osteoinductivity of a variety of polymers and scaffold architectures (produced from thermally induced phase separation [31] and [32], solvent casting particulate leaching [33], rapid prototyping and, electrospinning [12] and microspheres [34] etc. Most studies focused on hydroxyapatite (HA)-based coating, other calcium phosphates have rarely reported. Therefore, there is a lack of understanding regarding the osteo-promotive effect of calcium phosphate coating composition.

Moreover, the current coating methods may take a long time (days or weeks) for a stable apatite deposition on scaffold, thus lead to the biodegradation of the polymer prior to its use [15, 35]. Furthermore, CaP minerals are likely to aggregate on the outer region of geometrically complex 3D porous scaffold, resulting in the formation of a non-uniform layer of calcium phosphate materials with increased thickness at the scaffold surface and interfere in the porous structure and lead to the hindrance of cell in-growth.

Therefore, the objective here was to develop a modified alternate soaking process that (1) is fast and able to achieve a calcium phosphate coating within a few hours, (2) can produce a uniform CaP coating, even for large dimensional scaffolds intended for clinical applications, and (3) able to tune the calcium phosphate composition and topography. To this end, the conventional alternate soaking process was modified in three specific ways: (1) the amount and the rate of calcium phosphate coating were controlled by reagent concentration and initial calcium to phosphorous ratio; (2) cycles of vacuum followed by a rapid release to atmospheric pressure were applied to facilitate the diffusion of ions and thus uniform coating; (3) the composition and topography of calcium phosphate was tuned by monitoring the pH of the reagents. Herein, we prepared a high quality uniform CaP coating within an hour on 3D porous polymeric scaffolds using a modified alternate soaking process.

3.2 Materials and methods

3.2.1 Materials

Sodium chloride (NaCl), calcium chloride ($CaCl_2$), potassium phosphate dibasic trihydrate ($K_2HPO_4 \cdot 3H_2O$) were obtained from Sigma-Aldrich Chemical Co. (St. Louis,

MO). The NaCl particles in the range of 212- 425 µm were selected and used as a porogen in scaffold fabrication. 1,4-Dioxane was obtained from Fischer Scientific (Pittsburgh, PA).

3.2.2 Scaffold fabrication

3D porous scaffolds were fabricated from E1001(1k) using a combination of salt leaching and freeze-drying methods. Briefly, the polymer was first dissolved in deionized (DI) water and 1,4-dioxane overnight. The polymer solution was mixed uniformly with salt particles. The mixture was then casted into a Teflon mold, quenched in liquid nitrogen and freeze-dried for 2 days. Disk-shaped scaffolds were punched out using custom-designed cutting tools. Salt particles were leached out in distill water, and the nonporous skin was sliced off. Finally, the scaffolds were dried in a lyophilizer for 1 day.

3.2.3 Modified alternate soaking process

This method utilized the precipitation of calcium phosphate from the reaction between calcium chloride and potassium phosphate dibasic trihydrate. To produce a uniform calcium phosphate coating throughout the thickness of scaffold, cycles of vacuum up to 30 inHg followed by a rapid release to atmospheric pressure were used to force the calcium and phosphate solutions into the interior of scaffold construct. The coating scheme is shown in Fig. 3.1A. Each scaffold was placed in $CaCl_2$ solution. Vacuum up to 30 inHg was applied to the chamber for 1 min, followed by a rapid release to atmospheric pressure. This step was repeated 5 times to completely wet scaffolds with $CaCl_2$ solution. Then, the scaffolds were taken out and excess solution on scaffold

surface was removed by kimwipe. Each scaffold was then transferred to THE K_2HPO_4•$3H_2O$ solution. The same vacuum and atmospheric pressure cycles were used to facilitate the diffusion of phosphate solution into the interior of 3D scaffolds, which reacted with $CaCl_2$ to form a uniform calcium phosphate coating. Then the scaffolds were washed with DI water for 3 times and transferred back to $CaCl_2$ solution. The scaffolds were alternated in calcium and phosphate solutions for desired number of cycles. After completing the cycles, the scaffolds were soaked in DI water for 2 hours to wash off the byproducts. Finally, the mineralized scaffolds were dried in a lyophilizer for 1 day. To design an efficient and reproducible process, a custom-designed coating apparatus (Fig. 3.1B) was built. This apparatus consists of 16 independent cylindrical chambers that are 25 mm in diameter and 8 cm in height, where 16 scaffolds can be mineralized each time without interference from each other.

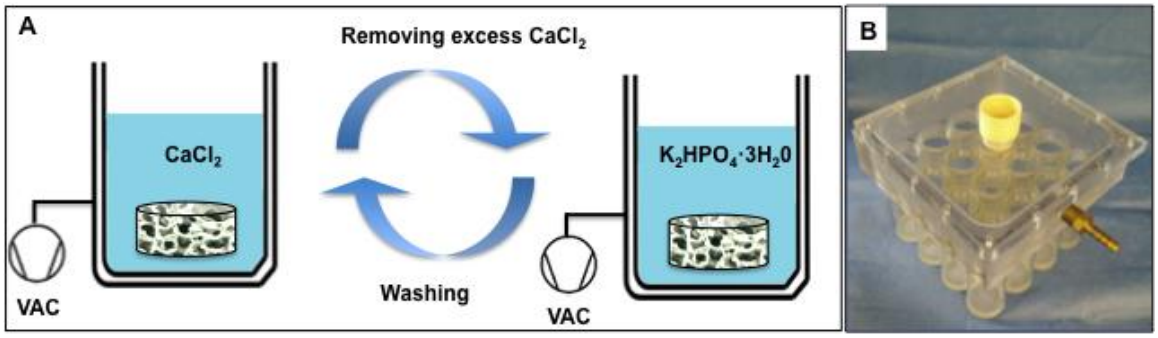

Figure 3.1 (A) scheme of modified alternate soaking process. (B) Custom-designed apparatus for efficient and reproducible calcium phosphate coating.

3.2.4 Calcium phosphate coating using various reagents pH

CaP coatings on E1001(1k) scaffolds were produced using calcium solution and phosphate solution at various pH according to Table 3.1. The concentrations of $CaCl_2$ and $K_2HPO_4 \cdot 3H_2O$ were 1M and 2M respectively in each condition. Three alternate calcium and phosphate cycles were used for all conditions, as well as for experiments in Section 3.2.5, and 3.2.6.

3.2.5 DCPD coating using various reagent concentrations, Ca/P ratio and pH of calcium solution.

From Section 3.2.4, hydroxyapatite (HA) or dicalcium phosphate dihydrate (DCPD) or biphasic of HA and DCPD coatings were produced. The objective in this section was to optimize DCPD coating by studying the effect of reagent concentration, Ca/P ratio and pH of calcium solution. Calcium phosphate coatings were produced according to conditions in Table 3.2.

3.2.6 HA coating using different Ca/P ratio

The objective in this section was to optimize HA coating by investigating the effect of Ca/P ratio on HA formation. Ca/P was varied from 0.125 to 1.67 according to Table 3.3.

Table 3.1 Calcium phosphate coating using various reagents pH

Conditions	$CaCl_2$ pH	$K_2HPO_4 \cdot 3H_2O$ pH
a	10	2
b	10	4
c	10	6
d	10	8
e	10	10
f	2	10
g	6	10
h	8	10

Table 3.2 DCPD coating using various reagent concentrations, Ca/P ratio and pH of calcium solution.

Conditions	Ca/P	$CaCl_2$, concentration	$CaCl_2$ pH	$K_2HPO_4 \cdot 3H_2O$, concentration	$K_2HPO_4 \cdot 3H_2O$ pH
a	1	1M	10.13	1M	6.02
b	1	0.5 M	10.01	0.5M	6.1
c	0.5	1M	10.12	2 M	6.08
d	1	1M	2.62	1M	6.28
e	1	1M	4.37	1M	6.21
f	1	1M	5.82	1M	6.19
g	1	1M	7.16	1M	6.2
h	1	1M	10.13	1M	6.02

Table 3.3 HA coating using different Ca/P ratio

Conditions	Ca/P	$CaCl_2$, concentration	$CaCl_2$ pH	$K_2HPO_4 \cdot 3H_2O$, concentration	$K_2HPO_4 \cdot 3H_2O$ pH
a	1.67	0.5 M	5.6	0.3 M	10.46
b	1	0.5 M	5.51	0.5M	10.59
c	0.5	0.5 M	6.06	1M	10.59
d	0.25	0.5 M	6.32	2M	10.56
e	0.125	0.5 M	6.08	4M	10.88

3.2.7 Scaffold characterization

Scaffolds fabricated in Sections 3.2.4-3.2.6 were characterized using the following technique.

Samples of the freeze-dried scaffolds were cut using a razor blade and sputter coated with gold/palladium (30 mA, 2 min, SCD 004 sputter coater). The scaffold morphology and microstructure were observed using a scanning electron microscope (SEM, AMRAY-1830I) at an acceleration potential of 20 kV. To investigate the uniformity in scaffold structure, samples from different region of scaffolds were assessed.

X-ray diffraction (XRD) patterns of scaffolds were obtained using a Philips X'Pert X-ray diffractometer operating at 40 kV and 40 mA (Cu-K α radiation: λ=1.5406). The scaffolds were scanned from 5° to 90° at step size of 0.02° and scan step time of 1 sec. The X-ray diffractogram was analyzed using PANalytical HighScore Plus software and compared with the standard library of known diffraction patterns, International Centre for

Diffraction Data (ICDD) to identify the phase of the calcium phosphate present in the scaffolds.

The amount of calcium phosphate coating onto scaffold surface was quantified by measuring the mass of scaffold prior to and post coating process.

3.3 Results

3.3.1 Tunable calcium phosphate composition and tomography by controlling the reagent's pH

The phase and the amount of calcium phosphate coating greatly depended on the pH of phosphate solution (Fig. 3.2). Fig. 3.2a shows the XRD diffraction pattern for the polymer scaffold without mineralization. After coating the scaffold using low pH of 2 or 4, minimal amount (≈ 0.5mg) of calcium phosphate was measured and only a small peak at two-theta of 11.65° was observed in the XRD diffraction (Fig.3.2b and c). Using medium phosphate solution pH of 6, about 30 mg calcium phosphate was deposited onto a scaffold. XRD analysis shows peaks at 11.65°, 20.949° and 29.296° (Fig.3.2d), which was determined as DCPD (ICDD # 01-072-0713). Using basic phosphate solution pH of 8 or 10, about 103 mg or 100 mg calcium phosphate was measured respectively. In addition to DCPD, peaks at 25.9 ° and 32.0 were also observed which were identified as HA (Fig. 3.2e and f). Although, the intensity of HA peaks appeared to be lower than that of DCPD due to the low refractive index of HA, Rietveld refinement analysis revealed that the majority was HA.

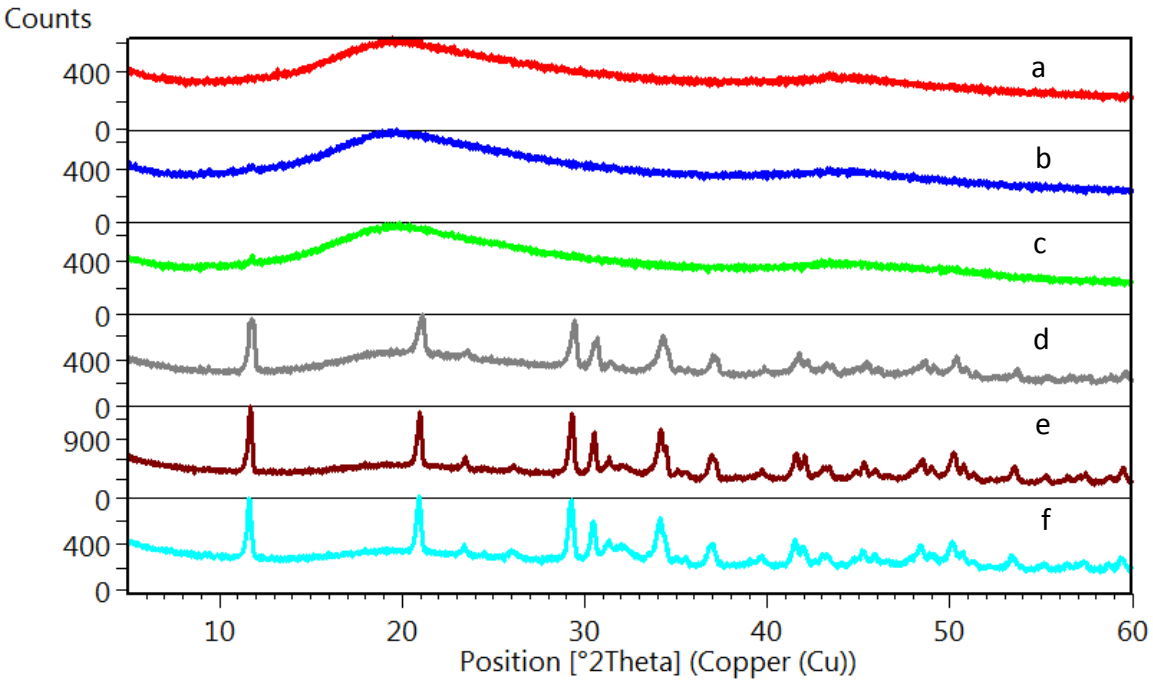

Figure 3.2 X-ray diffraction patterns of (a) polymer alone scaffold, and calcium phosphate deposited onto 3D porous scaffolds using various pH of phosphate solutions: (b) pH = 2, (c) pH = 4, (d) pH = 6, (e) pH = 8 and (f) pH = 10. The pH of $CaCl_2$ was 10. The concentrations of $CaCl_2$ and $K_2HPO_4 \cdot 3H_2O$ were 1 M and 2 M respectively. Three alternate cycles were used.

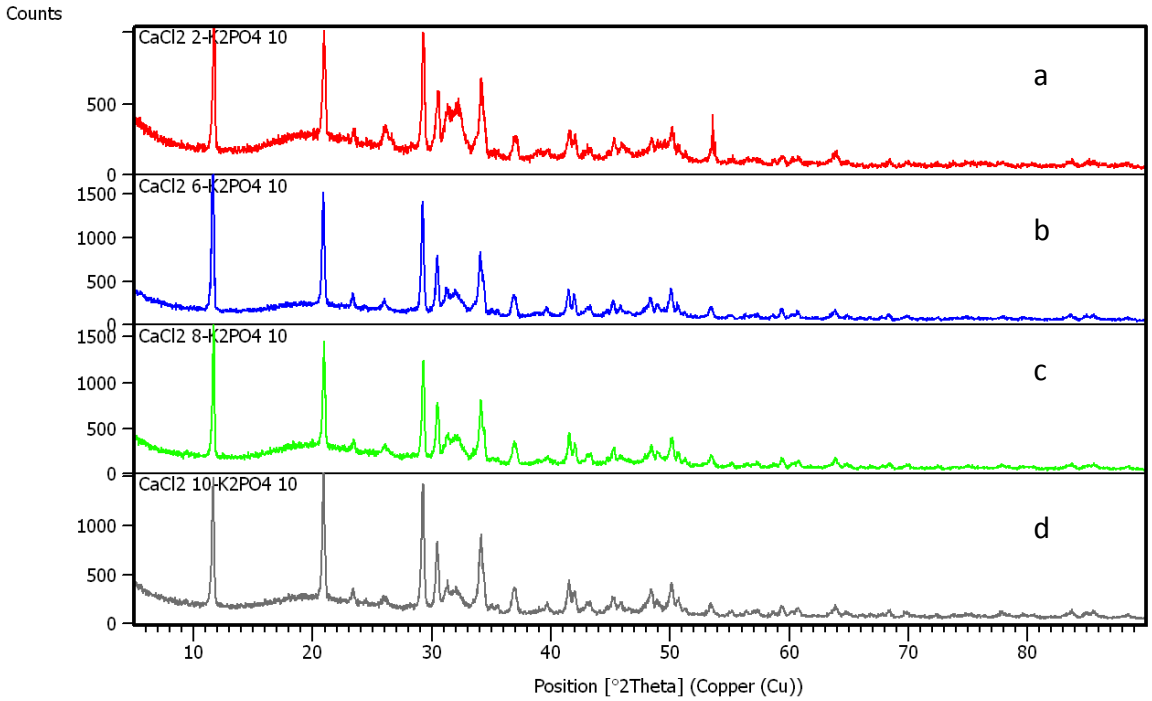

Figure 3.3 X-ray diffraction pattern of calcium phosphate deposited onto 3D porous scaffolds using various $CaCl_2$ pH: (a) pH = 2, (b) pH = 6, (c) pH = 8, and (d) pH = 10, The pH of K_2HPO_4• $3H_2O$ solution was 10. The concentrations of $CaCl_2$ and K_2HPO_4• $3H_2O$ were kept the same at 1 M and 2 M respectively. Three alternate cycles were used.

When using phosphate solution at pH 10 and varying calcium solution pH from 2 to 10, similar XRD profiles (Fig. 3.3) and SEM morphology (data not shown) were observed. All conditions yielded about 100 mg of calcium phosphates that is a mixture of HA and DCPD. Rietveld refinement analysis revealed that the majority of the mixture was HA with only a small amount of DCPD, which could be easily converted to HA after soaking in DI water or eliminated using lower reagent concentration.

3.3.2 The effect of reagent concentration, Ca/P ratio and pH of calcium solution on DCPD formation

Using the pH conditions listed in Table 3.2, DCPD was the only phase formed (Fig. 3.4), regardless of reagent concentration, Ca/P and pH of calcium solution. As the concentration of reagents increased, the amount of DCPD deposited onto scaffolds was increased as well, resulting in higher XRD intensity and more crystals filling the pores of scaffolds (Fig.3.5).

3.3.3 The effect of Ca/P ratio on HA formation

The formation of HA had a great dependence on Ca/P (Fig. 3.6). It seemed that for Ca/P ratio $\leq$ 1, HA was the major phase that was precipitated with a small amount of DCPD. For Ca/P ratio = 1.67, more DCPD was precipitated along with HA. DCPD was readily converted to HA after soaking in DI water for 2 hours.

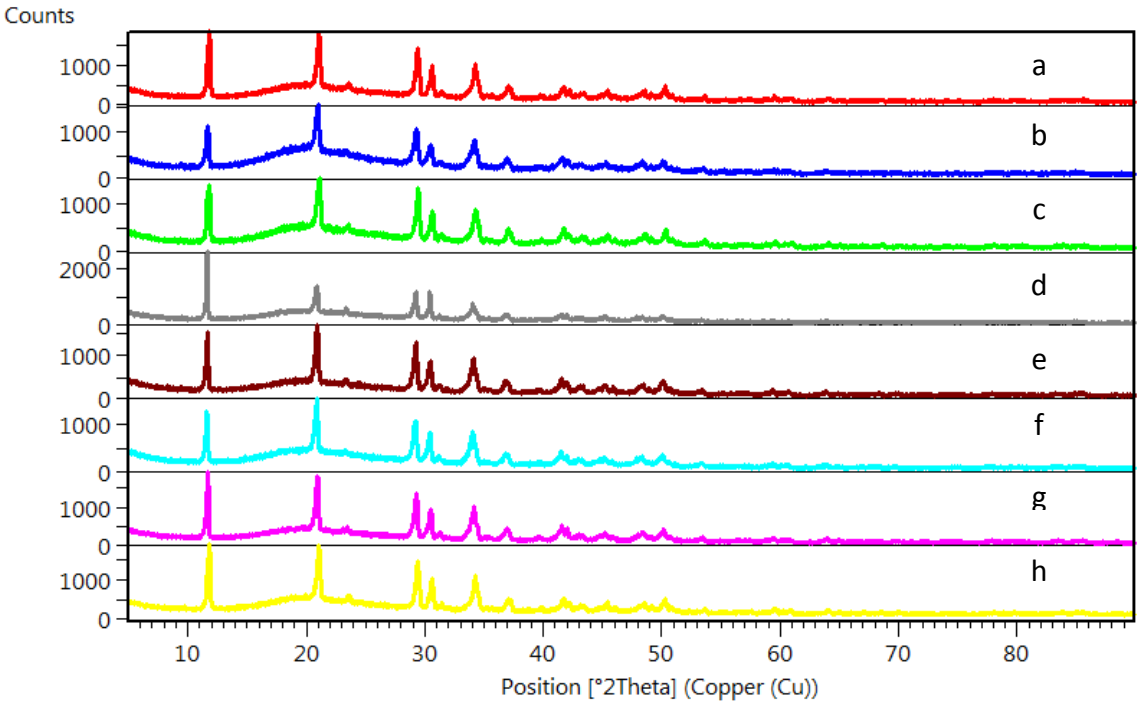

Figure 3.4 X-ray diffraction pattern of DCPD deposited onto 3D porous scaffolds using coating conditions listed in Table 3.2.

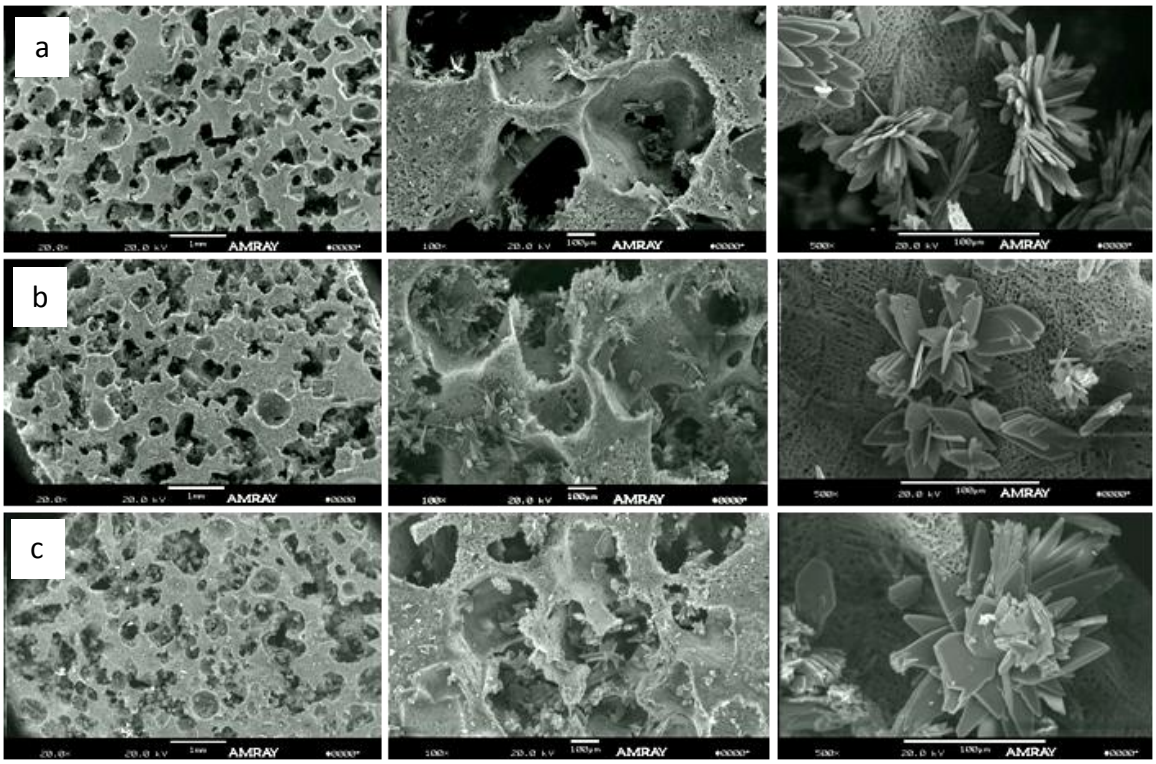

Figure 3.5 Scanning electron microscope images of polymer scaffolds after alternately soaked in $CaCl_2$ solution (pH 10) and $K_2HPO_4 \cdot 3H_2O$ (pH 6) solution at concentrations of (a) 0.5 M and 0.5 M, (b) 1 M and 1 M and (c) 1 M and 2 respectively.

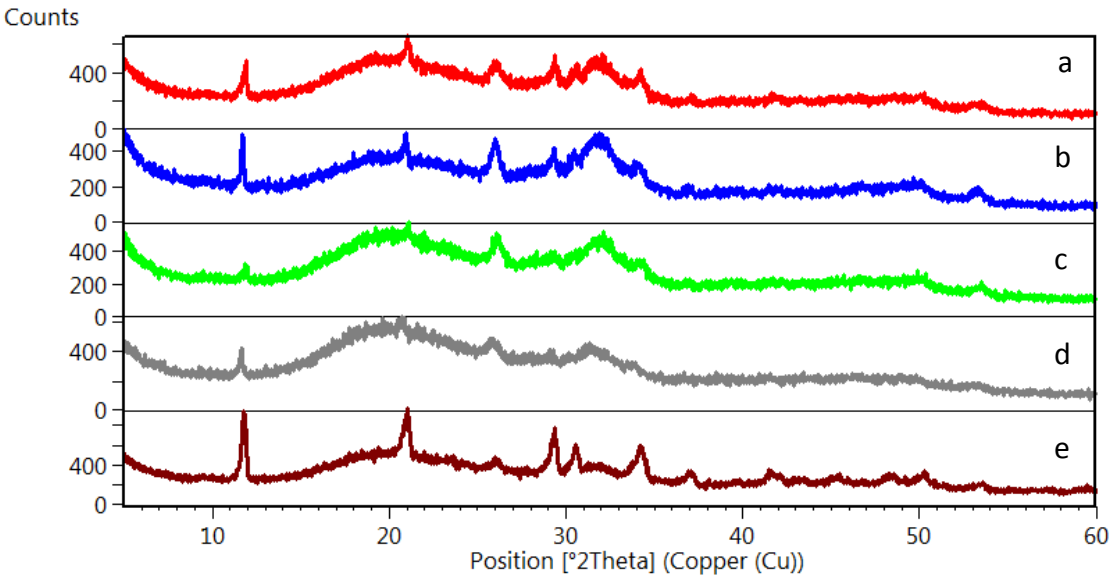

Figure 3.6 X-ray diffraction pattern of DCPD deposited onto 3D porous scaffolds using coating conditions listed in Table 3.3.

3.4 Discussion

Calcium phosphate coating on polymeric scaffold has been used as a power strategy to enhance the osteoconductivity and osteointegrativity of implants [13, 35]. In this study, a strightforward, fast and versatile modified alternate soaking method to mineralize polymer scaffolds was developed. It offers significant advantages over the conventional ASP mineralization of scaffolds.

First, a high quality mineral coating was achieved within an hour by precisely controlling the process parameters including reagents concentration and Ca/P ratio. The conventional biomimitic coating methods take serveral days to weeks to form a stable mineralization layer and leading to the biodegradation of polymer materials prior to their use in the tissue engineering application [15, 35].

Second, the modified alternate soaking process provides a control over the surface topography and chemical composition of calcium phosphate deposits to meet the requirements for cell growth and bone regeneration. Calcium phosphate coating of HA or DCPD or biphasic of HA and DCPD was produced by varying the process parameter, mainly pH of phosphate solution. Numerous studies have shown that surface topography is one of the main mechanisms that affect cell attachment, proliferation and differentiation [36, 37]. Dalby et al. have demonstrated that introducing a level of disorder in the nano-topography of the culture substrate, it is possible to drive the differentiation of human mesenchymal stem cells into osteoblasts [38]. Others have shown that an increased surface roughness favors cellular attachment and enhances bone formation [37, 39]. In **Chapter 5**, the effect of two different calcium phosphate coating formulations (HA or DCPD) on *in vitro* cellular response and *in vivo* bone formation was investigated. The pH-dependent calcium phosphate formation is attributed to the dissociation species of phosphoric acid in water at different pH (Equation 1). At acidic pH (6), $K_2HPO_4 \bullet 3H_2O$ dissociates into primary HPO_4^{2-} ions and when they react with Ca^{2+} ions, DCPD is formed. At basic pH (8 and 10), $K_2HPO_4 \bullet 3H_2O$ dissociates into primary PO_4^{3-} ions and when they react with Ca^{2+} ions, HA is the primary phase that is precipitated [40, 41]. At pH 2 and 4, precipitation was not observed due to high solubility of calcium phosphate under the acidic condition. The reaction schemes are shown in Equation 2 and 3. HA is a thermodynamically stable phase. DCPD is metastable or thermodynamically unstable but kinetically favored. It was formed along with HA at high reagent concentration. Together with other process parameters such as reagents concentration [42], number of cycles, and Ca to P ratio [43], the modified alternate

soaking process described herein offers a variety degree of freedom to tailor the properties of the calcium phosphate coating.

Equation 3.1 Dissociation of phosphoric acid

$$H_3PO_4 \rightarrow H_2PO_4^- + H^+$$

$$H_2PO_4^- \rightarrow HPO_4^{2-} + H^+$$

$$HPO_4^{2-} \rightarrow PO_4^{3-} + H^-$$

Equation 3.2 HA formation scheme

$$5CaCl_2 + 3K_2HPO_4 \cdot 3H_2O \rightarrow Ca_5(PO_4)_3OH + 6KCl + 4HCl + 8H_2O$$

Equation 3.3 DCPD formation scheme

$$CaCl_2 + K_2HPO_4 \cdot 3H_2O \rightarrow CaHPO_4 \cdot 2H_2O + 2KCl + H_2O$$

Third, the coatings deposited onto the E1001(1k) scaffolds was homogeneously distributed throughout the thickness of the samples as the cycles of vacuum and followed by a rapid release to atmospheric pressure facilitated the diffusion of calcium and phosphate solutions into the scaffold's core. Therefore, the coating did not result in the formation of non-uniform layer of calcium phosphate materials with increased thickness at the out region of scaffolds, as has been reported in the literature using traditional immersion methods, especially for scaffolds without adequate pore size and interconnectivity or large dimensional scaffolds for translational clinical application. This

is of significance, as a thick CaP coating can impede cell migration both *in vitro* and *in vivo*, thereby jeopardizing the regenerative outcome. Using this modified alternate soaking process, 20 mm (diameter) × 6 mm (height) scaffolds were uniformly coated with calcium phosphate and supported bone formation in goat calvarial critical size defects (**Chapter 6**).

3.5 Conclusion

In this study, a straightforward, fast, and versatile modified alternate soaking process was developed that offers significant advantages over the conventional ASP. Calcium phosphate coating can be achieved within an hour, significantly faster than conventional method. In addition, the surface topography and chemical composition of the deposits can be tailored by varying the process parameters. Moreover, cycles of vacuum, followed by a rapid release to atmospheric pressure facilitate uniform coating even for large dimensional scaffolds.

Reference

[1] De Long WG, Jr., Einhorn TA, Koval K, McKee M, Smith W, Sanders R, et al. Bone grafts and bone graft substitutes in orthopaedic trauma surgery. A critical analysis. J Bone Joint Surg Am 2007;89:649-58.

[2] Amini AR, Laurencin CT, Nukavarapu SP. Bone Tissue Engineering: Recent Advances and Challenges. Critical reviews in biomedical engineering 2012;40:363-408.

[3] Salgado AJ, Coutinho OP, Reis RL. Bone tissue engineering: state of the art and future trends. Macromol Biosci 2004;4:743-65.

[4] Stevens MM. Biomaterials for bone tissue engineering. Materials Today 2008;11:18-25.

[5] Ambrosio AM, Sahota JS, Khan Y, Laurencin CT. A novel amorphous calcium phosphate polymer ceramic for bone repair: I. Synthesis and characterization. J Biomed Mater Res 2001;58:295-301.

[6] Li J, Baker BA, Mou X, Ren N, Qiu J, Boughton RI, et al. Biopolymer/Calcium phosphate scaffolds for bone tissue engineering. Adv Healthc Mater 2014;3:469-84.

[7] Pilia M, Guda T, Appleford M. Development of Composite Scaffolds for Load-Bearing Segmental Bone Defects. BioMed Research International 2013;2013:15.

[8] Zhang Y, Zhang M. Synthesis and characterization of macroporous chitosan/calcium phosphate composite scaffolds for tissue engineering. J Biomed Mater Res 2001;55:304-12.

[9] Wei G, Ma PX. Structure and properties of nano-hydroxyapatite/polymer composite scaffolds for bone tissue engineering. Biomaterials 2004;25:4749-57.

[10] Haaparanta AM, Haimi S, Ella V, Hopper N, Miettinen S, Suuronen R, et al. Porous polylactide/beta-tricalcium phosphate composite scaffolds for tissue engineering applications. J Tissue Eng Regen Med 2010;4:366-73.

[11] Cao L, Duan PG, Wang HR, Li XL, Yuan FL, Fan ZY, et al. Degradation and osteogenic potential of a novel poly(lactic acid)/nano-sized beta-tricalcium phosphate scaffold. Int J Nanomedicine 2012;7:5881-8.

[12] Andiappan M, Sundaramoorthy S, Panda N, Meiyazhaban G, Winfred S, Venkataraman G, et al. Electrospun eri silk fibroin scaffold coated with hydroxyapatite for bone tissue engineering applications. Prog Biomater 2013;2:1-11.

[13] Surmenev RA, Surmeneva MA, Ivanova AA. Significance of calcium phosphate coatings for the enhancement of new bone osteogenesis – A review. Acta Biomaterialia 2014;10:557-79.

[14] Nandakumar A, Yang L, Habibovic P, van Blitterswijk C. Calcium Phosphate Coated Electrospun Fiber Matrices as Scaffolds for Bone Tissue Engineering. Langmuir 2010;26:7380-7.

[15] Seyedjafari E, Soleimani M, Ghaemi N, Shabani I. Nanohydroxyapatite-Coated Electrospun Poly(l-lactide) Nanofibers Enhance Osteogenic Differentiation of Stem Cells and Induce Ectopic Bone Formation. Biomacromolecules 2010;11:3118-25.

[16] Vaquette C, Ivanovski S, Hamlet SM, Hutmacher DW. Effect of culture conditions and calcium phosphate coating on ectopic bone formation. Biomaterials 2013;34:5538-51.

[17] Narayanan R, Seshadri SK, Kwon TY, Kim KH. Calcium phosphate-based coatings on titanium and its alloys. J Biomed Mater Res B Appl Biomater 2008;85:279-99.

[18] Yang Y, Kim K-H, Ong JL. A review on calcium phosphate coatings produced using a sputtering process—an alternative to plasma spraying. Biomaterials 2005;26:327-37.

[19] Lu X, Leng Y. Theoretical analysis of calcium phosphate precipitation in simulated body fluid. Biomaterials 2005;26:1097-108.

[20] Kokubo T, Takadama H. How useful is SBF in predicting in vivo bone bioactivity? Biomaterials 2006;27:2907-15.

[21] Liu Y, Wu G, de Groot K. Biomimetic coatings for bone tissue engineering of critical-sized defects. J R Soc Interface 2010;6:19.

[22] Yang F, Wolke JGC, Jansen JA. Biomimetic calcium phosphate coating on electrospun poly(ε-caprolactone) scaffolds for bone tissue engineering. Chemical Engineering Journal 2008;137:154-61.

[23] Taguchi T, Kishida A, Akashi M. Apatite formation on/in hydrogel matrices using an alternate soaking process (III) : Effect of physico-chemical factors on apatite formation on/in poly(vinyl alcohol) hydrogel matrices. Journal of Biomaterials Science, Polymer Edition 1999;10:795-804.

[24] Taguchi T, Kishida A, Akashi M. Hydroxyapatite Formation on/in Poly(vinyl alcohol) Hydrogel Matrices Using a Novel Alternate Soaking Process. Chemistry Letters 1998:711-2.

[25] Furuzono T, Taguchi T, Kishida A, Akashi M, Tamada Y. Preparation and characterization of apatite deposited on silk fabric using an alternate soaking process. Journal of Biomedical Materials Research 2000;50:344-52.

[26] Taguchi T, Kishida A, Akashi M. Apatite formation on/in hydrogel matrices using an alternate soaking process: II. Effect of swelling ratios of poly(vinyl alcohol) hydrogel matrices on apatite formation. Journal of Biomaterials Science, Polymer Edition 1999;10:331-9.

[27] Strange DGT, Oyen ML. Biomimetic bone-like composites fabricated through an automated alternate soaking process. Acta Biomaterialia 2011;7:3586-94.

[28] Suzuki K, Yumura T, Mizuguchi M, Taguchi T, Sato K, Tanaka J, et al. Apatite-Silica Gel Composite Materials Prepared by a New Alternate Soaking Process. Journal of Sol-Gel Science and Technology 2001;21:55-63.

[29] Li H, Zhu R, Sun L, Xue Y, Hao Z, Xie Z, et al. Effect of Thickness of HA-Coating on Microporous Silk Scaffolds Using Alternate Soaking Technology. BioMed Research International 2014;2014:8.

[30] Zhao J, Zhang Z, Wang S, Sun X, Zhang X, Chen J, et al. Apatite-coated Silk Fibroin Scaffolds to Healing Mandibular Border Defects in Canines. Bone 2009;45:517-27.

[31] Chen Y, Mak AFT, Wang M, Li J. Composite coating of bonelike apatite particles and collagen fibers on poly L-lactic acid formed through an accelerated biomimetic coprecipitation process. Journal of Biomedical Materials Research - Part B Applied Biomaterials 2006;77:315-22.

[32] Zhang R, Ma PX. Biomimetic polymer/apatite composite scaffolds for mineralized tissue engineering. Macromolecular Bioscience 2004;4:100-11.

[33] Murphy WL, Kohn DH, Mooney DJ. Growth of continuous bonelike mineral within porous poly(lactide-co- glycolide) scaffolds in vitro. Journal of Biomedical Materials Research 2000;50:50-8.

[34] Popp JR, Laflin KE, Love BJ, Goldstein AS. In vitro evaluation of osteoblastic differentiation on amorphous calcium phosphate-decorated poly(lactic-co-glycolic acid) scaffolds. Journal of Tissue Engineering and Regenerative Medicine 2011;5:780-9.

[35] He C, Xiao G, Jin X, Sun C, Ma PX. Electrodeposition on Nanofibrous Polymer Scaffolds: Rapid Mineralization, Tunable Calcium Phosphate Composition and Topography. Advanced Functional Materials 2010;20:3568-76.

[36] Anselme K, Ponche A, Bigerelle M. Relative influence of surface topography and surface chemistry on cell response to bone implant materials. Part 2: biological aspects. Proc Inst Mech Eng H 2010;224:1487-507.

[37] Deligianni DD, Katsala ND, Koutsoukos PG, Missirlis YF. Effect of surface roughness of hydroxyapatite on human bone marrow cell adhesion, proliferation, differentiation and detachment strength. Biomaterials 2000;22:87-96.

[38] Dalby MJ, Gadegaard N, Tare R, Andar A, Riehle MO, Herzyk P, et al. The control of human mesenchymal cell differentiation using nanoscale symmetry and disorder. Nature Materials 2007;6:997-1003.

[39] Deligianni DD, Katsala N, Ladas S, Sotiropoulou D, Amedee J, Missirlis YF. Effect of surface roughness of the titanium alloy Ti–6Al–4V on human bone marrow cell response and on protein adsorption. Biomaterials 2001;22:1241-51.

[40] Santos MH, Oliveira Md, Souza LPdF, Mansur HS, Vasconcelos WL. Synthesis control and characterization of hydroxyapatite prepared by wet precipitation process. Materials Research 2004;7:625-30.

[41] Song Y, Hahn H, Hoffmann E. Effects of pH and Ca/P ratio on the precipitation of phosphate. Chemical Water and Wastewater Treatment, Vol VIIIWA Publishing Alliance House, London, UK 2002:349-62.

[42] Yokoi T, Kawashita M, Kikuta K, Ohtsuki C. Biomimetic mineralization of calcium phosphate crystals in polyacrylamide hydrogel: Effect of concentrations of calcium and phosphate ions on crystalline phases and morphology. Materials Science and Engineering: C 2010;30:154-9.

[43] Raynaud S, Champion E, Bernache-Assollant D, Thomas P. Calcium phosphate apatites with variable Ca/P atomic ratio I. Synthesis, characterisation and thermal stability of powders. Biomaterials 2002;23:1065-72.

4

Comparative study on bone regeneration by octacalcium phosphate, beta-tricalcium phosphate and strontium in tyrosine-derived polycarbonate scaffolds using rabbit calvarial defect model

4.1 Abstract

Three-dimensional, porous scaffolds based on E1001(1k), a member of a large combinatorial library of tyrosine-derived polycarbonates (TyrPC), have been previously shown to promote bone regeneration *in vivo*. In this study, E1001(1k) scaffolds were used as a platform to study the effects of various calcium phosphates (CaPs) on osteoconductivity and biocompatibility in an *in vivo* model. Specifically, beta-tricalcium phosphate (β-TCP), octacalcium phosphate (OCP), and strontium (Sr) were added to E1001(1k) scaffolds and evaluated for their osteogenic capacity in an 8 mm rabbit calvarial non-critical size defect model (four defects per cranium). The harvested explants were analyzed by micro-computed tomography (microCT) and histology 4 weeks postoperatively. The microCT data revealed that all E1001(1k)-based scaffolds supported mineralization and bone formation. Defects treated with E1001(1k)/β-TCP scaffolds had higher new bone volume as compared to those treated with E1001(1k)/OCP (with and without Sr) scaffolds, E1001(1k) alone (no CaP) scaffolds, and empty controls. These results are likely due to differences in calcium phosphate content and type, as well as

scaffold 3D architecture. Histological images revealed significant new bone formation at the defect margins and excellent osseointegration between the new bone and implants. The scaffolds exhibited well-maintained structures, and promoted collagen deposition and blood vessel formation throughout the defect space. In conclusion, E1001(1k)-based scaffolds demonstrated excellent *in vivo* biocompatibility and osteoconductivity, and are promising substrates for bone regeneration.

4.2 Introduction

Large bone defects resulting from trauma, tumor resection, congenital abnormalities or reconstructive surgery are challenging clinical problems that are usually treated with autografts and allografts [1]. However, autograft donor site morbidity, supply shortage, and the limited bioactivity of allografts have stimulated the development of synthetic bone graft substitutes as potential alternatives for bone repair and augmentation [2].

Scientific literature has shown that there is a critical need for a synthetic bone graft substitute with physicochemical, mechanical, and degradation properties matching that of native bone [2, 3]. The family of aliphatic polyesters, such as poly(lactic acid) (PLA), poly(glycolic acid) (PGA) and their copolymers (poly(lactic-co-glycolic acid), PLGA), are currently the most widely used synthetic polymers for bone implants, but these suffer from acidic degradation products, which may adversely affect wound healing and the osteogenic outcome [4-6]. A solution to this critical need may be three-dimensional (3D) porous composite scaffolds based on E1001(1k), a member of a large combinatorial library of tyrosine-derived polycarbonates (TyrPC) [5-8]. One of the key advantages of this particular family of polymers is that they do not produce acidic by-products during

degradation [9]. Bone regeneration scaffolds prepared from E1001(1k) are nontoxic, possess suitable mechanical and degradation properties, and demonstrate excellent *in vivo* biocompatibility [8, 10]. However, bone regeneration was marginal when scaffolds made of E1001(1k) alone were tested. Thus, the addition of bioactive materials, such as calcium phosphates, are required to improve the biological performance of E1001(1k)-based scaffolds.

Calcium phosphates, such as hydroxyapatite (HA) and beta-tricalcium phosphate (β-TCP), are intrinsically bioactive and osteoconductive due to their chemical similarity to bone [11, 12]. Numerous studies have reported that β-TCP supports the *in vitro* attachment, proliferation and differentiation of osteoblastic progenitor cells and exhibits excellent *in vivo* biocompatibility and osteoconductivity [13-15]. An added advantage is that β-TCP resorbs faster than sintered HA, thereby fostering better bone regeneration in various *in vivo* models [16, 17]. Recently, octacalcium phosphate (OCP) has attracted great interest as a bone substitute material because of its potential to promote a higher volume of newly formed bone as compared to other calcium phosphates, such as HA, by acting as loci for bone induction [18-20]. In addition, OCP is of biological interest because it has been suggested as a precursor of biological apatite in bone and tooth [21, 22]. Moreover**,** reports have suggested that trace elements such as strontium (Sr), zinc, magnesium and fluoride in calcium phosphates may further enhance osteogenesis and bone healing [23]. Therefore, we hypothesized that the addition of calcium phosphate (β-TCP, OCP, or strontium-substituted OCP (SrOCP) would enhance the osteoconductive and osteoinductive properties of E1001(1k)-based scaffolds.

The primary objective of this study was to compare the *in vivo* performance of 3D porous E1001(1k) scaffolds containing different calcium phosphates (30 wt% β-TCP, OCP, or SrOCP) in the 8 mm rabbit calvarial non-critical size defect model. A secondary objective was to study the dose response of β-TCP (10, 30, or 50 wt%) in this model. All scaffolds were fabricated by a combination of porogen leaching and freeze-drying, characterized, and bone regeneration was determined using micro-computed tomography (microCT) and histological analyses.

4.3 Materials and methods

4.3.1 Materials

Calcium acetate, Sr acetate, sodium phosphate and sodium chloride (NaCl) were purchased from Sigma-Aldrich Chemical Co. (St. Louis, MO). The NaCl particles were sieved to obtain sizes between 212-425 μm and used as a porogen during scaffold fabrication. β-TCP (100 nm powders) was purchased from Berkeley Advanced Biomaterials, Inc. (Berkeley, CA). 1,4-Dioxane was obtained from Fischer Scientific (Pittsburgh, PA). E1001(1k) (MW=300 kDa), an abbreviation for poly(DTE-co-10 mol% DT-co-1 mol% PEG_{1k} carbonate), was synthesized at the New Jersey Center for Biomaterials, Rutgers University (Piscataway, NJ) according to published procedures [5] and used as the scaffold material. DTE stands for deaminotyrosyl tyrosine ethyl ester, DT for desaminotyrosyl tyrosine, and PEG_{1k} for poly(ethylene glycol) with a molecular weight of 1k. The detailed polymer structure and nomenclature can be found in previous publications [5, 24].

4.3.2 Octacalcium phosphate (OCP) and strontium-substituted OCP (SrOCP) synthesis

OCP powders were synthesized using a wet precipitation method according to the procedure published by LeGeros [25]. Briefly, 250 ml calcium acetate solution (0.08 M) was prepared and added dropwise into 750 ml sodium phosphate solution (0.09 M) over a period of 2-3 hours, with constant heating at 60 °C and stirring. After completing the addition, the precipitates were filtered and washed several times with deionized water. Finally, the precipitates were dried for 24 hours in a lyophilizer (Labconco 2.5L benchtop freeze-dry system, Kansas City, MO). For Sr-substituted OCP (SrOCP), a solution of calcium acetate (6.5 g) and Sr acetate (0.5 g) in 250 ml deionized water was used.

4.3.3 Composite scaffold fabrication

Composite scaffolds were prepared by a minor modification to our previously published procedure [5]. Briefly, E1001(1k) polymer was dissolved in deionized water and 1,4-dioxane overnight. The solution was uniformly mixed with salt particles and calcium phosphate. The weight ratios of polymer to salt was kept constant at 1:9. Composite scaffolds containing 10, 30 and 50 wt% β-TCP, 30 wt% OCP and 30 wt% SrOCP were fabricated. The mixture was then poured into a Teflon mold (50 mm in diameter × 15 mm in height), quenched in liquid nitrogen, and subsequently lyophilized for 48 hours. After lyophilization, disk-shaped scaffolds (8 mm in diameter × 3 mm in height) were punched out from the mold using a custom-designed puncher. The salt particles were completely removed by washing the disks in distilled water for 24 hours.

The non-porous skin layer was removed using a razor blade. Finally, the scaffolds were dried in a lyophilizer for 24 hours.

4.3.4 Scaffold characterization

Cross-sectional surfaces were carefully cut from the scaffolds and sputter coated with gold/palladium (30 mA, 2 min., SCD 004 sputter coater). Scaffold pore structure and morphology was assessed by scanning electron microscopy (SEM, AMRAY-1830I) at 20 kV.

The phase of the calcium phosphates was determined using an X-ray diffractometer (Philips X'Pert, Cu-K α radiation: λ=1.5406) operating at 40 kV and 40 mA. The samples were scanned from 3° to 90 ° at a step size of 0.02° and scan step time of 1 sec. The obtained X-ray diffraction patterns were analyzed using PANalytical HighScore Plus software and compared with the standard library of known diffraction patterns (International Centre for Diffraction Data, ICDD).

To determine the amount of calcium phosphate in the scaffold matrix, thermal gravimetric analysis (TGA) was performed at a heating rate of 10°C/ min from 25 to 800°C under flowing nitrogen.

The substitution of Sr into OCP was confirmed via elemental analysis using inductively coupled plasma optical emission spectrometry (ICP-OES, Intertek). The Sr to Ca ratio was determined.

4.3.5 Scaffold sterilization

Scaffolds were sterilized using a tabletop ethylene oxide (EtO) sterilizer (AN74i, Anderson Products). Sterility was verified using a Steritest (AN-80, Anderson Products).

4.3.6 Rabbit calvarial surgery and necropsy

All surgical procedures involving animals were approved by the Institutional Animal Care and Use Committee (IACUC) at Rutgers University and the Department of Defense United States Army Medical Research and Material Command Animal Care and Use Review Office (ACURO). Proper handling, housing, care, and standard food were given to the animals according to the guidelines established by the Rutgers University IACUC, the Animal Welfare Act, and the National Institutes of Health.

Seventeen adult male New Zealand white rabbits weighing 3.2-4.2 kg were used in this study. The animals were anesthetized by a subcutaneous injection of ketamine, xylazine and glycopyrrolate. Anesthetic maintenance was performed through inhalation of isoflurane gas. A 3-4 cm incision was made through the skin and the parietal and frontal bone exposed. Two circular defects 8 mm in diameter were created on each side of the sagittal suture, totaling four defects per calvarium per animal (Fig.4.1). The defects were created using a surgical drill equipped with a trephining bit. The surgical site was continuously irrigated with physiological saline during the drilling process to prevent heat buildup. Scaffolds were then randomly inserted into the craniotomy sites in each rabbit. The groups were : (1) empty control, (2) E1001(1k) scaffold, (3) E1001(1k)/10% β-TCP, (4) E1001(1k)/30% β-TCP, (5) E1001(1k)/50% β-TCP, (6) E1001(1k)/30% OCP, and (7) E1001(1k)/30% SrOCP scaffolds (N= 4-10). The soft tissue was closed with

absorbable sutures and the skin with surgical staples. After 4 weeks post-operation, all rabbits were euthanized. The samples were explanted with the surrounding bone and grossly examined for signs of infection, inflammation and bone resorption. The bone blocks were immediately fixed in 10% neutral buffered formalin and prepared for microCT and histological analyses.

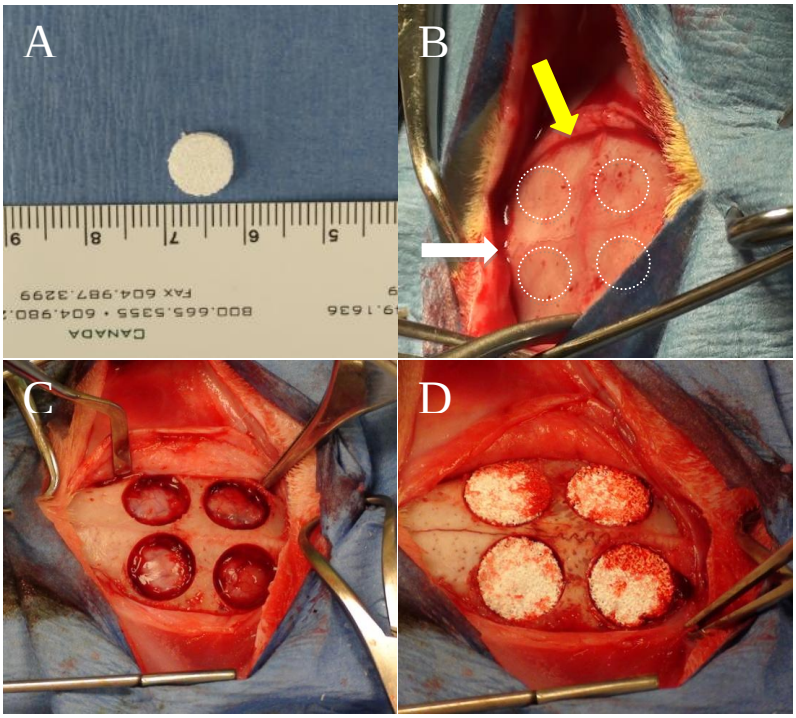

Figure 4.1 (A) Photograph of an E1001(1k)-based scaffold with dimensions of 8 mm diameter × 3 mm thick (ruler is in mm). Photographs of an exposed rabbit calvarium (B) prior to the creation of the bone defects (white circles indicate the location of the four circular defects (8 mm diameter) to be created on each side of the sagittal suture (yellow arrow) and coronal suture (white arrow), (C) after the creation of the four defects, and (D) after implantation of the scaffolds into the defects

4.3.7 Micro-computed tomography (microCT)

X-ray projections of the explants were collected using a GE eXplore Locus microCT (GE Healthcare, 80kVp, 500mA, 30 min/sample, and 20 μm voxel resolution) [8]. The projection images were then reconstructed into 3D volumes using a modified tent-FDK cone beam algorithm. After 3D reconstruction, each volume was scaled according to predefined Hounsfield Unit thresholds (calcium phosphate, cortical bone, trabecular/woven bone, and scaffold content, >3000, 2000-3000, 750-2000, and 300-750, respectively). Trabecular bone volume in each defect site was calculated. Trabecular bone volume (BV) was divided by the region of interest (ROI) volume (total volume, TV) and multiplied by 100 to calculate the percentage of BV per defect (BV/TV%).

4.3.8 Histological analysis

The specimens were dehydrated in ascending concentrations of ethanol, cleared in xylene at 4 °C, then embedded in polymethylmethacrylate (PMMA). The PMMA blocks were then cut and grounded to 5 μm thick sections with an Exakt diamond band saw and MicroGrinder (Exakt Technologies, Oklahoma City, OK). Coronal plane sections cut from the center of the defect were stained with Gomori Trichrome, which stains bone blue, collagen light blue, and cells and osteoid red.

4.3.9 Statistical analysis

Statistical analysis was performed on GraphPad Prism 6 software package using single factor analysis of variance (ANOVA) followed by the multiple comparison post-hoc test

with a significance level established as $p \leq 0.05$. All data were reported as the mean ± standard deviation (SD).

4.4 Results

4.4.1 Scaffold fabrication and characterization

The microstructure of E1001(1k) scaffolds (Fig. 4.2) was analyzed by SEM. All scaffolds had a highly porous and interconnected structure with macropores ranging from 200 to 400 μm. E1001(1k) scaffolds containing 50 wt% β-TCP, 30 wt% OCP, or 30 wt% SrOCP showed a slightly less open macroporous architecture than E1001(1k) scaffolds and scaffolds containing 10 or 30 wt% β-TCP, likely due to an increase in the viscosity of the polymer-salt-calcium phosphate mixture. Images at high magnification show the surface topography of the scaffold walls surrounding the macropores. The pore walls of E1001(1k) scaffolds were highly porous with micropores less than 20 μm aligned along the direction of the freezing front. For E1001(1k) scaffolds containing calcium phosphate, the particles were uniformly dispersed within the polymer matrix. An increase in the β-TCP content from 10 to 30 wt% resulted in scaffolds with smaller and more randomly distributed micropores. E1001(1k) scaffolds containing 50 wt% β-TCP exhibited a rougher wall topography due to the presence of β-TCP granules compared to scaffolds containing 10 or 30 wt% β-TCP. The micropores were significantly smaller and not as prevalent, and in some cases completely obliterated, in scaffolds containing 50 wt% β-TCP, 30 wt% OCP, or 30 wt% SrOCP. These results suggest that the 3D porous structure of E1001(1k) scaffolds depends on the calcium phosphate phase and content, and probably the viscosity of the polymer-salt-calcium phosphate mixture.

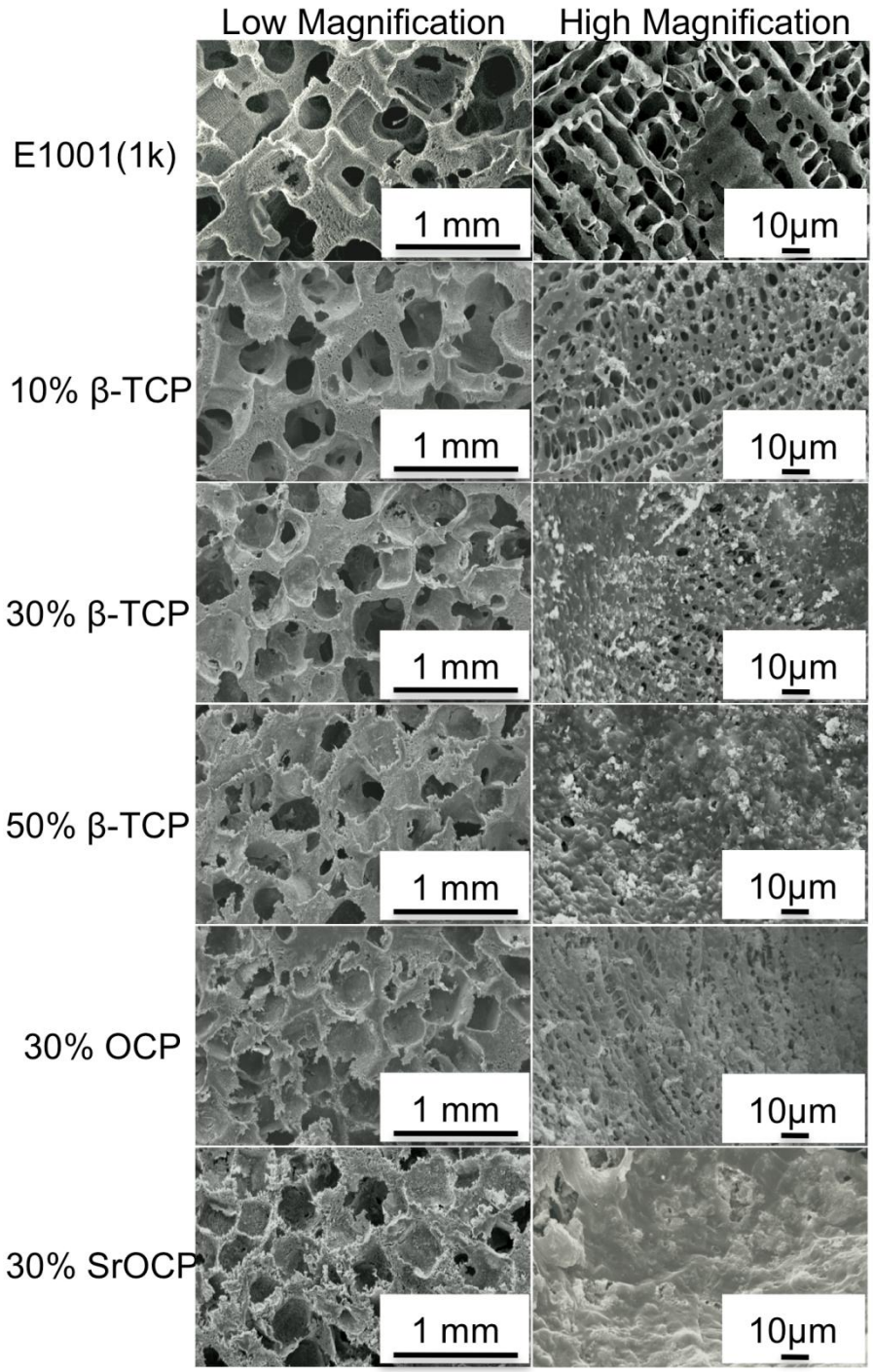

Figure 4.2 Representative SEM images of E1001(1k) scaffolds containing varying concentrations (0, 10, 30, or 50 wt%) of different calcium phosphates (β-TCP, OCP, or SrOCP) at low (left panel, scale bar = 1 mm) and high (right panel, scale bar = 10 μm) magnification.

X-ray diffraction patterns of the calcium phosphate powders and scaffolds containing calcium phosphates were obtained (Fig.4.3) and analyzed to determine the effects of the scaffold fabrication process on the phase of the calcium phosphate. The purchased β-TCP powders without modification showed characteristic peaks at 27.8°, 31° and 34.4° (Fig. 4.3A). The peak intensities of scaffolds containing 10 wt% β-TCP were significantly lower than scaffolds containing 30 or 50 wt%. This is likely due to the difference in the presence of the calcium phosphate at the surface, where scaffolds containing 10 wt% β-TCP had significantly fewer granules present at the surface (Fig. 4.2). These data suggest that the surface chemistry and topography of E1001(1k)/β-TCP scaffolds greatly depend on the ratio of the polymer to β-TCP used in the manufacturing process. The powders synthesized using the wet precipitation method exhibited characteristic peaks at 4.7° (Fig. 4.3B), and were identified as OCP (ICDD # 44-0778). In addition, elemental analysis determined that the ratio of calcium to Sr was 8.4:1, confirming that Sr was successfully substituted into OCP. No change in the XRD diffractogram was observed, indicating that the amount of Sr substituted was not high enough to affect the crystal lattices of OCP.

During the salt leaching step of the manufacturing process, it was observed that loosely-bound calcium phosphate particles were washed away. TGA was used to determine the actual amount of calcium phosphate that was incorporated into the scaffold. Quantitative analysis of the thermograms (Fig.4.4) confirmed that the actual percent weight of calcium phosphate incorporated into the scaffold was close to the theoretical concentrations (Table insert in Fig.4.4).

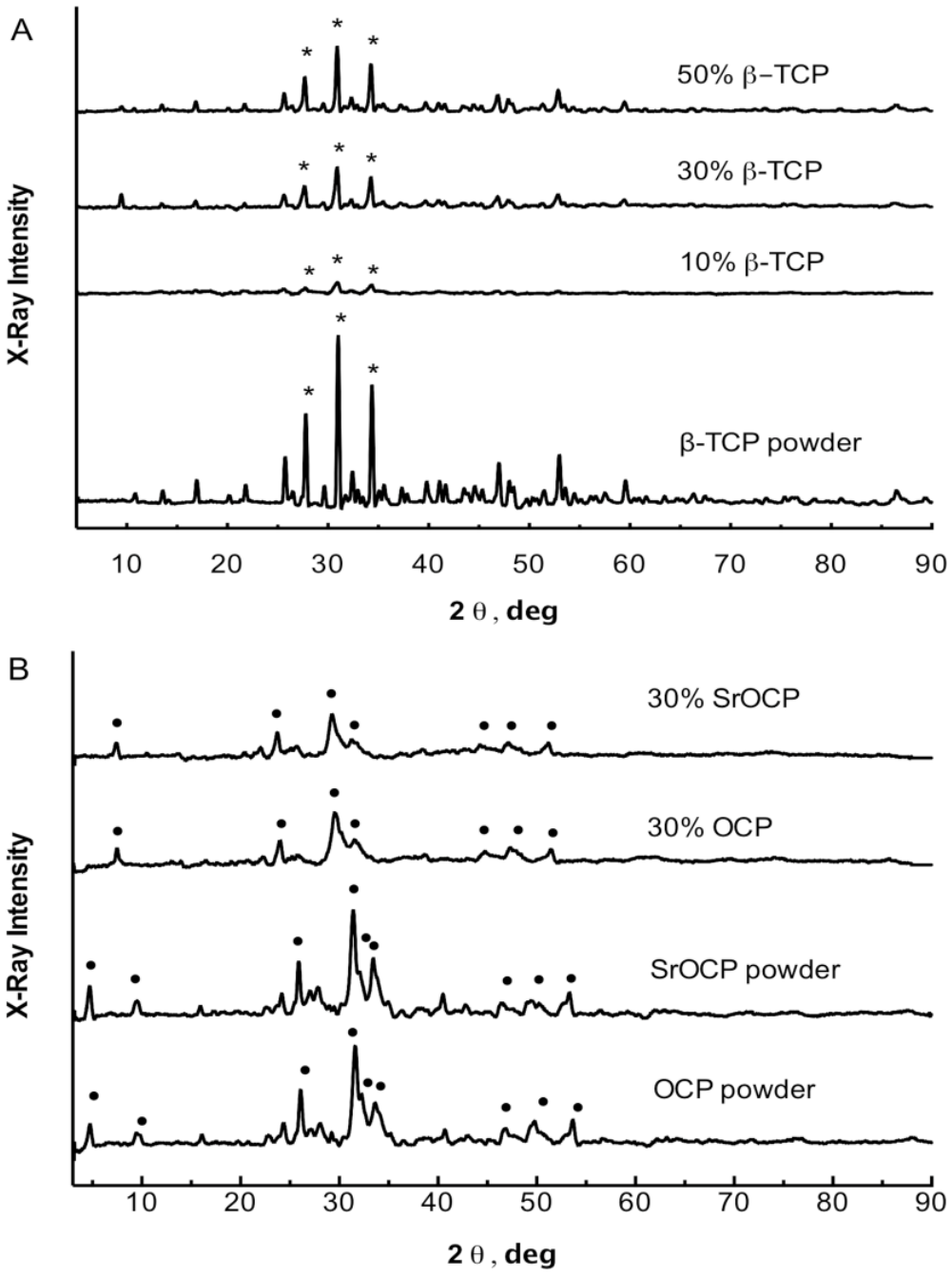

Figure 4.3 X-ray diffractograms of (A) β-TCP powder and E1001(1k) scaffolds containing 10, 30, or 50 wt% β-TCP, and (B) OCP and Sr-substituted OCP (SrOCP) powders and E1001(1k) scaffolds containing 30 wt% OCP or SrOCP.

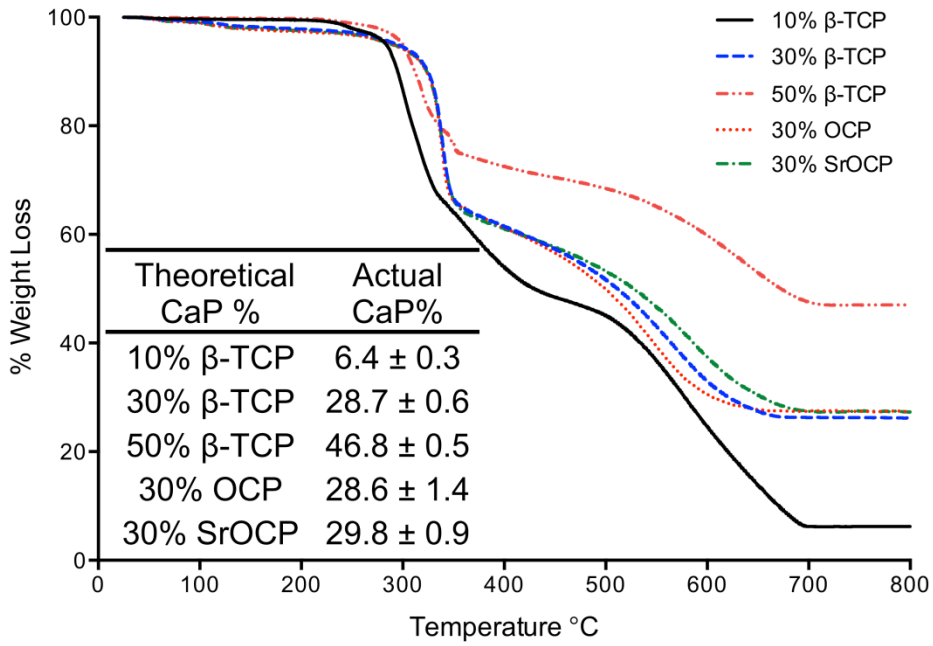

Figure 4.4 TGA thermograms of E1001(1k) scaffolds containing 10, 30 or 50 wt% β-TCP, 30 wt% OCP, or 30 wt% SrOCP. Percent weight loss is plotted as a function of temperature, which is used to determine the amount of calcium phosphate (CaP) incorporated into each scaffold. The table insert reports the theoretical and actual content (weight %) of calcium phosphate in each type of scaffold.

4.4.2 Ex vivo microCT evaluation

Fig. 4.5A depicts typical microCT images for implant sites in the rabbit calvarial defects at 4 weeks. A light gray area was observed in all defects at the interface between the scaffold and native bone indicating mineralization and bone formation in all groups. The empty defects showed spontaneous bone formation at 4 weeks due to the non-critical size of the defects. In the defects treated with scaffolds containing β-TCP, remaining calcium phosphate particles (bright white spots in 2D transverse and coronal images)

were present at 4 weeks. The amount of regenerated bone in each defect was quantified and plotted in Fig.4.5B as BV/TV %. Defects treated with E1001(1k) scaffolds had a similar amount of bone formation as compared to empty defects. Defects treated with scaffolds containing β-TCP had a higher average BV/TV % as compared to all other groups. In particular, scaffolds containing 10% or 30% β-TCP promoted significantly more new bone formation than scaffolds containing 30 wt% OCP or 30 wt% SrOCP. The average bone mineral density (Fig. 4.5C) was also higher in defects treated with β-TCP-containing scaffolds, but the differences were not statistically significant from the other groups.

To better delineate new bone formation near the scaffold-native bone interface and at the center of the implant site, the total defect was separated into a donut-shaped outer region (2 mm wide on each side) and a circular inner region (4 mm diameter) (Fig.4. 6A). Figure 4.6B shows that the woven bone volume in the outer region was almost equal to the total bone volume. In addition, a minimal amount of new bone (less than 2 mm^3) was present in the inner region of the defect, irrespective of treatment. These data suggest that new bone formation predominantly originated from the defect margins.

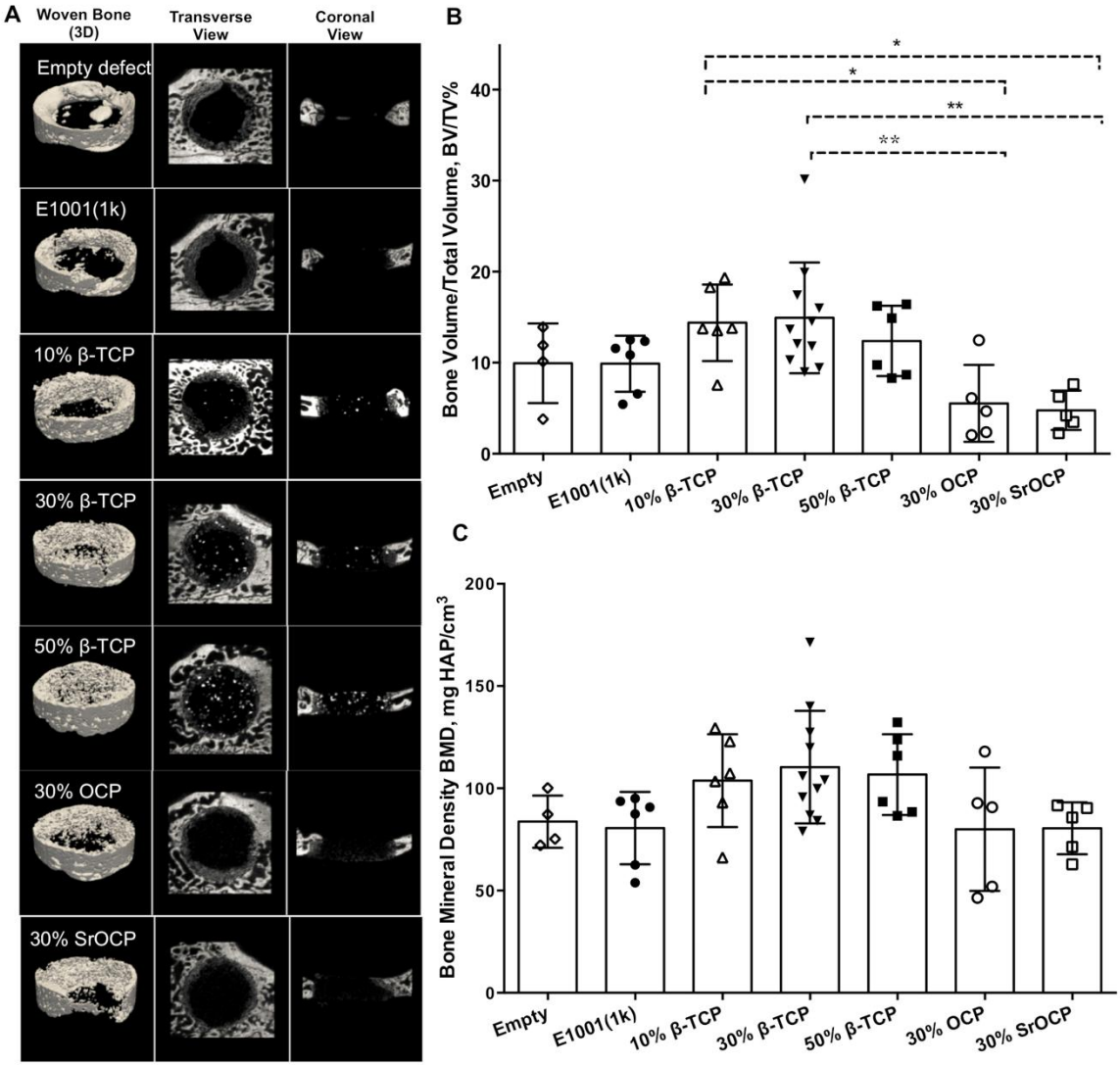

Figure 4.5 (A) Representative microCT images of bone regeneration in the 8 mm rabbit calvarial defects treated with E1001(1k) scaffolds and scaffolds containing 10, 30 or 50 wt% β-TCP, 30 wt% OCP, or 30 wt% SrOCP at 4 weeks post-implantation. Empty defect was included as controls. (B) Quantitative analyses of the percentage of trabecular bone volume of the total volume (BV/TV%) and (C) bone mineral density (BMD) of newly formed bone based on the microCT data. Data are reported as the mean ± SD for $n \geq 4$. An asterisk (*) indicates a statistical significant difference with $p \leq 0.05$, ** indicates $p \leq 0.01$.

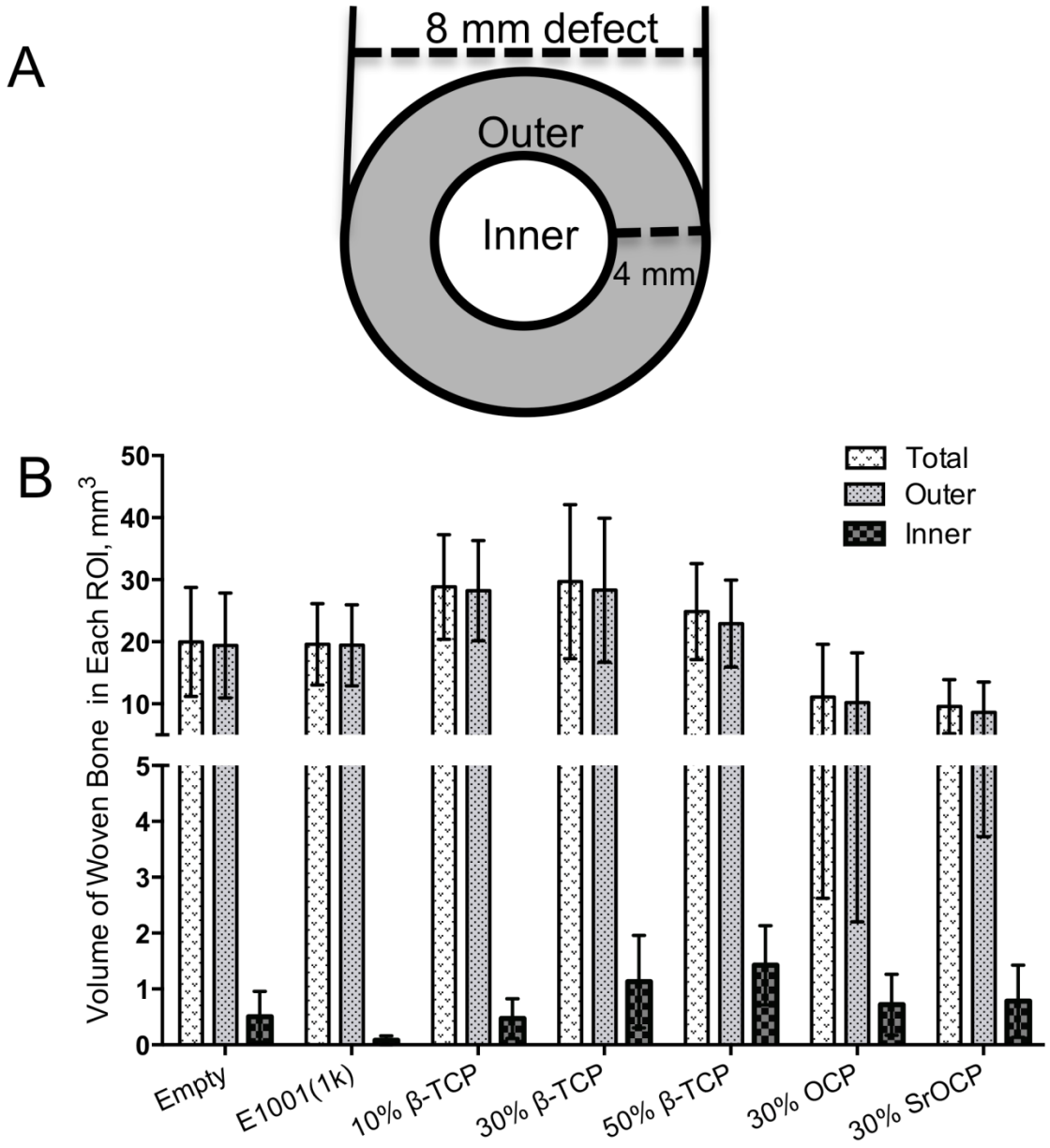

Figure 4.6 (A) Schematic of the defect area (region of interest) delineating the outer, donut-shaped region (shaded gray) and inner region (white) for quantitative analysis of microCT images. (B) Quantitative analysis of the absolute woven bone volume in the total region of interest (ROI), outer region and inner region.

4.4.3 Ex vivo histological analysis

Normal cellular infiltration and bone healing with no signs of a persistent inflammatory response were observed for all treatment groups (Fig. 4.7). At 4 weeks, the empty defects contained minimal amounts of triangular-shaped bone originating from the defect margins and isolated bone appeared toward the dura mater and the endocranial surface (Fig. 4.7A). The defect spaces were collapsed and filled with thin layers of avascular fibrous tissue. In contrast, treated defects showed that the scaffold implant occupied the defect space and exhibited a well-maintained structure (Fig. 4.7B-E). At 4 weeks, the macropores of the scaffolds were occupied by dense connective tissue of extracellular matrix comprised of collagen (stained light blue). In addition, new bone was directly in contact with the scaffold surface and osteoid and osteoblasts were observed along the newly formed bone (images at 20x). Furthermore, blood vessels were present in the pores of the scaffolds and interspersed throughout the entire implant site. These data suggest that the interconnectivity and porosity of the scaffolds supported angiogensis and osteogenesis. A distinctive difference in the deposited collagen matrix and bone formation was observed in defects treated with scaffolds containing β-TCP, OCP or SrOCP. For defects treated with 10, 30 or 50 wt% β-TCP scaffolds, the deposited collagen matrix and newly formed bone were well-interconnected and resembled the trabecular network. The difference among the 10, 30, and 50 wt% β-TCP groups was minimal; therefore, only images from the 30 wt% group were displayed in Fig. 4.7C. In contrast, defects treated with E1001(1k)/30 wt% OCP (Fig. 4.7D) and E1001(1k)/30 wt% SrOCP (Fig. 4.7E) exhibited collagen and bone deposition that were cuboidal in shape with little interconnectivity (images at 5x).

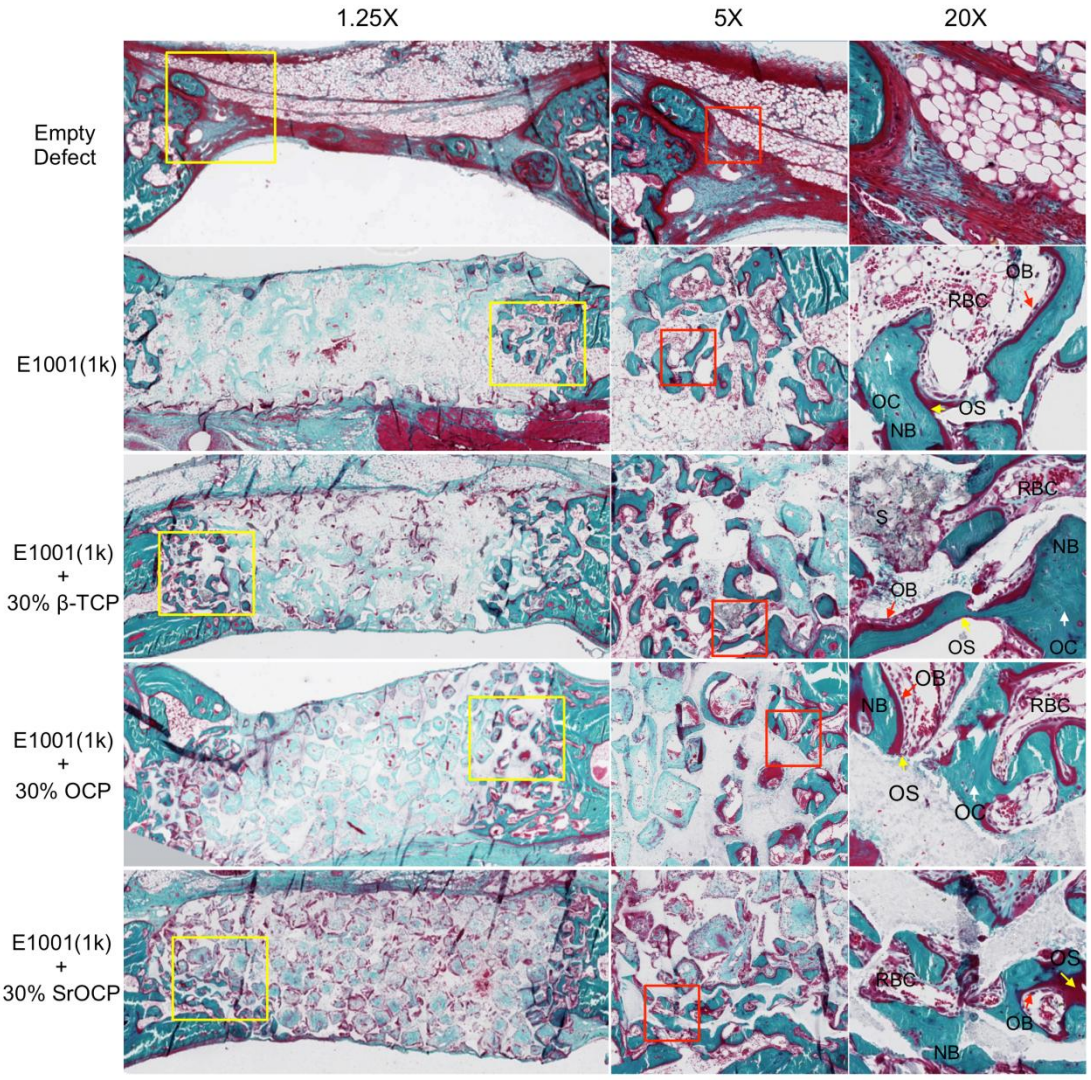

Figure 4.7 Representative histological images 4 weeks post-injury of (A) empty defects, and defects treated with (B) E1001(1k) scaffolds, (C) E1001(1k)/30% β-TCP scaffolds, (D) E1001(1k)/30% OCP scaffolds, and (E) E1001(1k)/30% SrOCP scaffolds. Sections from the coronal plane were stained with Gomori Trichrome, which stains new bone blue, collagen light blue, nonmineralized osteoid and cells red, and residual scaffold black. Figures on the left are at 1.25x magnification. Figures in the middle are higher magnification (5x) images of the areas indicated by the yellow boxes. Figures on the right are higher magnification (20x) images of the areas indicated by the red boxes. Abbreviations - NB: new bone, OB: osteoblast (red arrow), OS: osteoid (yellow arrow), OC: osteocyte (white arrow), RBC: red blood cell, S: scaffold. Histological images for defects treated with E1001(1k)/10% β-TCP or E1001(1k)/50% β-TCP scaffolds were similar to those shown in (C), and are therefore, not shown here.

4.5 Discussion

The osteoconductivity of a scaffold is one important characteristic that can promote successful bone regeneration. Osteoconductivity is an inherent property of E1001(1k) scaffolds [8], but can be further enhanced by the addition of calcium phosphate [26]. However, it is unclear if the type of calcium phosphate incorporated into the scaffold affects bone regeneration. Therefore, the objectives of this study were to (a) compare the *in vivo* performance of E1001(1k) scaffolds containing three different calcium phosphates (30 wt% β-TCP, OCP, and SrOCP) on bone regeneration at 4 weeks in an 8 mm rabbit calvarial non-critical size defect model, and (b) study the dose response of a commonly used calcium phosphate (0, 10, 30, and 50 wt% β-TCP) in conjunction with E1001(1k) scaffolds in this model.

The 8 mm rabbit calvarial non-critical size defect model was selected as a high throughput screening model to compare the *in vivo* performance of different scaffold formulations. Rabbit calvarial defects in the range of 10-15 mm have been considered in various studies [8, 27, 28] as critical size defects (CSDs) and have been used to evaluate the effectiveness of newly developed biomaterials in bone regeneration. However, only one or two defects can be created per cranium. The use of an 8 mm model allows for the creation of four defects per cranium, which reduces the operation time, cost and number of animals. Although an 8 mm defect model is uncommonly used for evaluating reossification, it has been suggested as a useful defect model to compare the early-phase healing (e.g., 4 weeks post-injury) response of graft materials [29, 30].

First, the performance of E1001(1k) scaffolds (no calcium phosphate) was compared to empty defect controls in this model. A comparable amount of new bone

formation was measured in both groups 4 weeks post-injury, confirming that the polymer itself was biocompatible and the scaffold's architecture did not hinder new bone formation. Some scaffolds have been reported to occupy the defect space and hinder bone regeneration in the same animal model [31]. Histological examination of the defects showed that E1001(1k) scaffolds promoted osteoconductivity and angiogenesis. This is likely due to a variety of factors, such as the inherent chemistry of the polymer, bimodal pore size and distribution (200 to 400 μm for macropores and < 20 μm for micropores), overall porosity (~90%), and extensive pore interconnectivity, some of which have been reported as optimal for bone regeneration [3, 8]. In addition, the presence of the E1001(1k) scaffolds provided structure to the defect space, which led to more organized collagen deposition, whereas the empty defect controls were collapsed and filled with thin layers of fibrous tissue. It is possible that space maintenance provided by the scaffold implants could be particularly useful to treat defects that are exposed to increased pressure from the dura mater and surrounding tissue [29].

Next, the performance of scaffolds containing three different calcium phosphates was compared. β-TCP has been used as synthetic bone substitutes for over 30 years because of its well-known bioactivity and osteoconductivity [16]. Recently, several studies have reported that synthetic OCP is more effective than β-TCP for the regeneration of bone because it resorbs at a faster rate [21, 32, 33]. In addition, SrOCP may be advantageous over OCP because studies have suggested that the release of Sr into the microenvironment may further enhance osteogenesis and bone healing [34]. However, our results showed that less bone regeneration was measured for E1001(1k)/30% OCP scaffolds and E1001(1k)/30% SrOCP compared to E1001(1k)/30%

β-TCP scaffolds. This unexpected osteogenic outcome may be attributed to their less-open and interconnected 3D macroporous structure and obliteration of the micropores. Several studies have shown that bone regeneration scaffolds with both macroporosity and microporosity support and induce bone growth more effectively than scaffolds with only macroporosity [35]. The obliteration of the micropores may have limited the influx of nutrients, removal of waste products, and migration of cells throughout the scaffold, thus, resulting in less regeneration. In addition, recent studies clarified that the osteoconductivity and biocompatibility of OCP depend on a variety of characteristics such as crystal stoichiometry [36], granule size [37, 38] and mictructure [39], which were determined by the conditions used to prepare them [21]. Therefore, the development of an effective E1001(1k)/OCP composite scaffold will require the optimization of mineral content, calcium phosphate physicochemical properties, and scaffold 3D architecture. The results from this study should be regarded as a preliminary indication that a more detailed investigation is needed to assess the potential of OCP and SrOCP to enhance bone regeneration in combination with E1001(1k) scaffolds.

Finally, a dose response of β-TCP was studied because the content of β-TCP in the composite scaffolds is an important factor for mineralization and osteogenesis. Cao et al. fabricated PGA)/β-TCP composite scaffolds using a similar method and reported that PGA/β-TCP (1:3) exhibited greater bone regeneration than PGA/β-TCP (1:1) in a rat femoral defect model [16]. In this study, a similar increasing trend was observed for E1001(1k) scaffolds containing 10% or 30% β-TCP. Studies have reported that increased calcium phosphate content in a polymer scaffold may increase scaffold surface roughness [3, 40], and permit more direct calcium phosphate to cell contact, which may contribute

to enhanced progenitor cell attachment, proliferation, differentiation and osteogenic outcome [41]. However, bone regeneration peaked in defects treated with E1001(1k)/30% β-TCP, and decreased in those treated with E1001(1k)/50% β-TCP. This decrease is likely due to the difference in scaffold architecture where E1001(1k)/50% β-TCP scaffolds had a less open macroporous structure and lacked micropores, as compared to E1001(1k) scaffolds containing 10 or 30% β-TCP, which may have affected cellular infiltration. Cao et al. studied the influence of 10, 30 and 50% β-TCP on the biological performance of PLA composite scaffolds in rabbit muscular pockets [42], and showed that the optimal scaffold formulation was PLA/30% β-TCP. This study confirms that calcium phosphate content in a polymer scaffold can influence its 3D structure and subsequently *in vivo* bone regeneration.

4.6 Conclusion

The results from this study demonstrated the *in vivo* biocompatibility of E1001(1k)-based scaffolds and their potential usefulness as osteoconductive scaffolds for bone regeneration. E1001(1k) scaffolds containing 10 and 30 wt% β-TCP exhibited a highly interconnected and porous structure that promoted the highest amount of new bone formation among the treatment groups. On the other hand, E1001(1k) scaffolds containing 30 wt% OCP and 30 wt% SrOCP had a less open 3D structure, resulting in less bone regeneration. The results indicate that *in vivo* bone regeneration greatly depends on calcium phosphate content and type, as well as scaffold 3D architecture.

References

[1] Amini AR, Laurencin CT, Nukavarapu SP. Bone tissue engineering: recent advances and challenges. Crit Rev Biomed Eng 2012;40:363-408.

[2] De Long WG, Jr., Einhorn TA, Koval K, McKee M, Smith W, Sanders R, et al. Bone grafts and bone graft substitutes in orthopaedic trauma surgery. A critical analysis. J Bone Joint Surg Am 2007;89:649-58.

[3] Karageorgiou V, Kaplan D. Porosity of 3D biomaterial scaffolds and osteogenesis. Biomaterials 2005;26:5474-91.

[4] Gunatillake PA, Adhikari R. Biodegradable synthetic polymers for tissue engineering. Eur Cell Mater 2003;5:1-16.

[5] Magno MHR, Kim J, Srinivasan A, McBride S, Bolikal D, Darr A, et al. Synthesis, degradation and biocompatibility of tyrosine-derived polycarbonate scaffolds. Journal of Materials Chemistry 2010;20:8885-93.

[6] Choueka J, Charvet JL, Koval KJ, Alexander H, James KS, Hooper KA, et al. Canine bone response to tyrosine-derived polycarbonates and poly(L-lactic acid). J Biomed Mater Res 1996;31:35-41.

[7] Kim J, Magno MH, Alvarez P, Darr A, Kohn J, Hollinger JO. Osteogenic differentiation of pre-osteoblasts on biomimetic tyrosine-derived polycarbonate scaffolds. Biomacromolecules 2011;12:3520-7.

[8] Kim J, Magno MH, Waters H, Doll BA, McBride S, Alvarez P, et al. Bone regeneration in a rabbit critical-sized calvarial model using tyrosine-derived polycarbonate scaffolds. Tissue Eng Part A 2012;18:1132-9.

[9] Tangpasuthadol V, Pendharkar SM, Kohn J. Hydrolytic degradation of tyrosine-derived polycarbonates, a class of new biomaterials. Part I: study of model compounds. Biomaterials 2000;21:2371-8.

[10] Tangpasuthadol V, Pendharkar SM, Peterson RC, Kohn J. Hydrolytic degradation of tyrosine-derived polycarbonates, a class of new biomaterials. Part II: 3-yr study of polymeric devices. Biomaterials 2000;21:2379-87.

[11] LeGeros RZ. Calcium phosphate-based osteoinductive materials. Chem Rev 2008;108:4742-53.

[12] LeGeros RZ. Properties of osteoconductive biomaterials: calcium phosphates. Clin Orthop Relat Res 2002;395:81-98.

[13] Metsger DS, Driskell TD, Paulsrud JR. Tricalcium phosphate ceramic--a resorbable bone implant: review and current status. J Am Dent Assoc 1982;105:1035-8.

[14] Horch HH, Sader R, Pautke C, Neff A, Deppe H, Kolk A. Synthetic, pure-phase beta-tricalcium phosphate ceramic granules (Cerasorb®) for bone regeneration in the reconstructive surgery of the jaws. International Journal of Oral and Maxillofacial Surgery 2006;35:708-13.

[15] Neamat A, Gawish A, Gamal-Eldeen AM. beta-Tricalcium phosphate promotes cell proliferation, osteogenesis and bone regeneration in intrabony defects in dogs. Arch Oral Biol 2009;54:1083-90.

[16] Cao H, Kuboyama N. A biodegradable porous composite scaffold of PGA/β-TCP for bone tissue engineering. Bone 2010;46:386-95.

[17] Ogose A, Hotta T, Kawashima H, Kondo N, Gu W, Kamura T, et al. Comparison of hydroxyapatite and beta tricalcium phosphate as bone substitutes after excision of bone tumors. J Biomed Mater Res B Appl Biomater 2005;72:94-101.

[18] Fuji T, Anada T, Honda Y, Shiwaku Y, Koike H, Kamakura S, et al. Octacalcium phosphate-precipitated alginate scaffold for bone regeneration. Tissue Eng Part A 2009;15:3525-35.

[19] Kawai T, Anada T, Honda Y, Kamakura S, Matsui K, Matsui A, et al. Synthetic octacalcium phosphate augments bone regeneration correlated with its content in collagen scaffold. Tissue Eng Part A 2009;15:23-32.

[20] Suzuki O, Imaizumi H, Kamakura S, Katagiri T. Bone regeneration by synthetic octacalcium phosphate and its role in biological mineralization. Curr Med Chem 2008;15:305-13.

[21] Suzuki O. Octacalcium phosphate (OCP)-based bone substitute materials. Japanese Dental Science Review 2013;49:58-71.

[22] Johnsson MS, Nancollas GH. The role of brushite and octacalcium phosphate in apatite formation. Crit Rev Oral Biol Med 1992;3:61-82.

[23] Hoppe A, Güldal NS, Boccaccini AR. A review of the biological response to ionic dissolution products from bioactive glasses and glass-ceramics. Biomaterials 2011;32:2757-74.

[24] Bourke SL, Kohn J. Polymers derived from the amino acid l-tyrosine: polycarbonates, polyarylates and copolymers with poly(ethylene glycol). Advanced Drug Delivery Reviews 2003;55:447-66.

[25] LeGeros R. Preparation of octacalcium phosphate (OCP): A direct fast method. Calcif Tissue Int 1985;37:194-7.

[26] Mohamad Yunos D, Bretcanu O, Boccaccini A. Polymer-bioceramic composites for tissue engineering scaffolds. J Mater Sci 2008;43:4433-42.

[27] Pripatnanont P, Nuntanaranont T, Vongvatcharanon S. Proportion of deproteinized bovine bone and autogenous bone affects bone formation in the treatment of calvarial defects in rabbits. Int J Oral Maxillofac Surg 2009;38:356-62.

[28] Xu S, Lin K, Wang Z, Chang J, Wang L, Lu J, et al. Reconstruction of calvarial defect of rabbits using porous calcium silicate bioactive ceramics. Biomaterials 2008;29:2588-96.

[29] Hwang JW, Park JS, Lee JS, Jung UW, Kim CS, Cho KS, et al. Comparative evaluation of three calcium phosphate synthetic block bone graft materials for bone regeneration in rabbit calvaria. J Biomed Mater Res B Appl Biomater 2012;100:2044-52.

[30] Sohn J-Y, Park J-C, Um Y-J, Jung U-W, Kim C-S, Cho K-S, et al. Spontaneous healing capacity of rabbit cranial defects of various sizes. Journal of Periodontal & Implant Science 2010;40:180-7.

[31] Park J-Y, Yang C, Jung I-H, Lim H-C, Lee J-S, Jung U-W, et al. Regeneration of rabbit calvarial defects using cells-implanted nano-hydroxyapatite coated silk scaffolds. Biomater Res 2015;19:1-10.

[32] Kamakura S, Sasano Y, Shimizu T, Hatori K, Suzuki O, Kagayama M, et al. Implanted octacalcium phosphate is more resorbable than beta-tricalcium phosphate and hydroxyapatite. J Biomed Mater Res 2002;59:29-34.

[33] Tanuma Y, Matsui K, Kawai T, Matsui A, Suzuki O, Kamakura S, et al. Comparison of bone regeneration between octacalcium phosphate/collagen composite and beta-tricalcium phosphate in canine calvarial defect. Oral Surg Oral Med Oral Pathol Oral Radiol 2013;115:9-17.

[34] Boanini E, Torricelli P, Fini M, Sima F, Serban N, Mihailescu IN, et al. Magnesium and strontium doped octacalcium phosphate thin films by matrix assisted pulsed laser evaporation. J Inorg Biochem 2012;107:65-72.

[35] Polak SJ, Levengood SK, Wheeler MB, Maki AJ, Clark SG, Johnson AJ. Analysis of the roles of microporosity and BMP-2 on multiple measures of bone regeneration and healing in calcium phosphate scaffolds. Acta Biomater 2011;7:1760-71.

[36] Miyatake N, Kishimoto KN, Anada T, Imaizumi H, Itoi E, Suzuki O. Effect of partial hydrolysis of octacalcium phosphate on its osteoconductive characteristics. Biomaterials 2009;30:1005-14.

[37] Tanuma Y, Anada T, Honda Y, Kawai T, Kamakura S, Echigo S, et al. Granule Size–Dependent Bone Regenerative Capacity of Octacalcium Phosphate in Collagen Matrix. Tissue Engineering Part A 2012;18:546-57.

[38] Murakami Y, Honda Y, Anada T, Shimauchi H, Suzuki O. Comparative study on bone regeneration by synthetic octacalcium phosphate with various granule sizes. Acta Biomater 2010;6:1542-8.

[39] Honda Y, Anada T, Kamakura S, Morimoto S, Kuriyagawa T, Suzuki O. The effect of microstructure of octacalcium phosphate on the bone regenerative property. Tissue Eng Part A 2009;15:1965-73.

[40] Huang H-H, Ho C-T, Lee T-H, Lee T-L, Liao K-K, Chen F-L. Effect of surface roughness of ground titanium on initial cell adhesion. Biomolecular Engineering 2004;21:93-7.

[41] Vaquette C, Ivanovski S, Hamlet SM, Hutmacher DW. Effect of culture conditions and calcium phosphate coating on ectopic bone formation. Biomaterials 2013;34:5538-51.

[42] Cao L, Duan PG, Wang HR, Li XL, Yuan FL, Fan ZY, et al. Degradation and osteogenic potential of a novel poly(lactic acid)/nano-sized beta-tricalcium phosphate scaffold. Int J Nanomedicine 2012;7:5881-8.

5

Calcium phosphate-coated tyrosine-derived polycarbonate scaffolds enhance osteogenic differentiation of stem cells and induce ectopic bone formation

5.1 Abstract

In the present study, a straightforward, fast and versatile modified alternte soaking process was developed and utilized to deposit hydroxyapatite (HA) or dicalcium phosphate dihydrate (DCPD) coating on preformed three-dimensional porous scaffolds based on E1001(1k), a member of large combinational library of tyrosine-derived polycarbonates (TyrPC). The capacity of the fabricated scaffolds for bone formation was investigated *in vitro* using human mesenchymal stem cells (hMSCs) and *in vivo* in the rat subcutaneous pockets loaded with different doses of recombinant human bone morphogenetic protein-2 (rhBMP-2: 0, 1 and 5 μg), and compared with uncoated scaffolds and bulk composite of E1001(1k) scaffold mineralized with beta-tricalcium phosphate (β-TCP). It was demonstrated that the deposition of calcium phosphate coating on the surface of scaffolds showed favorable osteoconductive properties as confirmed by increased alkaline phosphatase (ALP) activity in basal and osteognic media. After 6 weeks implantation, micro-computed tomography (microCT) data revealed that rhBMP-2

loaded onto calcium phosphate coated scaffolds exhibited an osteoinductive effect including more bone formation than the controls. In addition, more animals in calcium phosphate coated groups induced bone formation when a minimal dosage of 1 μg rhBMP-2 was supplemented. Histology results mirrored with microCT data and demonstrated tissue mineralization immediately adjacent to the scaffold surface. In addition, E1001(1k)/HA scaffold showed the capacity for ectopic bone formation in the absence of exogenous osteogenic growth factor. It also yielded the most bone at the low discriminating rhBMP-2 dose. The results in this study suggest that the osteoinductive effect is durface- and dose- dependent. Moreover, a synergistic effect between calcium phosphate coating and rhBMP-2 delivery was observed.

5.2 Introduction

Treatment of large critical size bone defects due to various disease or trauma remains an unsolved clinical challenge that affects millions military and civilian populations [1, 2]. The developing field of bone tissue engineering aims to regenerate osseous defect by combining osteogenic cells with highly porous osteonductive scaffolds and osteoinductive growth factors has emerged as a promising strategy to restore or replace bony defects [2]. Among the materials used as bone regenerating scaffolds, calcium phosphates (CaPs) are the most widely used to fill bone void space because their chemical compositions are similar to bone, which render them to have excellent osteoconductivity and osteointergration [3-6]. Despite their favorable biological properties, the clinical applications of CaPs scaffolds have been limited due to their low mechanical strength and high brittleness [7].

Inspired by the nature of bone, researchers have combined organic polymer with CaP to address some of the limitations associated with CaP-based materials. These composites have been fabricated in a number of ways, e.g., by forming bulk composite scaffolds [8-10] or by coating the polymer surface [11-15] with a calcium phosphate layer, which both have drawbacks. In the bulk composite method, where CaP particles are blended with polymer matrix as fillers, although most often used, embedding of CaP within the polymer often resulting the formation of a thin layer of polymer skin covering the inorganic particles that may lead to the masking of its bioactivity [16-18]. The current biomimetic coating methods based on the immersion of implants in simulated body fluid (SBF) [14, 19-21] or alternate soaking process (ASP) [15, 22, 23], which immerse the biomaterials in the alternate cycles of calcium-ions and phosphate-ions containing solutions, may take a long time (days and weeks) for a stable apatite deposition on scaffold [17, 18]. Furthermore, CaP minerals are likely to aggregate on the outer region of geometrically complex 3D porous scaffold, resulting in the formation of a non-uniform layer of calcium phosphate materials with increased thickness at the scaffold surface and interfere in the porous structure and lead to the hindrance of cell in-growth [24].

Herein, we prepared a high quality uniform CaP coating within an hour on 3D porous polymeric scaffolds using a modified alternate soaking process. The coating process developed in this study is a straightforward, fast and versatile technique to fabricate mineralized polymer scaffolds. Furthermore, the surface topography and chemical composition of the deposits can be tailored to meet the requirements for cell growth and bone regeneration. Our group have developed a E1001(1k) scaffold produced by porogen leaching combined with freeze-drying method for bone regeneration [25-28].

E1001(1k) is a member of a large combinatorial library of tyrosine-derived polycarbonate (TyrPC) whose properties can be tailored for different tissue engineering applications by varying the composition of the monomers (desaminotyrosyl-tyrosine alkyl ester (DTR), deasaminotyrosl-tyrosine (DT) and poly(ethylene glycol(PEG)) [25, 29, 30]. E1001(1k) scaffold features a favorable pore size, porosity and interconnectivity for permitting *in vivo* bone and vascular ingrowth and therefore it is considered as a good candidate for bone regeneration [26, 28].

In this study, using the modified alternate soaking process, two calcium phosphate coating materials were deposited on 3D E1001(1k) scaffolds. The effect of calcium phosphate coating materials have been evaluated for bone formation *in vitro* using human mesenchymal stem cells (hMSCs) and *in vivo* after subcutaneous implantation in rats loaded with different doses of recombinant human bone morphogenetic protein 2 (rhBMP-2, 0, 1 and 5 μg per scaffold). To the best of our knowledge, there is no study on the effect of these calcium phosphate formulations and simultaneous delivery of rhBMP-2 on ectopic bone formation of coated polymeric implants. Two calcium phosphate coating formulations were selected, hydroxyapatite (HA) and dicalcium phosphate dihydrate (DCPD), each has unique properties that promote osseointegration and bioactivity *in vivo*. HA is the most widely investigated calcium phosphate and supports osteogenesis [4, 5]. DCPD has attracted great attention recently because it is believed to be one of the precursors of biological apatite in bone and tooth [31-33]. We hypothesized that the osteogenic potential of E1001(1k) scaffold may be enhanced by the deposition of a calcium phosphate layer on its surface. The bone formation capacity of HA or DCPD coated E1001(1k) scaffolds were compared to uncoated E1001(1k) scaffolds and

scaffolds mineralized with beta-tricalcium phosphate (β-TCP) prepared by bulk composite method.

5.3 Materials and methods

5.3.1 Materials

Sodium chloride (NaCl), calcium chloride ($CaCl_2$), potassium phosphate dibasic trihydrate ($K_2HPO_4 \cdot 3H_2O$) were obtained from Sigma-Aldrich Chemical Co. (St. Louis, MO). The NaCl particles in the range of 212- 425 μm were selected and used as a porogen in scaffold fabrication. β-TCP powders (100 nm) were purchased from Berkeley Advanced Biomaterials, Inc. (Berkeley, CA). 1,4-Dioxane was obtained from Fischer Scientific (Pittsburgh, PA). E1001(1k) denotes poly(DTE-co-10 mol% DT-co-1 mol% PEG_{1k} carbonate), was synthesized at the New Jersey Center for Biomaterials and used as the scaffold matrix. Detailed polymer structure, nomenclature, and synthetic procedure can be found in previous publications [25]. Recombinant human bone morphogenetic protein-2 (rhMBMP-2) were purchased from HumanZyme, Inc. (Chicago, IL)

5.3.2 Polymer scaffold fabrication

3D porous scaffolds were fabricated from E1001(1k) using a combination of salt leaching and freeze-drying methods [25-28]. Briefly, the polymer was first dissolved in deionized (DI) water and 1,4-dioxane overnight. The polymer solution was mixed uniformly with salt particles. The mixture was then casted into a Teflon mold, quenched in liquid nitrogen and freeze-dried for 2 days. Disk-shaped scaffolds were punched out

using custom-designed cutting tools. Salt particles were leached out in distill water, and the nonporous skin was sliced off. Finally, the scaffolds were dried in a lyophilizer for 1 day.

5.3.3 Mineralization of polymer scaffolds

To prepare consistent calcium phosphate coating for *in vitro* and *in vivo* experiments, a custom-designed coating apparatus was built. This apparatus consists of 16 independent cylindrical chambers that are 25 mm in diameter and 8 cm in height, where 16 scaffolds can be mineralized each time. HA or DCPD coating was deposited on E1001(1k) scaffolds using a modified alternate soaking process. Each scaffold was placed in 20 ml of 0.5 M $CaCl_2$ solution at pH 6 in each chamber. Vacuum (up to 30 inHg) was applied to the chamber for 1 min, followed by a rapid release to atmospheric pressure; this step was repeated 5 times to completely wet the scaffolds with $CaCl_2$ solution. Then, the scaffolds were removed from the $CaCl_2$ solution and pat-dried with a kimwipe to remove excess solution on the scaffold surface. Each scaffold was then transferred to 20 ml 0.5 M $K_2HPO_4 \cdot 3H_2O$ solution at pH 6 or 10 and the same vacuum and atmospheric pressure cycles were used to facilitate the diffusion of phosphate solution into the interior of the 3D scaffolds to react with the $CaCl_2$ to form a uniform calcium phosphate coating. The scaffolds were alternated in calcium (Ca) and phosphate (P) solutions for 3 or 5 cycles for phosphate solution at pH 10 or 6 respectively until 30% calcium phosphate by weight was obtained. Finally, the mineralized scaffolds were dried in a lyophilizer for 1 day. By controlling the phosphate solution pH (6 or 10), two

calcium phosphate formulations (DCPD or HA respectively) were deposited on the scaffolds as confirmed by XRD analysis.

β-TCP mineralized E1001(1k) scaffolds, denoted as E1001(1k)/β-TCP, were fabricated using the same salt leaching and freeze-drying method (Section 2.2) with the addition of β-TCP particles during the mixing step and the prepared scaffolds were used as one of the control in this study.

5.3.4 Scaffolds characterization

The morphology of the deposited calcium phosphate minerals and their effect on scaffold structure were assessed using a Scanning Electron Microscope (SEM, AMRAY-1830I). The phase of the deposited calcium phosphate was determined using X-Ray diffractometer (XRD, Philips X'Pert, Cu-K α radiation: λ = 1.5406, operating at 45 kV and 40 mA). The scaffolds were scanned from 5° to 90 ° at step size of 0.02° and scan step time of 1 sec. PANalytical HighScore Plus software was used to analyze the X-Ray diffraction patterns. The phase of the calcium phosphates was determined by matching the diffractogram with the standard library of known diffraction patterns, International Centre for Diffraction Data (ICDD). The scaffolds were also characterized using micro-computed tomography (microCT). The scans were performed in a microCT scanner (Skyscan 1172, Bruker-microCT, Belgium) at a resolution of 10 μm, a voltage of 60 kVp, a current of 170 mA, and with a 0.5 mm Aluminum filter. The reconstruction of projection images was performed using Skyscan system software package. The distribution of calcium phosphate minerals was assessed qualitatively using the projection images. The gray-scale index distribution of each scaffold was obtained.

5.3.5 Scaffold degradation and calcium phosphate dissolution in PBS

The effect of calcium phosphate coating on scaffold degradation profile was investigated. Each E1001(1k)-based scaffold was incubated in 10 mL Dulbecco's phosphate buffered saline (PBS) with 0.05% sodium azide added at 37 °C for a period up to 35 days and the incubation media was refreshed weekly. At pre-determined time points (3, 7, 14, 28 and 35 days), scaffolds (n=3) were characterized. The change in molecular weight, scaffold mass and mechanical properties were investigated (Supplementary Information). At each time point, the concentration of calcium ion in the PBS containing E1001(1k)-CaP scaffolds was measured using a calcium assay kit (BioVision) according to the manufacture procedure. The change in scaffold morphology and calcium phosphate phase was investigated using SEM and XRD.

5.3.6 Scaffold sterilization

Scaffolds were sterilized by ethylene oxide using a 12 hours cycle at room temperature and sterility is verified by a steritest (AN-80 Anderson Products, Haw River, NC).

5.3.7 hMSCs attachment, proliferation and differentiation

5.3.7.1 Seeding of hMSCs

Human mesenchymal stem cells (hMSCs) at passage 3 (hMSCs, donor # 8001L, Texas A&M Health Science Center College of Medicine) were used to determine the effect of calcium phosphate coating on cell attachment, proliferation and osteogenic

differentiation. Before cell seeding, the sterile scaffolds (10 mm diameter × 2 mm thick) were fully hydrated in cell culture media (α-MEM media, Invitrogen, CA) supplemented with 16% fetal bovine serum and 25 μg/ml gentamicin. The scaffolds were placed in the wells of non-attachment 48-well cell culture plate (CytoOne, FL). 100 μl of cell suspension was added onto the top of each scaffold at a density of 5×10^4 cell/scaffold for E1001(1k) scaffold, E1001(1k)/β-TCP scaffold and tissue culture polystyrene (TCPS) and 10×10^4 cell/scaffold for HA or DCPD coated scaffolds (preliminary result indicated that the cell seeding efficiency on CaP coated scaffolds was half of that of controls, therefore twice cells were seeded initially to ensure similar starting cell numbers on each type of scaffold). An additional 700 μl of media was added to each well after 3 h of incubation at 37°C in 5% CO_2 atmosphere and further cultured for 24 h. After 24 h of incubation, the media in each well was either replaced with the osteogenic media (the culture media supplemented with 10 mM β-glycerophosphate, 50 μg/mL of ascorbic acid, and 1μM dexamethasone) or continue cultured in basal media. The media was changed every other day.

5.3.7.2 hMSCs attachment and proliferation

Cultured scaffolds were analyzed for the attachment and proliferation of hMSCs using SEM and PicoGreen assay respectively. For cell attachment, at day 1, cultured scaffolds were fixed in 4% PBS buffered paraformaldehyde overnight. The scaffolds were rinsed in PBS, dehydrated through graded ethanol and critical-dried. The dried scaffold samples were sputter coated for SEM examination. For proliferation, the cultured scaffolds were rinsed with PBS three times and transferred to a new plate. 200 μl

of 1X cell lysis buffer (Cell Signalling Technology) was added to each scaffold, followed by three thaw/freeze cycles (30 min of thawing at 37°C and 30 min of freezing at -80°C) to extract DNA. The cell lysate was collected and centrifuged at 12000 rpm for 5 min, after which the supernatant was collected for analysis.The DNA content was quantified using a fluorometric Quanti-iT^{TM} PicoGreen dsDNA kit (Invitrogen) according to the manufacture's procedure and the fluorescence was measured using a microplate reader (Tecan) with excitation at 485 nm and emission at 535 nm.

5.3.7.3 Biochemical analysis: alkaline phosphatase (ALP) activities

Cultured scaffolds were analyzed for alkaline phosphatase (ALP) activities of hMSCs using ALP fluorometric Kit (Biovision) according to manufacture procedure. Briefly, at each time point, 80 μl of assay buffer, 30 μl of cell lysate and 20 μl of 0.5 mM working substrate solution were added to each well of a 96-well plate. The plate was incubated at room temperature on an orbital shaker for 45 min, and the reaction was stopped by the addition of stop solution. The fluorescence was measured using a microplate reader (Tecan) with excitation at 360nm and emission at 440 nm. The value of ALP activities was normalized to the amount of DNA in the sample.

5.3.8 Subcutaneous implantation in rats

The use of the animals in this experiment was approved by the Institutional Animal Care and Use Committee (IACUC) at Rutgers University and the Department of Defense United States Army Medical Research and Material Command Animal Care and Use Review Office (ACURO). Fifteen adult male Sprague Dawley rats ordered from

Charles River Laboratories, weighting 280-400 g were used in this study. The rats were anaesthetized by intraperitoneal injections of a mixture of Ketamine and Xylazine, and inhalation of isoflurane. The back of each rat was shaved and aseptically prepared using povidone-iodine and 70% isopropyl alcohol. Two small midline incisions (1 cm) were made between the shoulders and toward the tail. From these incisions, subcutaneous pockets were created using a pair of surgical scissors on the right and left side of the midline incisions. Each individual pocket held one scaffold of each of the following groups: (1) no rhBMP-2, (2) 1 μg rhBMP-2, and (3) 5 μg rhBMP-2. In each group, there were four types of scaffolds: (1) E1001(1k), (2) E1001(1k)/β-TCP, (3) E1001(1k)/DCPD, and (4) E1001(1k)/HA. Then the incisions were closed with surgical staples. The animals were monitored for local symptoms at the wound area on a daily basis for three days. The animals were sacrificed after six weeks and the implants were retrieved and fixed in 10% neutral buffered formalin for further analysis.

5.3.9 MicroCT scanning and analysis

The scans were performed in a micro-computed tomography (microCT) scanner (Skyscan 1172, Bruker-microCT, Belgium) at a resolution of 10 μm, a voltage of 60 kVp, a current of 170 mA, and with a 0.5 mm Aluminum filter. The reconstruction of projection images was performed using Skyscan system software package. The volume of bone in scaffolds was obtained using CTAn v.1.13 software. The average of the negative controls (scaffolds without rhBMP-2) was subtracted from the value of the corresponding experiment groups.

5.3.10 Histological analysis

The specimens were cut in half, dehydrated through ascending concentrations of ethanol, cleared in xylene, and infiltrated with paraffin. Next, the scaffold halves were embedded cut side down into a mold. Paraffin sections were taken at 8 μm after cutting into each block 400-500 μm to remove area of potential compression artifact. The sections were stained with hematoxylin and eosin (H&E).

5.3.11 Statistics

Statistical analyses were performed using single factor analysis of variance (ANOVA) followed by a multiple comparison post-hoc test (Tukey-Kramer method) with a significance level established as $p \leq 0.05$. All statistical analyses were carried out using GraphPad Prism 6 software package. All data were reported as mean ± standard deviation (SD).

5.4 Results

5.4.1 Scaffolds fabrication and characterization

Using the modified alternate soaking process, about 30 weight% of calcium phosphate was deposited onto E1001(1k) scaffold within an hour. The phase composition and surface topography of the deposits was tailored by controlling the pH of phosphate solution: two distinctive calcium phosphate phases, DCPD or HA, were deposited throughout the thickness of scaffolds. Using calcium and phosphate solutions at pH 6, micro-size crystals were observed adhering to the scaffold pore wall (Fig. 5.1A, third row). Images at high magnification revealed that those calcium phosphate minerals were either plate-like or flower-like structure composed of fine lamellae clustered themselves. X-ray diffraction analysis (Fig. 5.2) of this calcium phosphate showed peaks at 11.65°, 20.949° and 29.296°, which are characteristic of DCPD or Brushite (ICDD # 01-072-0713). On the other hand, after alternately soaked in calcium solution at pH 6 and phosphate solution at pH 10, SEM revealed a thin layer of calcium phosphate mineral deposited onto E1001(1k) scaffolds (Fig.5.1 A, fourth row). This layer fully covered the scaffold pore walls surface and displayed the typical morphology of carbonated hydroxyapatite obtained by alternate soaking process, that is nano-textured fluffy-like aggregates of fine grains. X-ray diffraction analysis confirmed this calcium phosphate was carbonated hydroxyapatite (ICDD # 01-070-0795) with characteristics peaks at 25.9° and 32.0° (Fig.5.2). The HA peaks were broad indicating that the crystals are nano-size. The SEM images (Fig. 5.1) and XRD diffractograms (Fig. 5.2) of controls: E1001(1k) and E1001(1k)/β-TCP, are also displayed . E1001(1k) scaffolds displayed a highly porous and interconnected structure with bimodal pore size distribution of macropores

(200-400 μm) and micropores (< 20 μm). The E1001(1k)/β-TCP control scaffold exhibited a similar porous structure as the E1001(1k) control with uniform distribution of β-TCP particles throughout the polymer matrix.

SEM assessments of samples taking along the depth as well as cross the coronal surface of calcium phosphate mineralized scaffolds revealed that DCPD or HA coating or β-TCP was homogeneously distributed throughout the surface and the thickness of the scaffolds. Fig.5.3 shows the 2D coronal images of scaffolds from the microCT scan, which also confirmed uniform calcium phosphate distribution. The results indicated that the technique of vacuum, followed by a rapid release to atmospheric pressure was effective in facilitating ions diffusions.

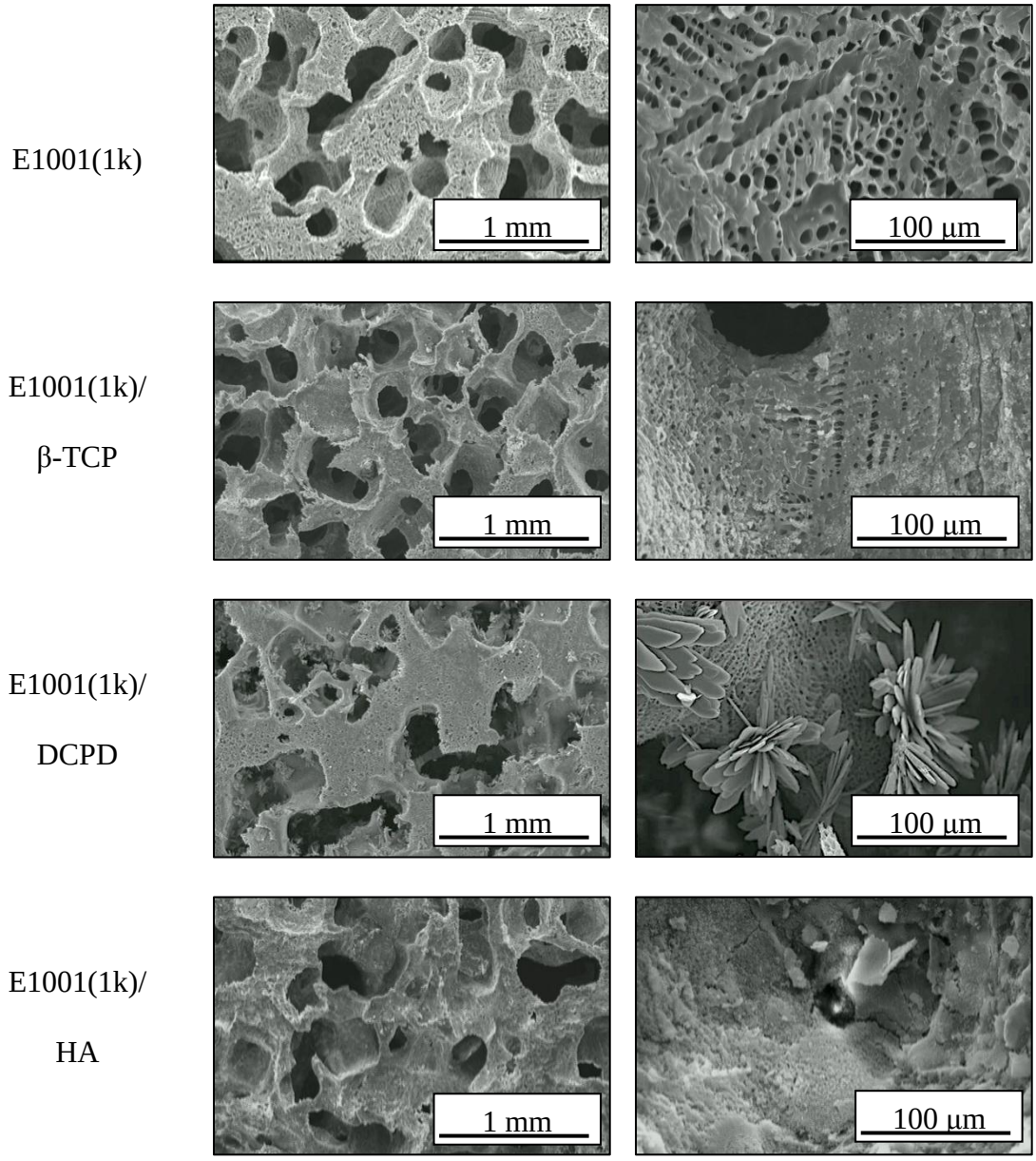

Figure 5.1 Representative scanning electron microscopy images of the macroporous networks (first panel) and surface topologies (second panel) of E1001(1k), E1001(1k)/β-TCP, E1001(1k)/DCPD and E1001(1k)/HA scaffolds at low and high magnifications respectively.

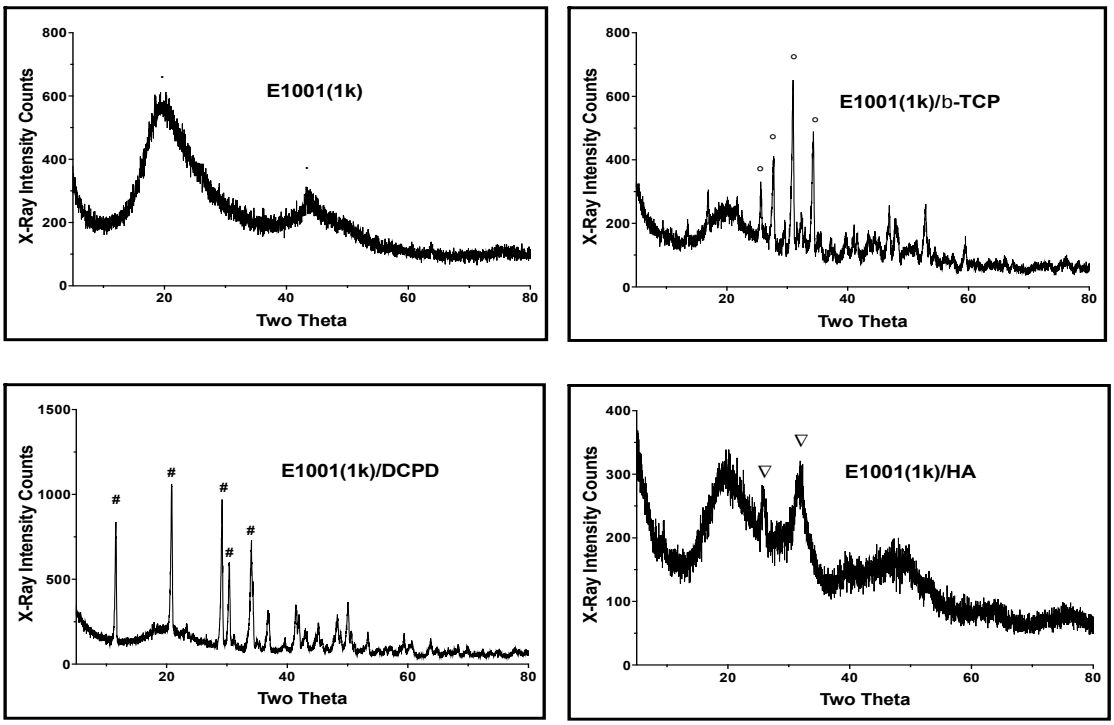

Figure 5.2 X-ray diffractograms of E1001(1k), E1001(1k)/β-TCP, E1001(1k)/DCPD and E1001(1k)/HA scaffolds

.

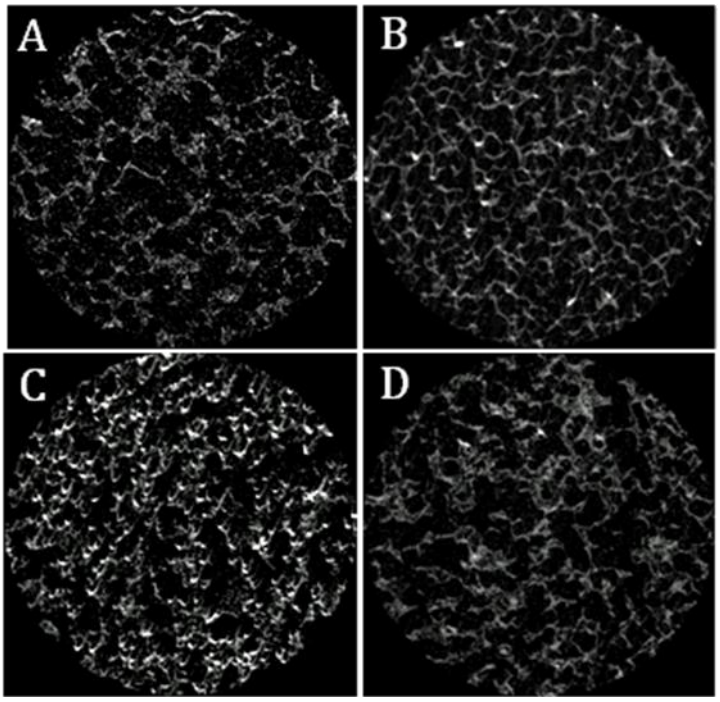

Figure 5.3 2D coronal images of scaffolds from the micro-computed topography (microCT) scans (A) E1001(1k), (B) E1001(1k)/β-TCP, (C) E1001(1k)/DCPD and (D) E1001(1k)/HA scaffolds.

5.4.2 Ca^{2+} release profile and *in vitro* conversion of DCPD to HA

It is well known that the calcium cations released from the CaP materials play important role in stimulating angiogenesis and osteogenesis *in vivo* and *in vitro*. Therefore, the Ca^{2+}concentration in PBS containing β-TCP, or DCPD or HA mineralized E1001(1k) scaffolds was measured up to 35 days (Fig. 5.4A). The result indicated that the Ca^{2+} concentration was similar (about 0.5 mg/dl) in PBS solutions containing E1001(1k)/HA or E1001(1k)/β-TCP scaffolds at all time points. On the other hand, immersion of E1001(1k)/DCPD in PBS showed 5-6 times higher Ca^{2+} concentration than the other groups at day 3, 7, 14. At day 21, the concentration started to decrease and

reached to a value equal to that of E1001(1k)/HA and E1001(1k)/β-TCP groups at day 28 and 35. Moreover, at day 14, SEM photomicrographs displayed needle-like crystal structure in addition to plate-like DCPD crystals, indicating partial transformation of DCPD crystals into another calcium phosphate phase (Fig. 5.4C). The X-ray diffraction analysis of this composition determined that the needle-like structure were carbonated-hydroxyapatite as indicated by the appearance of apatite peaks at 25.9° and 32.0° along with DCPD peaks (Fig. 5.4B). By the end of 4 weeks in PBS, only one phase was detected by XRD which is poorly crystalline carbonated apatite, all the DCPD peaks had disappeared indicating the complete conversion of DCPD to HA. SEM images also reveal that the plate-like DCPD have completely transformed to needle-like apatite. On the other hand, HA and β-TCP are thermodynamically stable and no phase transition occurred. Moreover, calcium phosphate coating did not influence scaffold degradation very much as similar molecular weight, scaffold mass and compressive elastic modulus retention profiles (data not shown) were observed as compared to scaffold without calcium phosphate.

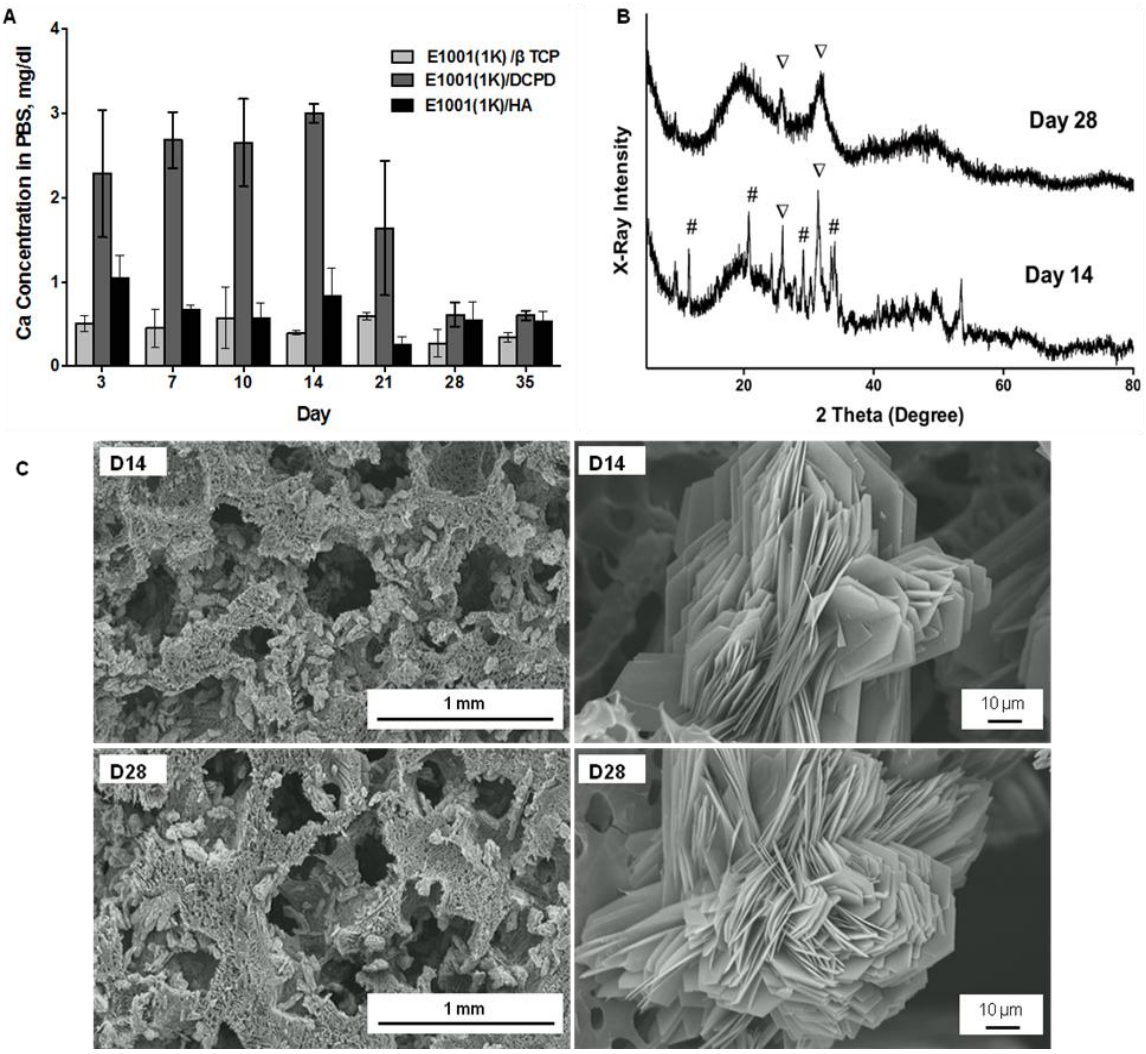

Figure 5.4 (A) Calcium ion concentration in phosphate buffered saline (PBS) containing E1001(1k)/β-TCP, E1001(1k)/DCPD and E1001(1k)/HA scaffolds at each time point. (B) XRD diffractograms and (C) scanning electron microscopy images of E1001(1k)/DCPD scaffold after soaking in PBS for 14 and 28 days.

5.4.3 *in vitro* study

To investigate the effects of calcium phosphate coating on cells responses, hMSCs were used. SEM images (Fig. 5.5) of cell-seeded scaffolds after 24 h culture showed that hMSCs attached very well on all scaffolds with spreading-out phenotype. Cells were connected with each other indicating good cell-to-cell interaction. The DNA content of hMSCs on scaffolds in cell culture media was measured at days 1, 4, and 7 as an indication of cell proliferation. The results, as shown in Fig. 5.6A, indicated that the cells have maintained their numbers in the scaffolds as the DNA content did not significantly vary over the entire culture period. The high cell seeding density may partially explain this that it is likely the cells stopped proliferating because they had reached confluence. Furthermore, no significant difference was observed between coated scaffolds and controls.

The normalized ALP expression of the hMSCs cultured on scaffolds in both basal and osteogenic media at day 7 is shown in Fig. 5.6B. The results revealed that DCPD or HA coated scaffolds induced a significantly higher ALP expression compared to the TPCS, E1001(1k) and E1001(1k)/β-TCP controls in media with or without osteoinduction. Moreover, in the basal media without osteoinduction, DCPD or HA coated scaffolds induced substantial ALP expression that was comparable to the level induced by osteogenic media for E1001(1k) scaffolds and higher than E1001(1k)/β-TCP, suggesting that the calcium phosphate coating may intrinsically promoting ALP expression.

E1001(1k)

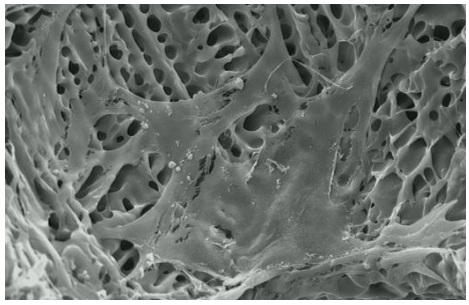

E1001(1k)/β-TCP

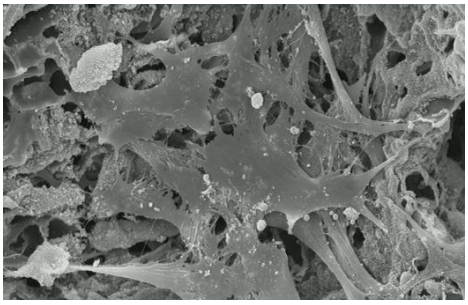

E1001(1k)/DCPD

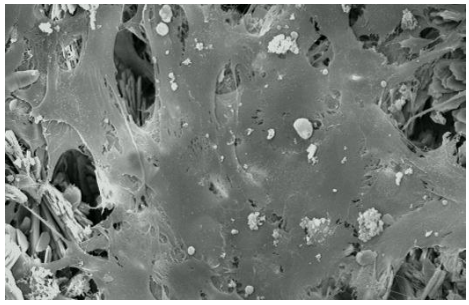

E1001(1k)/HA

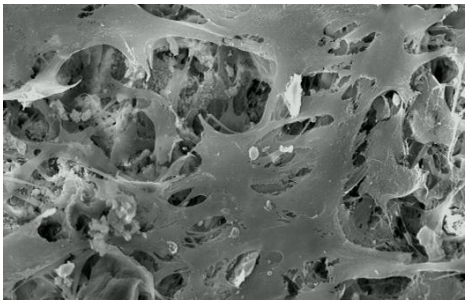

Figure 5.5 Scanning electron microscope of human mesenchymal stemm cells (hMSC) on coated scaffolds and controls under basal condition after 24 hour of *in vitro* culture.

A

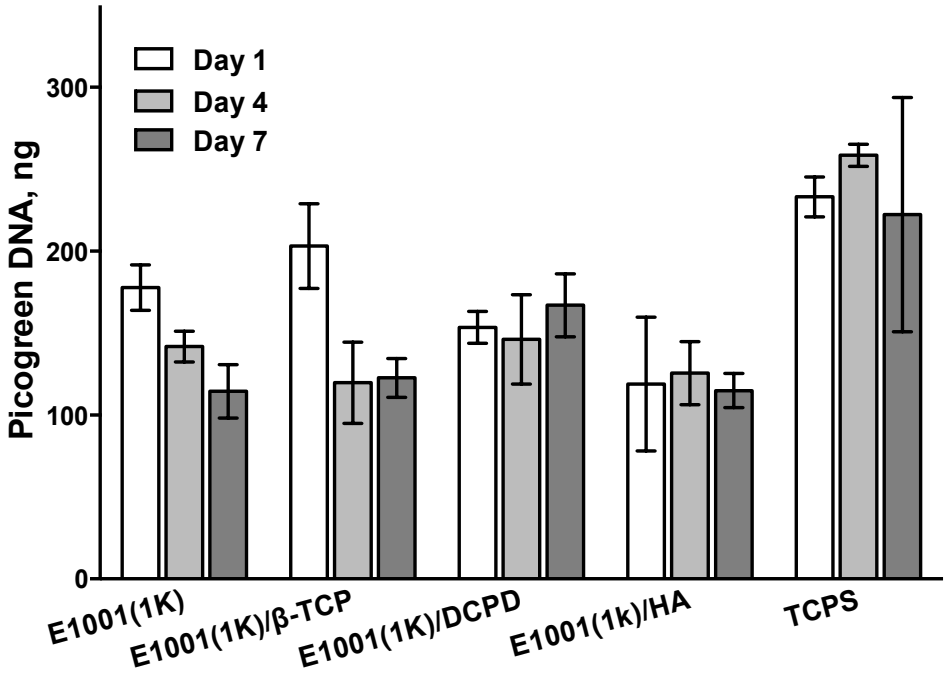

B

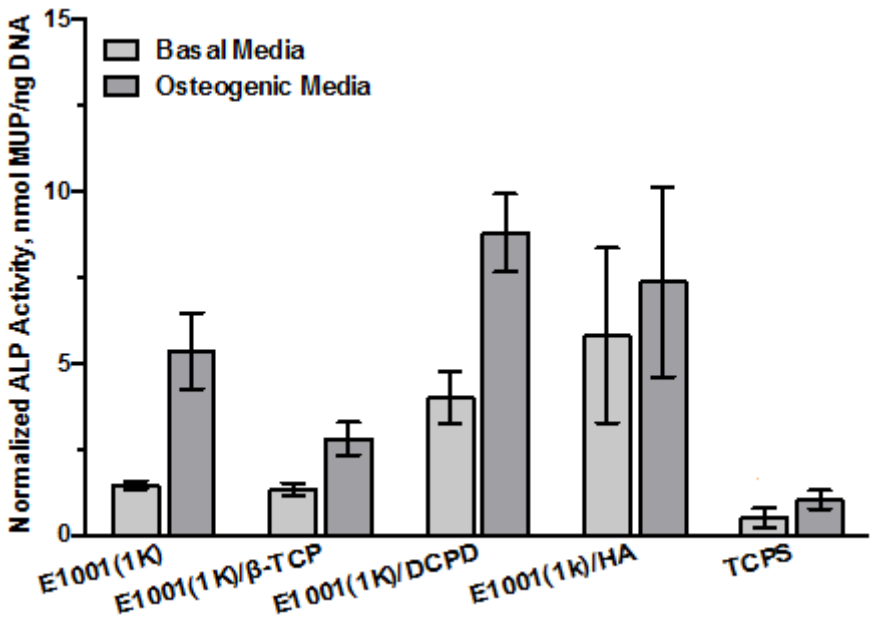

Figure 5.6 (A) DNA content for coated scaffolds and controls in basal condition. (B) Alkaline Phosphatase (ALP) activity for coated and controls with or without osteoinduction over y days of *in vitro* culture

5.4.4 *In vivo* subcutaneous implantation

No wound or implant infection was detected and all animals were alive and healthy at the end of the study. Upon sample collection, excellent scaffold integration in the subcutaneous pocket was observed and vascularization was present around the samples regardless of the groups.

Fig.5.7 shows the gray-scale index distribution (0 – 255, 0 is black, 255 is white, values between are shades of gray) of scaffolds prior to and post 6 weeks implantation without rhBMP-2, as an indicator of the change in scaffold radiodensity. The gray-scale index distribution of E1001(1k) scaffolds were concentrated on the lower end due to the low raiodensity of polymer. After the incorporation of radio-opaque calcium phosphates, the radiodensity of scaffolds was enhanced. After 6 weeks implantation, no significant change in the gray-scale index distribution (Fig.5.7B) was observed for E1001(1k) and E1001(1k)/β-TCP scaffolds. For E1001(1k)/DCPD scaffold, the radiodensity of scaffold decreased after implantation, suggesting possible degradation of DCPD particles. On the other hand, the rariodensity of E1001(1k)/HA scaffold increased, likely due to tissue mineralization, as confirmed by the histology results. It is worthy to note that the gray-scale index distribution of HA or β-TCP mineralized scaffolds post implantation overlapped with that of induced bone in the rhBMP-2 treated groups. Therefore, in the calculation of bone volume formation within each scaffold, the average of the negative controls (scaffolds without rhBMP-2) was subtracted from the value of the corresponding experiment groups.

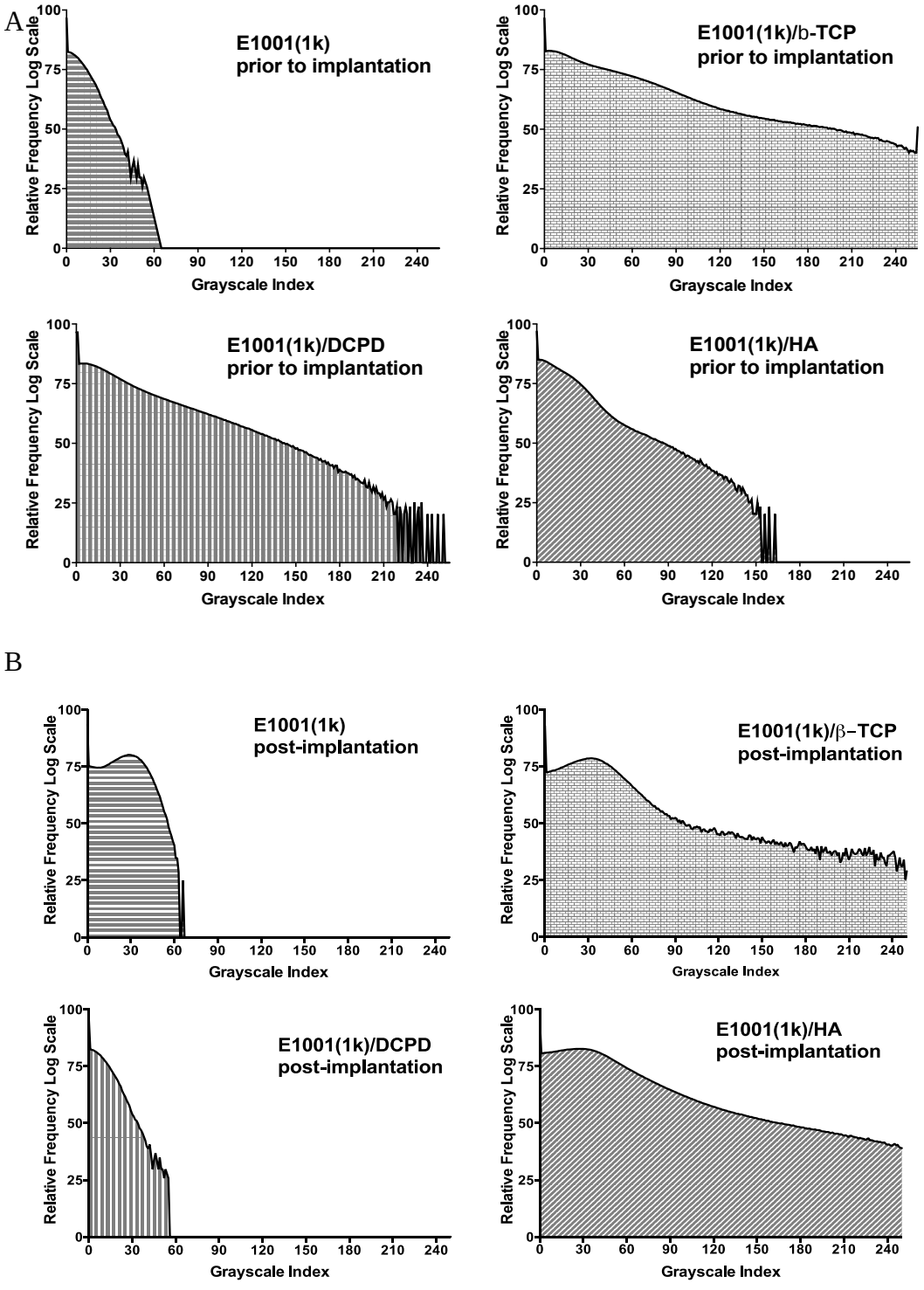

Figure 5.7 The gray-scale index distribution of coated scaffolds and controls (A) prior to and (B) post subcutaneous implantation.

The X-ray projection images of scaffolds prior to and post implantation with 0, 1 and 5 μg rhBMP-2 are shown in Fig. 5.8. The projection images of E1001(1k) scaffolds prior to implantation were translucent due to the low radiodensity of the polymer. With calcium phosphate mineralization, the scaffold images became opaque revealing the enhancement in scaffolds radiodensity due to the uniform distribution of calcium phosphate minerals throughout the scaffolds. In rhBMP-2 treated groups, dense mineralized tissue was observed (Fig.5.8 third and fourth row). For scaffolds with 1 μg rhBMP-2, minimal bone formation was observed in 2/5, 0/5, 2/5 and 5/5 animals for E1001(1k), E1001(1k)/β-TCP, E1001(1k)/DCPD and E1001(1k)/HA groups respectively (Table 5.1). This result was also confirmed by using histology. A clear dose-dependent response of bone formation on rhBMP-2 was observed. With 5 μg rhBMP-2, all animals had bone induction (Fig.5.8, fourth row) and the amount of bone formation was significantly greater. In the controls groups, bone formation was observed in some regions within a scaffold, rather than being uniformly distributed throughout the scaffold matrix and there were no preferred regions for bone formation that was observed in the center of the implant in some cases and in the periphery in other cases**.** In contrast, scaffolds coated with HA or DCPD, 4/5 or 2/5 animals had bone uniformly distributed throughout the entire scaffolds. The average volume of bone induction in E1001(1k), E1001(1k)/β-TCP, E1001(1k)/DCPD and E1001(1k)/HA scaffolds were 0.65, 0.73, 2.42 and 4.93 mm^3 respectively (Fig.5.9). Significantly greater bone induction was observed in scaffolds with DCPD or HA coating.

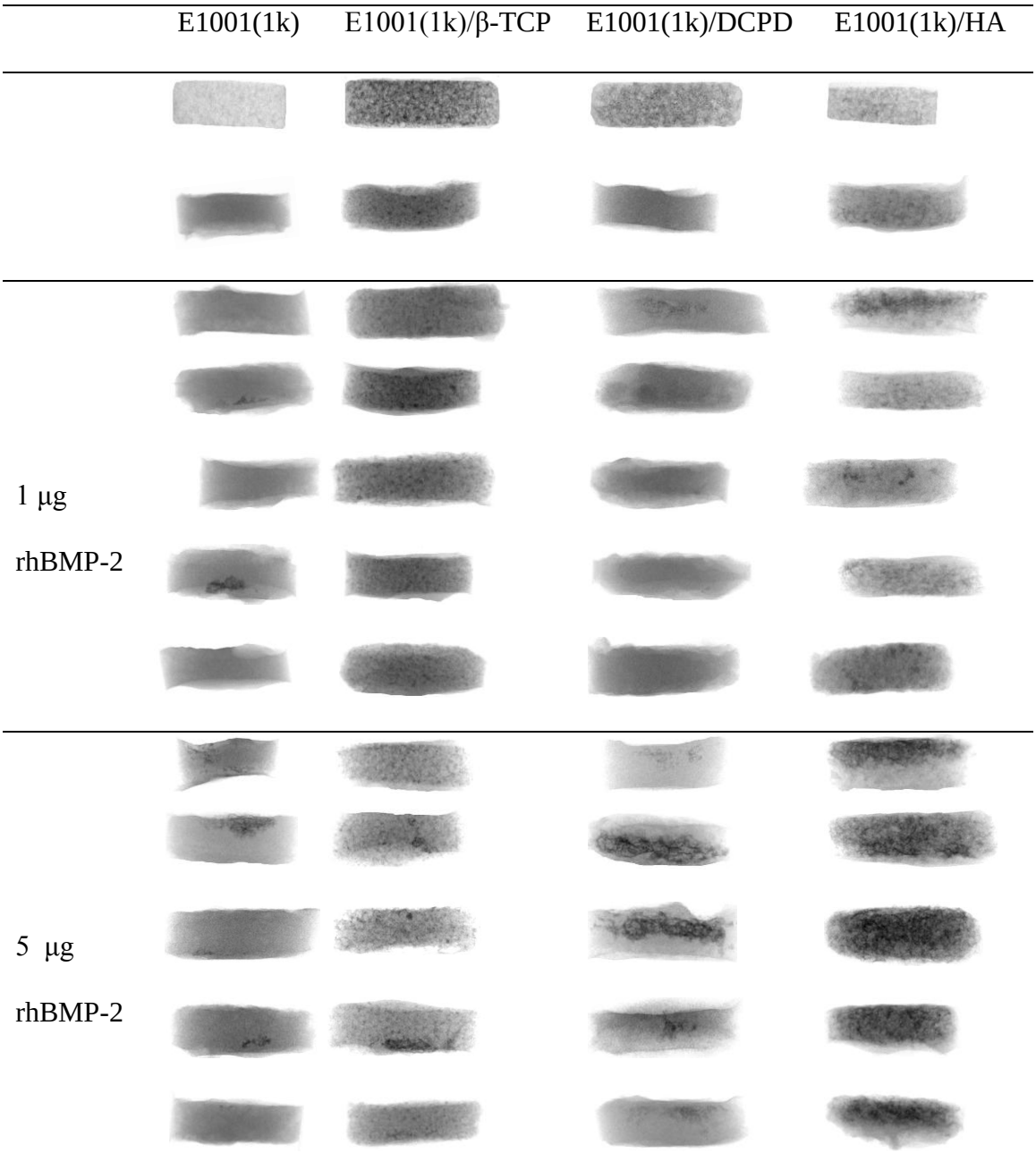

Figure 5.8 Micro-computed tomography (microCT) project images of calcium phosphate coated scaffolds and controls prior to implantation (first row), after subcutaneous implantation in rat loaded with 0 (second row), 1 (third row) and 5 μg (fourth row) recombinant human bone morphogenetic protein-2.

Table 5.1 Number of animals induced bone formation in rat subcutaneous implantation after 6 weeks for each type of scaffold in each group

Scaffolds	0 μg rhBMP-2	1 μg rhBMP-2	5 μg rhBMP-2
E1001(1k)	0/4	2/5	5/5
E1001(1k)/β-TCP	0/4	0/5	5/5
E1001(1k)/DCPD	0/6	2/5	5/5
E1001(1k)/HA	4/4	5/5	5/5

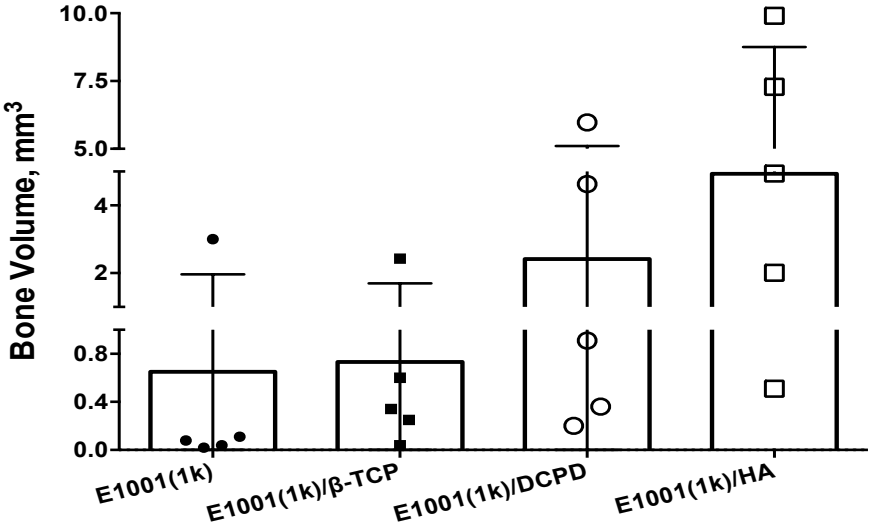

Figure 5.9 Quantified bone volume in mm3 for groups loaded with 5 μg recombinant human bone morphogenetic protein-2.

Histological analysis revealed that tissue infiltration had fully occurred 6 weeks post-implantation in all scaffolds as shown in Fig. 5.10. The macropores of scaffolds were filled with fibrous connective tissue that was characterized by good vascularization. Furthermore, cells migrated into micropores. Coated scaffolds and controls displayed similar tissue response with mild to moderate inflammation reaction. They are surrounded by a thin fibrous capsule. Scattered macrophages and multinucleated giant cells could be seen at the surface of the scaffolds. Occasional accumulation of inflammatory cells was observed. Microscopic examination of the sections taken from the group that received E1001(1k)/HA showed scattered mineralizing tissue throughout the scaffolds without rhBMP-2 supplement in all 4 samples.

ın the bone forming samples, that is, 1 and 5 μg rhBMP-2 groups, mineralized bone tissue was found in direct contact with the scaffold surface along the contour of macropores, with adjacent osteoblast-like cells, indicating osteoconductivity of calcium phosphate coating. The histological bone formation results mirrored with microCT data that calcium phosphate coated scaffolds induced significantly higher amount of bone formation than uncoated scaffolds and scaffolds mineralized with β-TCP. HA coated scaffolds yielded the most bone. The osteoinfucitve effect was surface-and dose-dependent.

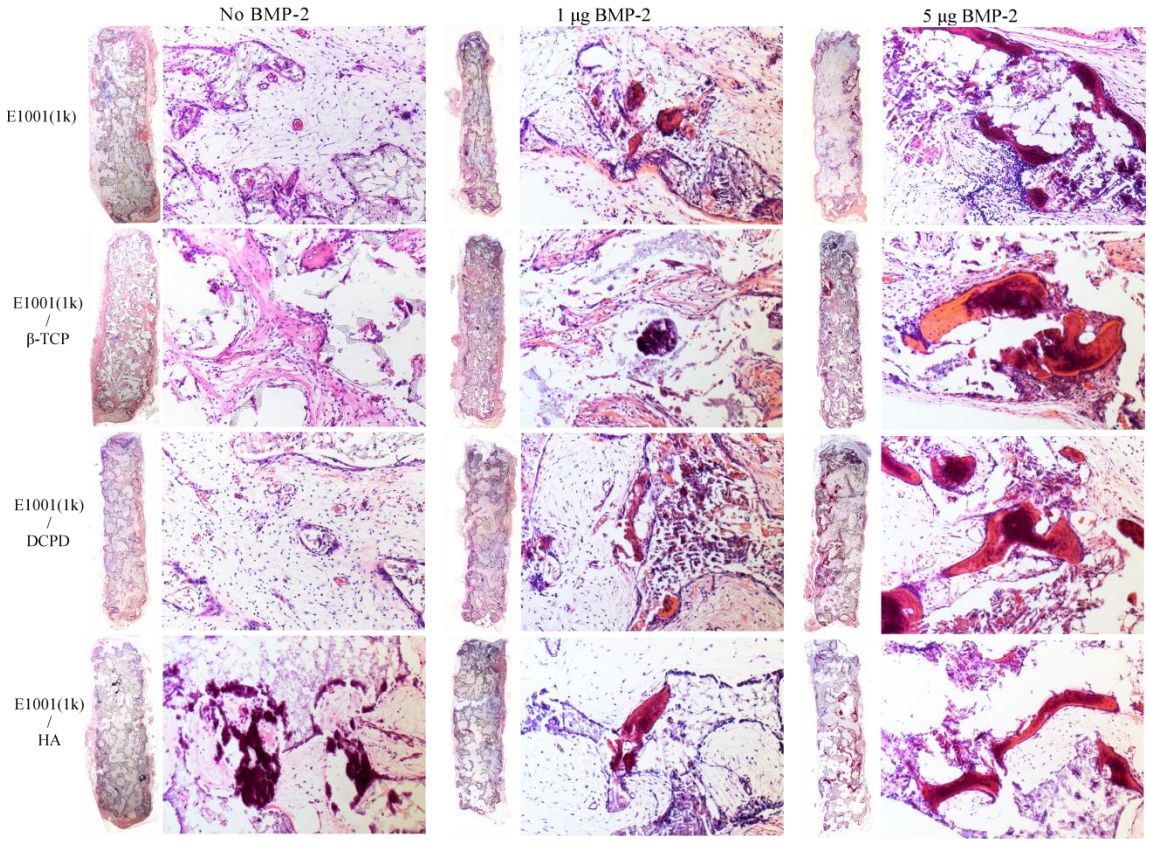

Figure 5.10 Haematoxylin and esosin staining of the scaffolds with 0, 1 and 5 µg rhBMP-2 in rat subcutis.

5.5 DISCUSSION

Alternate soaking process, coats the biomaterials with a calcium phosphate layer, has been recently utilized as a powerful method to increase the osteoconductivity of porous scaffolds [15, 22, 23]. However, the conventional ASP possesses several drawbacks including a long time for a stable apatite deposition and CaP may aggregate on the outer region of scaffolds and lead to the hindrance of cell in-growth [16, 18]. In this study, a straightforward, fast and versatile modified alternate soaking process was developed and utilized to deposit HA or DCPD on preformed E1001(1k) scaffolds. We

demonstrated that calcium phosphate coating significantly enhanced osteogenic differentiation of hMSCs *in vitro*. A synergistic effect of calcium phosphate coating and rhBMP-2 was observed in rat subcutaneous implantation. Moreover, HA coated E1001(1k) scaffolds induced tissue mineralization without any osteogenic growth factor.

The modified alternate soaking process offers significant advantages over the conventional ASP mineralization of scaffolds. First, It is fast, a substaintial amount (30 wt%) of high quality mineral coating was achieved within an hour by controlling the processing parameters precisely. The conventional biomimitic coating methods take serveral days to weeks to form a stable mineralization layer and lead to the biodegradation of polymer materials prior to their use in the tissue engineering application [17, 18, 34].

Second, the surface topography and chemical composition of the deposits can be tailored to meet the requirements for cell growth and bone regeneration. The strategy chosen in this study was to produce two different calcium phosphate coating formulations, HA or DCPD, using basic or acidic phosphate solution respectively. The mechanism of pH dependent calcium phosphate formation is well known that at acidic/basic condition, $K_2HPO_4 \bullet 3H_2O$ can dissociate into primary HPO_4^{2-} / PO_4^{3-} ions and form DCPD/HA respectively when react with Ca^{2+} ions [35-42]. The physical characterization of scaffolds has demonstrated that HA and DCPD have distinctive surface topography, crystal size (nano vs. micro respectively, Fig. 5.1A) and dissolution properties (slow vs. fast respectively, Fig. 5.3A), which are expected to have a significant effect on human bone cells, especially on their proliferation and differentiation [12, 43]. Together with other processing parameters such as Ca^{2+} and HPO_4^{2-} or PO_4^{3-}

concentration [22, 42, 44, 45], number of cycles , and Ca to P ratio [36, 40, 46], the modified alternate soaking process described herein offers a variety degree of freedom to tailor the properties of the calcium phosphate coating.

Third, the coatings deposited onto the E1001(1k) scaffolds was homogeneously distributed throughout the thickness of the samples as the cycles of vacuum, followed by a rapid release to atmospheric pressure facilitated the diffusion of calcium and phosphate solutions into the scaffold's core. Therefore, the coating did not result in the formation of non-uniform layer of calcium phosphate materials with increased thickness at the outer region of scaffolds [24], as has been reported in the literature using traditional immersion methods, especially for scaffolds without adequate pore size and interconnetivity [17, 47-49] or large dimensional scaffolds for translational clinical application. This is of significance, as a thick CaP coating can impede cell migration both *in vitro* and *in vivo*, thereby jeopardizing the regenerative outcome. Using this modified alternate soaking method, 20 mm (diameter) × 6 mm (height) scaffolds were uniformly coated with calcium phosphate and induced bone formation in goat calvarial critical size defects.

The deposition of calcium phosphate coatings on the surface of E1001(1k) scaffolds shows favorable osteoconductive properties as indicated by the increased ALP activity of hMSC in CaP coated samples regardless of culture media. Moreover, hMSC on DCPD or HA coated scaffolds cultured in basal media without osteoinduction, expressed comparable or even more ALP activity than that on E1001(1k) or E1001(1k)/β-TCP scaffolds respectively cultured in osteogenic media (Fig. 5.4C), suggesting that the calcium phosphate coating may be intrinsically osteoinductive. This is further confirmed by increased radiodensity (Fig.5.5) and ectopic tissue mineralization in rat subctis

(Fig.5.8) of E1001(1k) /HA scaffolds without rhBMP-2 after 6 weeks implantation by microCT and histology analyses respectively.

Moreover, a synergistic effect of rhBMP-2 and calcium phosphate coating was observed. In this study, the rhBMP-2 dosages (1 and 5 μg) were significantly less than the recommended dosage (10 -20 μg) [50, 51] for ectopic bone formation in rat subcutaneous pockets because we believe that calcium phosphate coating may prompt bone induction at significantly lower dosage and the high rhBMP-2 dosage is likely overshadow the effect of calcium phosphate coating. In deed, at very minimal dosage of 1 μg rhBMP-2, more animals in the calcium phosphate coated groups, especially HA coated samples, induced bone formation, as compared to uncoated scaffolds and E1001(1k)/β-TCP scaffolds. In addition, as indicated by microCT and histological analyses, for scaffolds received 5 μg rhBMP-2, significantly higher amount as well as more uniform bone formation was measured in HA or DCPD coated E1001(1k) scaffolds. Specially, E1001(1k)/HA scaffold loaded with 5 μg rhBMP-2 induced equivalent amount of bone as E1001(1k) with 10 μg rhBMP-2 (unpublished data).

Compare CaP coated vs. non-coated scaffolds, favorable *in vitro* and *in vivo* osteocnductive properties induced by calcium phosphate coating was observed. These results are in line with finding from other groups [12, 16, 18]. The deposition of a calcium phosphate coating on the surface of polymeric scaffold can promote osteogenic differentiation according to two distinct and most probably concomitant mechanisms: 1) the topography of the substrate and 2) the release of Ca^{2+} and P^{-} from the coating into the cell culture media and/or into the tissue microenvironment once implanted. It is believed that calcium phosphate coating could provide a favorable topography for cell attachment

and osteogenic differentiation by absorbing proteins and other macromolecules, leading to a biological layer that resembling a bone-like mineral matrix [6]. Furthermore, studies have suggested that the released Ca^{2+} ions [52-54]can drive specific molecular and cellular responses by directly activating intracellular mechanisms through Ca-sensing receptors [55] in osteoblastic cells, which play important role in bone formation and resportion. Moreover, the high local calcium ions concentration *in vivo* resembles the bone resorption microenvironment, thus may simulate osteogenic recruitment and differentiation and encourage bone mineralization [53, 54].

Compare to E1001(1k)/β-TCP scaffolds prepared by bulk composite method, HA or DCPD coated scaffolds have demonstrated to be more osteoconductive as well as better vehicles for rhBMP-2 delivery. Previous comparative evaluation of scaffolds without rhBMP-2 using goat calvarial defect model has shown that CaP coated scaffolds regenerated significantly more bone than E1001(1k)/β-TCP scaffolds, likely due to more exposed calcium phosphate on scaffold surface. In this study, we further demonstrated that, loaded with the same amount of rhBMP-2, calcium phosphate coated scaffolds induced a higher amount bone than E1001(1k)/ β-TCP scaffolds after rat subcutaneous implantation, suggesting that they are better vehicles for rhBMP-2 delivery. The superior osteoconductivity and osteoinductivity of calcium phosphate coated scaffolds can be attributed to the methods of scaffold preparation. In the bulk composite method, where CaP particles are blended with polymer matrix as fillers, although the most often used, embedding of CaP within the polymer often results the formation of a thin layer of polymer skin covering the inorganic particles that may lead to the masking of its bioactivity and rhBMP-2 binding sites [16, 18]. Calcium phosphate coating provides

increased CaP-cell contact [12], thus attributed to its increased osteoconductivity and osteoinductivity. Moreover, calcium phosphate coating provides exposed surface sites for rhBMP-2 binding and retention, which is of significant because it has been suggested that prolong rhBMP-2 retention can further enhance bone regeneration.[56, 57]

The coatings were extensively characterized prior to implantation to understand the differences between materials, and ectopic bone induction to identify potential correlations regarding the relative efficacy of each coating. As revealed by SEM images, HA coating consisted of a layer of nano-sized fine grains that cover the surface of porous scaffolds. The nano-sized coating may be advantageous by providing enhanced surface area for cell attachment [58] and rhBMP-2 binding [59]. In this study, it was found that HA coating improved the hydrophilicity of the scaffold the most and allowed for rapid and uniform rhBMP-2 infiltration. In addition, HA coating on 3D porous scaffoled resembled the chemical composition as well as 3D strcutre of bone, which may contribute to its capacity for ectopic bone formation in the absence of exogenous osteogenic growth factor. On the other hand, DCPD minerals are micro-sized that did not cover the surface of scaffolds but filling the macropores instead. The high solubility of DCPD and its ability to convert to HA may be advantageous to accelerate bone formation at early healing stage [53, 54]. In the goat calvarial critical size defect study, we observed that DCPD coated scaffold bridged the 20 mm defect in 16 weeks. DCPD exhibited 5 to 6 time higher calcium ion concentration in PBS than HA. It degrades solely by dissolution [60] in PBS until day 14 and then transformed to a more thermodynamically stable HA phase. However, we found that DCPD did not convert to HA *in vivo*, but fully degraded after 6 weeks implantation, probably due to cellular decomposition mainly by

macrophages and giant cells [61]. Nevertheless, the results obtained in this study suggest that the coated scaffold platform demonstrated a synergistic effect between calcium phosphate coatings and rhBMP-2 delivery and may provide a promising platform for the functional restoration of large bone defects.

5.6 Conclusion

In the present study, we developed and utilized a modified alternate soaking process to deposit HA or DCPD coating on preformed E1001(1k) porous scaffolds. The capacity of fabricated scaffolds for bone formation was investigated *in vitro* using human mesenchymal stem cells (hMSCs) and *in vivo* in the rat subcutaneous pockets loaded with different doses of rhBMP-2 (0, 1 and 5 μg). The osteogenic outcomes were compared to uncoated scaffold and E1001(1k)/β-TCP scaffold, prepared as a bulk composite. It was demonstrated that the deposition of calcium phosphate coating on the surface of scaffolds showed favorable osteoconductive properties as confirmed by increased ALP activity. In addition, E1001(1k)/HA scaffold showed the capacity for ectopic bone formation in the absence of exogenous osteogenic growth factor. Furthermore, a synergistic effect was observed between calcium phosphate coatings and rhBMP-2 delivery. Therefore, calcium phosphate coated scaffold may provide a promising platform for the functional restoration of large bone defects.

Reference

[1] De Long WG, Jr., Einhorn TA, Koval K, McKee M, Smith W, Sanders R, et al. Bone grafts and bone graft substitutes in orthopaedic trauma surgery. A critical analysis. J Bone Joint Surg Am 2007;89:649-58.

[2] Amini AR, Laurencin CT, Nukavarapu SP. Bone Tissue Engineering: Recent Advances and Challenges. Critical reviews in biomedical engineering 2012;40:363-408.

[3] Legeros RZ. Biodegradation and bioresorption of calcium phosphate ceramics. Clinical materials 1993;14:65-88.

[4] LeGeros RZ. Calcium phosphate-based osteoinductive materials. Chemical reviews 2008;108:4742-53.

[5] LeGeros RZ. Properties of osteoconductive biomaterials: calcium phosphates. Clinical orthopaedics and related research 2002;395:81-98.

[6] Barrère F, van Blitterswijk CA, de Groot K. Bone regeneration: molecular and cellular interactions with calcium phosphate ceramics. international Journal of Nanomedicine 2006;1:317.

[7] Rezwan K, Chen Q, Blaker J, Boccaccini AR. Biodegradable and bioactive porous polymer/inorganic composite scaffolds for bone tissue engineering. Biomaterials 2006;27:3413-31.

[8] Wei G, Ma PX. Structure and properties of nano-hydroxyapatite/polymer composite scaffolds for bone tissue engineering. Biomaterials 2004;25:4749-57.

[9] Haaparanta AM, Haimi S, Ellä V, Hopper N, Miettinen S, Suuronen R, et al. Porous polylactide/β-tricalcium phosphate composite scaffolds for tissue engineering applications. Journal of tissue engineering and regenerative medicine 2010;4:366-73.

[10] Cao L, Duan P-G, Wang H-R, Li X-L, Yuan F-L, Fan Z-Y, et al. Degradation and osteogenic potential of a novel poly (lactic acid)/nano-sized β-tricalcium phosphate scaffold. international Journal of Nanomedicine 2012;7:5881.

[11] Andiappan M, Sundaramoorthy S, Panda N, Meiyazhaban G, Winfred SB, Venkataraman G, et al. Electrospun eri silk fibroin scaffold coated with hydroxyapatite for bone tissue engineering applications. Progress Biomater 2013;2.

[12] Surmenev RA, Surmeneva MA, Ivanova AA. Significance of calcium phosphate coatings for the enhancement of new bone osteogenesis–A review. Acta biomaterialia 2014;10:557-79.

[13] Nandakumar A, Yang L, Habibovic P, van Blitterswijk C. Calcium phosphate coated electrospun fiber matrices as scaffolds for bone tissue engineering. Langmuir 2009;26:7380-7.

[14] Lu X, Leng Y. Theoretical analysis of calcium phosphate precipitation in simulated body fluid. Biomaterials 2005;26:1097-108.

[15] Furuzono T, Taguchi T, Kishida A, Akashi M, Tamada Y. Preparation and characterization of apatite deposited on silk fabric using an alternate soaking process. Journal of biomedical materials research 2000;50:344-52.

[16] Vaquette C, Ivanovski S, Hamlet SM, Hutmacher DW. Effect of culture conditions and calcium phosphate coating on ectopic bone formation. Biomaterials 2013;34:5538-51.

[17] He C, Xiao G, Jin X, Sun C, Ma PX. Electrodeposition on nanofibrous polymer scaffolds: Rapid mineralization, tunable calcium phosphate composition and topography. Advanced functional materials 2010;20:3568-76.

[18] Seyedjafari E, Soleimani M, Ghaemi N, Shabani I. Nanohydroxyapatite-Coated Electrospun Poly(l-lactide) Nanofibers Enhance Osteogenic Differentiation of Stem Cells and Induce Ectopic Bone Formation. Biomacromolecules 2010;11:3118-25.

[19] Kokubo T, Takadama H. How useful is SBF in predicting in vivo bone bioactivity? Biomaterials 2006;27:2907-15.

[20] Liu Y, Wu G, de Groot K. Biomimetic coatings for bone tissue engineering of critical-sized defects. Journal of the Royal Society Interface 2010:rsif20100115.

[21] Yang F, Wolke J, Jansen J. Biomimetic calcium phosphate coating on electrospun poly (ε-caprolactone) scaffolds for bone tissue engineering. Chemical Engineering Journal 2008;137:154-61.

[22] Taguchi T, Kishida A, Akashi M. Apatite formation on/in hydrogel matrices using an alternate soaking process (III): Effect of physico-chemical factors on apatite formation on/in poly (vinyl alcohol) hydrogel matrices. Journal of Biomaterials Science, Polymer Edition 1999;10:795-804.

[23] Taguchi T, Kishida A, Akashi M. Hydroxyapatite Formation on/in Poly (vinyl alcohol) Hydrogel Matrices Using a Novel Alternate Soaking Process. Chemistry Letters 1998:711-2.

[24] Li H, Zhu R, Sun L, Xue Y, Hao Z, Xie Z, et al. Effect of Thickness of HA-Coating on Microporous Silk Scaffolds Using Alternate Soaking Technology. BioMed Research International 2014;2014:8.

[25] Magno MHR, Kim J, Srinivasan A, McBride S, Bolikal D, Darr A, et al. Synthesis, degradation and biocompatibility of tyrosine-derived polycarbonate scaffolds. Journal of Materials Chemistry 2010;20:8885-93.

[26] Kim J, Magno MHR, Waters H, Doll BA, McBride S, Alvarez P, et al. Bone regeneration in a rabbit critical-sized calvarial model using tyrosine-derived polycarbonate scaffolds. Tissue Engineering Part A 2012;18:1132-9.

[27] Kim J, Magno MHR, Alvarez P, Darr A, Kohn J, Hollinger JO. Osteogenic differentiation of pre-osteoblasts on biomimetic tyrosine-derived polycarbonate scaffolds. Biomacromolecules 2011;12:3520-7.

[28] Jinku K, Sean M, Amy D, Aniq D, Maria Hanshella RM, Jeffrey OH. Tyrosine-derived polycarbonate scaffolds for bone regeneration in a rabbit radius critical-size defect model. Biomedical Materials 2015;10:035001.

[29] Ertel SI, Kohn J. Evaluation of a series of tyrosine-derived polycarbonates as degradable biomaterials. Journal of biomedical materials research 1994;28:919-30.

[30] James K, Levene H, Parsons JR, Kohn J. Small changes in polymer chemistry have a large effect on the bone–implant interface:: evaluation of a series of degradable tyrosine-derived polycarbonates in bone defects. Biomaterials 1999;20:2203-12.

[31] Johnsson MS, Nancollas GH. The role of brushite and octacalcium phosphate in apatite formation. Crit Rev Oral Biol Med 1992;3:61-82.

[32] Kanzaki N, Onuma K, Treboux G, Ito A. Dissolution kinetics of dicalcium phosphate dihydrate under pseudophysiological conditions. Journal of Crystal Growth 2002;235:465-70.

[33] Bohner M. Calcium orthophosphates in medicine: from ceramics to calcium phosphate cements. Injury 2000;31, Supplement 4:D37-D47.

[34] Escada ALdA, Machado JPB, Claro APRA. Characterization of Calcium Phosphate Coating Produced by Biomimetic Method. Materials Research 2015;18:3-8.

[35] Dorozhkin SV. Calcium orthophosphates: Occurrence, properties, biomineralization, pathological calcification and biomimetic applications. Biomatter 2011;1:121-64.

[36] Mekmene O, Quillard S, Rouillon T, Bouler J-M, Piot M, Gaucheron F. Effects of pH and Ca/P molar ratio on the quantity and crystalline structure of calcium phosphates obtained from aqueous solutions. Dairy Sci Technol 2009;89:301-16.

[37] Toshima T, Hamai R, Tafu M, Takemura Y, Fujita S, Chohji T, et al. Morphology control of brushite prepared by aqueous solution synthesis. Journal of Asian Ceramic Societies 2014;2:52-6.

[38] Santos MH, Oliveira Md, Souza LPdF, Mansur HS, Vasconcelos WL. Synthesis control and characterization of hydroxyapatite prepared by wet precipitation process. Materials Research 2004;7:625-30.

[39] Marshall RW, Nancollas GH. Kinetics of crystal growth of dicalcium phosphate dihydrate. The Journal of Physical Chemistry 1969;73:3838-44.

[40] Osaka A, Miura Y, Takeuchi K, Asada M, Takahashi K. Calcium apatite prepared from calcium hydroxide and orthophosphoric acid. J Mater Sci: Mater Med 1991;2:51-5.

[41] Oliveira C, Ferreira A, Rocha F. Dicalcium Phosphate Dihydrate Precipitation: Characterization and Crystal Growth. Chemical Engineering Research and Design 2007;85:1655-61.

[42] Ferreira A, Oliveira C, Rocha F. The different phases in the precipitation of dicalcium phosphate dihydrate. Journal of Crystal Growth 2003;252:599-611.

[43] Barrère F, van Blitterswijk CA, de Groot K. Bone regeneration: molecular and cellular interactions with calcium phosphate ceramics. international Journal of Nanomedicine 2006;1:317-32.

[44] Strange DGT, Oyen ML. Biomimetic bone-like composites fabricated through an automated alternate soaking process. Acta biomaterialia 2011;7:3586-94.

[45] Monmaturapoj N. Nano-size hydroxyapatite powders preparation by wet-chemical precipitation route. Journal of Metals, Materials and Minerals 2008;18:15-20.

[46] Cheng P-T, Pritzker KP. Solution Ca/P ratio affects calcium phosphate crystal phases. Calcified tissue international 1983;35:596-601.

[47] Madurantakam PA, Rodriguez IA, Cost CP, Viswanathan R, Simpson DG, Beckman MJ, et al. Multiple factor interactions in biomimetic mineralization of electrospun scaffolds. Biomaterials 2009;30:5456-64.

[48] Mavis B, Demirtas TT, Gumusderelioglu M, Gunduz G, Colak U. Synthesis, characterization and osteoblastic activity of polycaprolactone nanofibers coated with biomimetic calcium phosphate. Acta Biomater 2009;5:3098-111.

[49] Yu HS, Jang JH, Kim TI, Lee HH, Kim HW. Apatite-mineralized polycaprolactone nanofibrous web as a bone tissue regeneration substrate. J Biomed Mater Res A 2009;88:747-54.

[50] Hall J, Sorensen RG, Wozney JM, Wikesjo UM. Bone formation at rhBMP-2-coated titanium implants in the rat ectopic model. J Clin Periodontol 2007;34:444-51.

[51] Lee J-H, Kim C-S, Choi K-H, Jung U-W, Yun J-H, Choi S-H, et al. The induction of bone formation in rat calvarial defects and subcutaneous tissues by recombinant human BMP-2, produced in Escherichia coli. Biomaterials 2010;31:3512-9.

[52] Hoppe A, Guldal NS, Boccaccini AR. A review of the biological response to ionic dissolution products from bioactive glasses and glass-ceramics. Biomaterials 2011;32:2757-74.

[53] Barradas AM, Fernandes HA, Groen N, Chai YC, Schrooten J, van de Peppel J, et al. A calcium-induced signaling cascade leading to osteogenic differentiation of human bone marrow-derived mesenchymal stromal cells. Biomaterials 2012;33:3205-15.

[54] Barradas AM, Monticone V, Hulsman M, Danoux C, Fernandes H, Tahmasebi Birgani Z, et al. Molecular mechanisms of biomaterial-driven osteogenic differentiation in human mesenchymal stromal cells. Integr Biol 2013;5:920-31.

[55] Marie PJ. The calcium-sensing receptor in bone cells: a potential therapeutic target in osteoporosis. Bone 2010;46:571-6.

[56] Winn SR, Uludag H, Hollinger JO. Sustained release emphasizing recombinant human bone morphogenetic protein-2. Advanced Drug Delivery Reviews 1998;31:303-18.

[57] Autefage H, Briand-Mésange F, Cazalbou S, Drouet C, Fourmy D, Gonçalvès S, et al. Adsorption and release of BMP-2 on nanocrystalline apatite-coated and uncoated hydroxyapatite/β-tricalcium phosphate porous ceramics. Journal of Biomedical Materials Research Part B: Applied Biomaterials 2009;91B:706-15.

[58] Heo SJ, Kim SE, Wei J, Kim DH, Hyun YT, Yun HS, et al. In vitro and animal study of novel nano-hydroxyapatite/poly(epsilon-caprolactone) composite scaffolds fabricated by layer manufacturing process. Tissue Eng Part A 2009;15:977-89.

[59] King WJ, Krebsbach PH. Growth factor delivery: How surface interactions modulate release in vitro and in vivo. Advanced Drug Delivery Reviews 2012;64:1239-56.

[60] Tas AC, Bhaduri SB. Preparation of brushite powders and their in vitro conversion to nanoapatites. Bioceramics: Materials and Applications V: Proceedings of the 106th Annual Meeting of The American Ceramic Society, Indianapolis, Indiana, USA 2004, Ceramic Transactions: Wiley-American Ceramic Society; 2005. p. 119.

[61] Theiss F, Apelt D, Brand B, Kutter A, Zlinszky K, Bohner M, et al. Biocompatibility and resorption of a brushite calcium phosphate cement. Biomaterials 2005;26:4383-94.

6

Novel Tyrosine-derived Polycarbonate / Dicalcium Phosphate Dihydrate Composite Scaffolds Induce Complete Bridging of Goat Critical Size Calvarial Defect

6.1 Abstract

Reconstruction of large segmental bone defects remains a significant clinical problem. Due to the limitations of autografts and allografts, there is an urgent demand for bone graft substitutes. In the present study, a novel three-dimensional (3D) porous bone regeneration scaffold based on E1001(1k), a member of large combinational library of tyrosine-derived polycarbonates (TyrPC) and dicalcium phosphate dihydrate (DCPD) were prepared and evaluated for bone regeneration in goat calvarial 20 mm critical size defects (CSD). The osteogenic outcomes were assessed using microcomputed tomography (microCT) and histological analyses16 weeks post-implantation and compared to a commercial bone graft substitute (chronOS) and E1001(1k) scaffolds mineralized with beta-tricalcium phosphate (β-TCP). The results from microCT and histomorphometric analyses revealed that E1001(1k)/DCPD scaffolds demonstrated significantly greater ostegenic regeneration and complete bridging of the defects was discovered in 3 out of 6 animals. It is for the first in the literature that complete bridging

of critical size defect in large animal model was observed using polymer/calcium phosphate composite scaffolds without the addition of any osteogenic growth factors. The results obtained in this study demonstrated that E1001(1k)/DCPD scaffolds have excellent bone regeneration capacity and may be the next-generation synthetic bone graft substrate for large bone defect repair.

6.2 Introduction

The reconstruction of critical size bone defects resulting from trauma, tumor resection, congenital abnormalities or reconstructive surgery remains a significant clinical problem [1, 2]. The current 'gold standard' to treat those bony defects is autograft, known to produce the best clinical outcome because it possesses osteoconductivity and osteoinductivity, two properties that contribute to successful bone regeneration [1, 3]. However, the use of autologous bone has its limitations such as donor site morbidity, increased surgery time, and limited available quantity [1, 4]. Due to these limitations, there remains a clinical demand for bone graft substitutes (BGS) that can treat large critical size bone defects.

Polymer scaffolds in combination with calcium phosphates (CaPs) have been widely investigated and designed as BGS to mimic the chemical composition and structure of human bone [1, 5]. Of the many CaPs, hydroxyapatite (HA) and beta tri-calcium phosphate (β-TCP) are the most commonly studied for bone applications and have been shown to promote new bone growth through enhanced biocompatibility [6, 7], osteoconductivity and osteointegration [6, 8]. Alternatively, our group has taken a particular interest in dicalcium phosphate dihydrate (DCDP) or brushite, which is

believed as one of the precursors of biological apatite in bone and tooth [9, 10]. Contrary to HA or β-TCP, DCPD is a metastable CaP phase at physiological conditions. Therefore, it has high solubility and resorbs much faster (the comparative solubility of these CaPs are as follows: DCPD > β-TCP > sintered HA) [11, 12]. Moreover, it has been used in hydraulic calcium phosphate cements and coatings for metallic implants since the 1990s [13, 14].

Although CaPs are commonly blended with the polymer to produce bulk composite scaffolds, these fabrication methods typically form a polymer skin that covers the CaP and masks its bioactivity. In deed, marginal bone regeneration is typically observed in large critical size defect and substantial amount of osteogenic growth factors such as recombinant human bone morphogenetic protein-2 (rhBMP-2) is often required to achieve considerable bone healing and regeneration. Recently, biomimetic coating methods based on immersion in simulated body fluid [15-17] or the alternate soaking process [18, 19] have been utilized to deposit a layer of calcium phosphate material on the surface of 3D porous scaffold [15, 20]. It is believed that CaP coating could provide a favorable topography for cell attachment and osteogenic differentiation [20]. Most of these studies have focused on the *in vitro* influences of the biomimetic coating at a cellular level, only a few *in vivo* studies, either ectopically and or in a critical size defect model, have been reported. There is still a lack of conclusive data regarding the osteo-promotive effect of biomimetic CaP-coated polymeric scaffolds, especially in large animal model.

Our group has developed a E1001(1k) scaffold produced by porogen leaching combined with freeze-drying method for bone regeneration. E1001(1k) is a member of a

large combinatorial library of tyrosine-derived polycarbonates (TyrPC) whose propertied can be tailored for different tissue engineering applications by tuning the compositions. E1001(1k) scaffolds have demonstrated favorable pore size, porosity and interconnectivity for permitting *in vivo* bone and vascular ingrowth in many rabbit calvarial and radius defect models.

The objective of this study was to investigate the safety and efficacy of E1001(1k) scaffolds containing CaP in the goat calvarial critical size 20 mm defect model. Two E1001(1k)-based scaffolds were evaluated: 1) E1001(1k) scaffolds fabricated as a bulk composite with β-TCP (abbreviated as E1001(1k)/β-TCP scaffolds), and 2) E1001(1k) scaffolds coated with DCPD (abbreviated as E1001(1k)/DCPD scaffolds). The bone regeneration potential of those scaffolds was compared to 1) a commercially available bone graft substitute made of poly(lactide co-ε-caprolactone) and β-TCP (chronOS), and 2) E1001(1k)/β-TCP supplemented with recombinant human bone morphogenetic protein (rhBMP-2, 400 μg/scaffold) as positive controls. To the best of our knowledge, this study is the first report on *in vivo* evaluation of a biomimetic CaP-coated polymeric scaffolds in a large animal model. The scaffolds were extensively characterized prior to implantation. The healing of the defect was assessed using microcomputed tomography (microCT) and histological analyses 16 weeks post-implantation.

6.3 Materials and methods

6.3.1 Materials

Sodium chloride (NaCl), calcium chloride ($CaCl_2$), potassium phosphate dibasic trihydrate ($K_2HPO_4 \cdot 3H_2O$) were obtained from Sigma-Aldrich Chemical Co. (St. Louis, MO). The NaCl particles were sieved to select particles with sizes in the range of 212-425 μm and used as a porogen in scaffold fabrication. β-TCP (100 nm) powders were purchased from Berkeley Advanced Biomaterials, Inc. (Berkeley, CA). 1,4-Dioxane was obtained from Fischer Scientific (Pittsburgh, PA). Poly(DTE-co-10 mol% DT-co-1 mol% PEG_{1k} carbonate), abbreviated E1001(1k), was synthesized according to published procedures [21] at the New Jersey Center for Biomaterials (Piscataway, NJ). DTE stands for deaminotyrosyl tyrosine ethyl ester, DT for desaminotyrosyl tyrosine, and PEG_{1k} for poly(ethylene glycol) with a molecular weight of 1 kDa. chronOS was obtained from DePuy Synthes (West Chester, PA). rhBMP-2 was purchased from Wyeth-Genetics Institute, Inc. (Cambridge, MA).

6.3.2 Scaffold fabrication

E1001(1k)/β-TCP scaffolds were prepared by a minor modification to our previously published salt leaching and freeze-drying method [7, 22]. Briefly, 12.2 g E1001(1k) polymer was dissolved in 8.54 ml deionized (DI) water and 52.46 ml 1,4-dioxane overnight. The polymer solution was uniformly mixed with 109.8 g NaCl and 12.2 g β-TCP powders using an overhead mixer (EuroStar Power Control Visc Stirrer, IKA® Works, Inc., Wilmington, NC) at 500 rpm for 10 min. The mixture was then

poured into two Teflon molds (60 mm in diameter × 20 mm in height). The samples were frozen at -50 ºC for 6 h, and freeze-dried at 0 ºC for 24 h and at 20 ºC for another 24 h using a computer-controlled large-scale lyophilizer (LD85, Millrock Technology, Kinston, NY). After drying, disk-shaped scaffolds (20 mm in diameter) were punched out from the molds using a custom-designed puncher. The salt particles were completely removed by washing the scaffolds in distilled water. Then, the top and bottom nonporous skins were sliced off using blades and a custom-designed holder to produce scaffolds with final dimensions of 20 mm in diameter × 6 mm in height. Finally, the scaffolds were dried in the lyophilizer at room temperature for 24 h.

E1001(1k)/DCPD scaffolds were prepared by coating E1001(1k) scaffolds with DCPD minerals using a modified alternate soaking process. Briefly, E1001(1k) scaffolds were first prepared using the salt leaching and freeze-drying process without β-TCP described above. Each E1001(1k) scaffold was placed into a separate well of a custom-designed alternate soaking chamber (16 wells per chamber) and immersed in 20 ml of 0.25 M $CaCl_2$ solution (pH = 6). Vacuum (up to 30 inHg) was applied to the chamber for 1 min, followed by the rapid release to atmospheric pressure; this step was repeated 5 times to completely wet the scaffolds with $CaCl_2$ solution. Then, the scaffolds were removed from the $CaCl_2$ solution and pat-dried with a kimwipe to remove excess solution on the scaffold surface. The scaffolds were then transferred to 0.25 M $K_2HPO_4 \cdot 3H_2O$ solution (pH = 6), and the same vacuum and atmospheric pressure cycles were used to force the phosphate solution into the interior of the 3D scaffolds to react with the $CaCl_2$ to form calcium phosphate. The scaffolds were alternated in calcium (Ca) and phosphate

(P) solutions until 50% calcium phosphate by weight was obtained. The solutions were refreshed after every 5 cycles. Finally, scaffolds were dried in a lyophilizer for 24 h.

6.3.3 Scaffold characterization

Samples of the freeze-dried scaffolds were cut using a razor blade and sputter coated with gold/palladium (30 mA, 2 min, SCD 004 sputter coater). The scaffold morphology and microstructure were observed using a scanning electron microscope (SEM, AMRAY-1830I) at an acceleration potential of 20 kV.

X-ray diffraction (XRD) patterns of scaffolds were obtained using a Philips X'Pert X-ray diffractometer operating at 40 kV and 40 mA (Cu-K α radiation: λ=1.5406). The scaffolds were scanned from 5° to 90° at step size of 0.02° and scan step time of 1 sec. The X-ray diffractogram was analyzed using PANalytical HighScore Plus software and compared with the standard library of known diffraction patterns, International Centre for Diffraction Data (ICDD), to identify the phase of the calcium phosphate present in the scaffolds. The percent of Ca and P (by weight) incorporated into the scaffolds was determined via elemental analysis using inductively coupled plasma optical emission spectrometry (ICP-OES, Intertek). The Ca to P ratio was calculated. Analysis was done in triplicate.

The porosity of the scaffolds was determined using a helium pycnometer (Porous Material, Inc). Brunauer-Emmett-Teller (BET) specific surface area of the scaffolds was determined using BET Sorptometer (Porous Material, Inc). Scaffolds prior to implantation were also scanned in an eXplore Locus microcomputed tomography (microCT, GE Healthcare) at a resolution of 20 μm, voltage of 80 kVp and current of 150

mA. 3D images of the scaffolds were reconstructed from the scans by the microCT system software package. The total porosity, total pore volume, and largest pore volume were obtained.

The compressive elastic moduli of scaffolds were measured using ReNew MTS Systems 4 (crosshead speed of 0.5 mm/min and a load cell of 100 N). To more accurately mimic the mechanical properties of scaffolds *in vivo,* the scaffolds were pre-wet in phosphate buffered saline (PBS) overnight and the mechanical tests were carried out in PBS at 37 °C. The data were collected and analyzed using TestWork 4 (Ver.4.11C; MTS Systems).

The molecular weight of the scaffolds was determined using gel permeation chromatography (GPC) relative to polystyrene standards following a published procedure [21].

6.3.4 Scaffold Sterilization

The scaffolds were sterilized using ethylene oxide (EtO) at Johnson & Johnson Sterility Assurance Group (Raritan, NJ). Scaffolds before and after sterilization were characterized according to Section 6.3.3 in triplicate.

6.3.5 Goat calvarial surgery and necropsy

The Institutional Animal Care and Use Committee (IACUC) at Allegheny Singer Research Institute (Pittsburgh, PA) and the Department of Defense United States Army Medical Research and Materiel Command Animal Care and Use Review Office (ACURO) approved all surgical procedures involving animals. Proper handling, housing,

care, and standard caprine food was given to the animals according to the guidelines posted by Allegheny Singer Research Institute's IACUC, the Animal Welfare Act, and the National Research Council.

Adult skeletally mature Boer Cross female goats weighting 36-57 kg were used for the study. A randomized experiment was conducted to determine the effect of scaffold composition on healing in a critical sized calvaria defect (CSD, 20 mm diameter). Animals were anaesthetized with an intravenous injection of propofol and anesthetic maintenance was performed through inhalation of isoflurane gas. A 7 cm incision was made through the skin and the periosteum was removed using Bovie electrocautery pen. A 20 mm calvarial defect (Fig.6.1) was created along the sagittal suture just slightly posterior to the intersection of the coronal suture using a surgical trephine with copious physiological saline for irrigation. The dura was kept intact. One scaffold per craniotomy per goat were then randomly inserted (press fit). The treatment groups (Table 1) are: (1) E1001(1k)/β-TCP scaffolds, (2) E1001(1k)/DCPD scaffolds, (3) E1001(1k)/ β-TCP scaffolds + 400 μg rhBMP-2, and (4) chronOS. For scaffolds containing rhBMP-2, 200 μg rhBMP-2 in 325 μl of PBS was delivered drop-wise via micropipette and dried in the biological safety cabinet (BSC) for 2 hours followed by a second 325uL aliquot on the other side of the scaffold and dried for an additional 2 hours in the BSC prior to insertion. Following insertion of the scaffold into the defect, deep tissue, including musculature, was closed with inverted resorbable sutures, and the skin was closed with a non-resorbable running/lock-stitch suture. Once the animals were upright and ambulatory, they were returned to the animal housing facility for the remainder of the study (16 weeks in life). At 16 weeks post-implantation, goats were euthanized humanely. The samples

were explanted with surrounding bone and grossly examined for signs of infection, inflammation and bone resorption. The bone blocks were fixed in 10% neutral buffered formalin and prepared for microCT and histological analyses.

Figure 6.1 Photographs of (A) an E1001(1k)-based scaffold with dimension of 20 mm diameter × 6 mm thick (ruler is in cm), (B) 20 mm goat calvarial critical size defect, (C) an implant fitted snuggly into the defect.

Table 6.1Treatment groups

Group No.	**Scaffold Formulation**	**Biologics**	**Number of Goats (n)**
1	E1001(1k)/DCPD	None	6
2	E1001(1k)/β-TCP	None	6
3	chronOS	None	7
4	E1001(1k)/β-TCP	400 μg rhBMP-2	7

6.3.6 Microcomputed tomography (microCT)

X-ray projections of the explants were collected using an eXplore Locus microCT (GE Healthcare) according to a published procedure (80 kVp; 500 mA, 30 min/sample, and 20 μm voxel resolution) [95]. Three-dimensional (3D) construction of the projection images was performed on a 4PC Unix Cluster (8 GB RAM, ~ 60 min to reconstruct each volume) using a modified tent-FDK cone beam algorithm. The images were segmented using predefined Housfield Unit thresholds (calcium phosphate, cortical bone, trabecular/woven bone, and scaffold content: >3000, 2000-3000, 750-2000, and 300-750, respectively) and a 3D histomorphometric analysis was performed using Matlab. The new bone volume (BV) and bone mineral density (BMD) were calculated. BV was normalized to total volume (TV) within the region of interest (ROI), as an indicator of the relative amount of newly formed bone.

6.3.7 Histology and histomorphometry

The specimens were dehydrated in ascending concentration of ethanol from 50% to 100%, infiltrated with a clearing agent, then embedded in polymethylmethacrylate (PMMA). The PMMA blocks were then cut and grounded to 60 μm thick sections with a Buegker Isomet low-speed diamond blade saw and Buehler Handimet. Plane sections cut at 45° from the sagittal suture through the center of the defects were stained with Stevenel's Blue and counterstained with van Gieson's picrofuchsin, which stains bone red and nonmineralized structures various shades of blue. Gigapixel images of the whole cross sections were obtained. A ROI was delineated and the percentage area of new bone was calculated in relation to the total ROI. The linear distance of new bone ingrowth

from the defect margins was measured and divided by the defect length to calculate linear ingrowth percentage (LI), an indicator of the spatial pattern of bone ingrowth.

6.3.8 Statistics

Statistical analyses were performed using single factor analysis of variance (ANOVA) followed by a multiple comparison post-hoc test (Tukey-Kramer method) with a significance level established as $p \leq 0.05$. All statistical analyses were carried out using GraphPad Prism 6 software package. All data were reported as mean ± standard deviation (SD).

6.4 Results

6.4.1 Scaffold preparation and characterization

The average dimensions of E1001(1k)-based scaffolds were 20.2 ± 0.1 mm (diameter) × 5.8 ± 0.1 mm (thick) and the average mass was 359 ± 18 mg (n = 60). The microstructure of the scaffolds was analyzed using SEM (Fig. 6.2A). Both E1001(1k)-based scaffolds displayed a highly porous and interconnected structure with macropores ranging from 200 to 400 μm (top row of Fig. 6.2A). In addition, many micropores with diameters less than 20 μm were observed within the walls of the macropores. Images at higher magnification (bottom row of Fig. 6.2A) show the detailed surface topography of the macropore walls. For E1001(1k)/β-TCP scaffolds, small particles were uniformly dispersed throughout the polymer matrix and some particles were embedded within the matrix. For E1001(1k)/DCPD scaffolds, large plate-liked crystals were well exposed on

the polymer surface and occupied some space within the macropores. In contract, chronOS appeared significantly less porous with minimal interconnectivity.

Fig. 6.2B shows XRD scans of CaP-containing scaffolds. The scans of E1001(1k)/β-TCP scaffold and chronOS displayed characteristic peaks at 27.8°, 31° and 34.4°, indicating the presence of β-TCP. Although chronOS contains a higher amount of β-TCP than E1001(1k)/β-TCP scaffolds (70 vs. 50 wt%, respectively), the characteristic peaks for β-TCP were at a lower intensity. This is likely due to the coverage of β-TCP particles by the polymer during the fabrication process of chronOS. The XRD scans of E1001(1k)/DCPD scaffolds showed peaks at 11.65°, 20.949° and 29.296°, which are characteristics of DCPD (ICDD #01-072-0713). The identify of calcium phosphates was further confirmed by calcium to phosphate ratio measured from elemental analysis using inductively coupled plasma optical emission spectrometry. It was measured that the Ca to P ratios of E1001(1k)/β-TCP scaffolds, E1001(1k)/DCPD scaffolds, and chronOS were 1.57 ± 0.05, 1.07 ± 0.01, and 1.46 ± 0.02, respectively, which agree with their theoretical values (1 for DCPD and 1.5 for β-TCP).

Helium pyconometry measurements showed that the porosity of E1001(1k)-based scaffolds with and without the incorporation of CaP was nearly 1.8 times higher than chronOS (90% vs. 50%, respectively) (Fig. 6.3A). In addition, BET specific surface area (SSA) measurements showed that E1001(1k)-based scaffolds had a SSA of 0.22-0.35 m^2/g, which was 5 times higher than that of chronOS (0.071 m^2/g) (Fig. 6.3B). The high SSA of E1001(1k)-based scaffolds may be attributed to the large quantity of micropores present on the scaffolds' pore walls, as shown in the SEM images of Fig 6.2A. Moreover, E1001(1k)-based scaffolds demonstrated a slightly higher, although not statistically

significant, compressive elastic modulus than ChronOS, (Fig. 6.3C). No significant effect of EtO sterilization on scaffold porosity, BET SSA, compressive elastic modulus and polymer molecular weight was measured (Fig. 6.3D). In addition, no significant change in scaffold morphology and CaP phase was observed (data not shown), suggesting that exposure to EtO gas is a suitable sterilization method for E1001(1k)-based scaffolds.

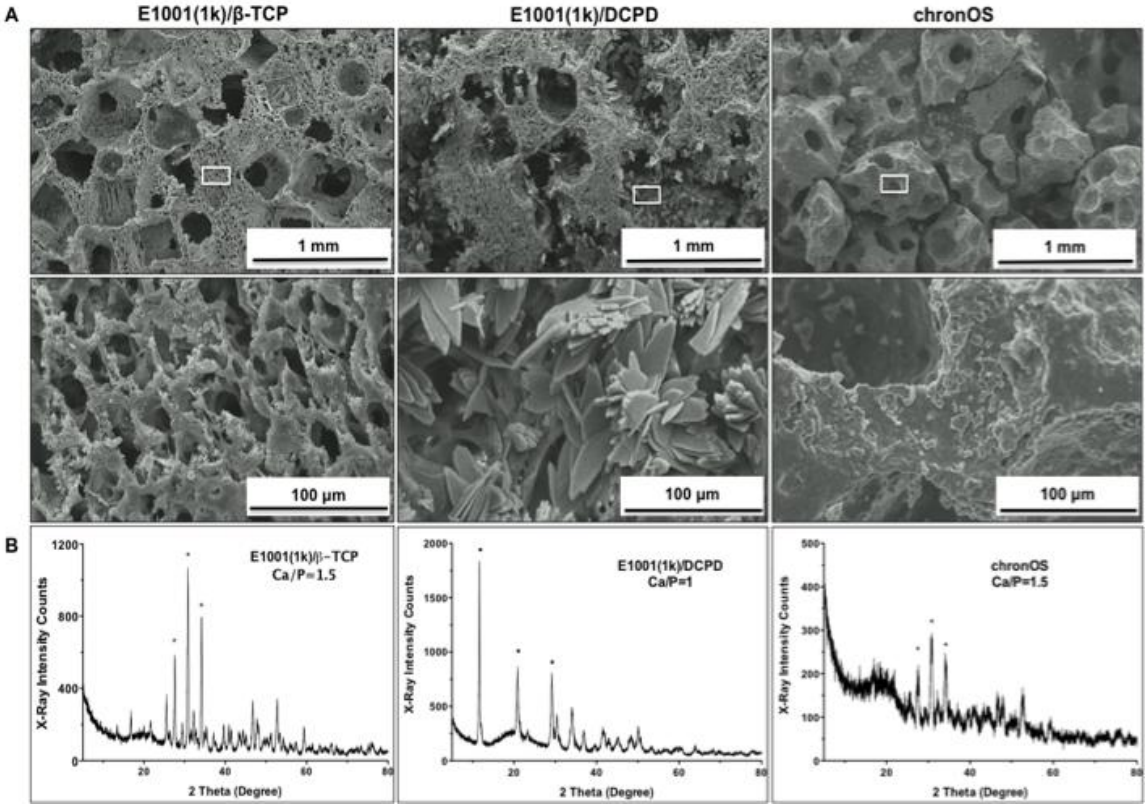

Figure 6.2 (A) Representative SEM images of the macroporous networks (top row) and surface topologies (bottom row) of E1001(1k)/β-TCP, E1001(1k)/DCPD and chronOS scaffolds at low and high magnifications respectively. (B) X-ray diffractograms of E1001(1k)/β-TCP, E1001(1k)/DCPD and chronOS

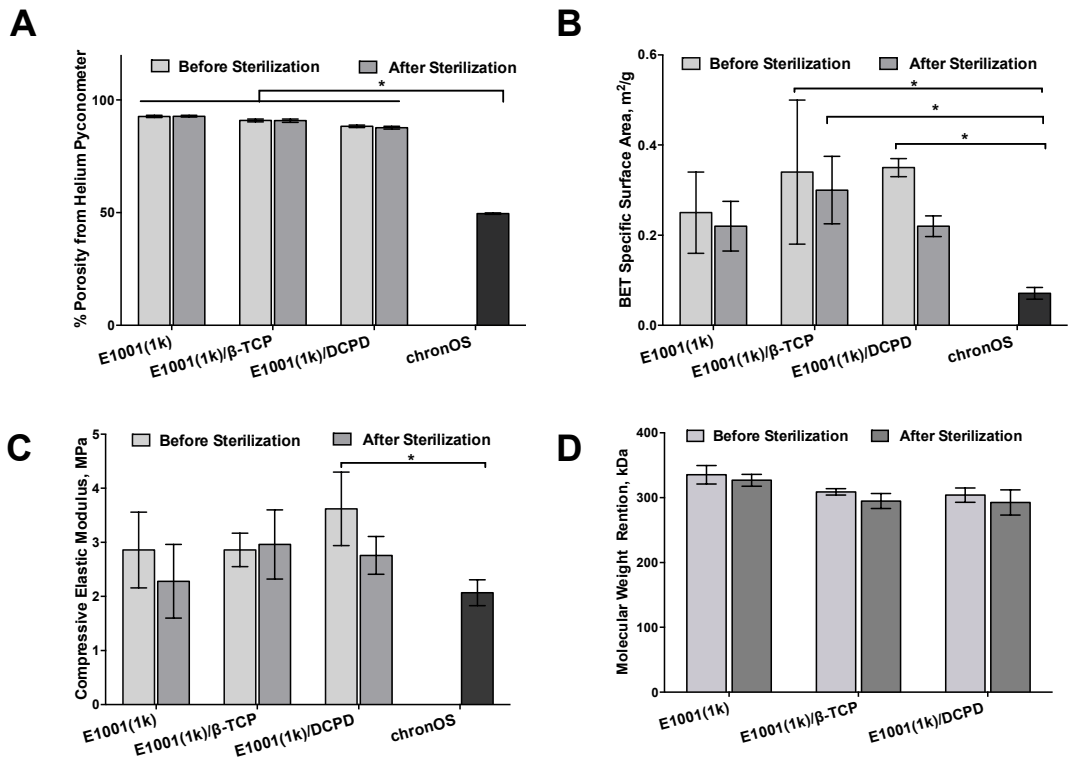

Figure 6.3 Physical properties of E1001(1k)/β-TCP and E1001(1k)/DCPD scaffolds before and after ethylene oxide sterilization: (A) total scaffold porosity obtained from helium pyconometer, (B) BET specific surface area in m2/g, (C) compressive elastic modulus in MPa, and (D) scaffold polymer molecular weight in kDa. chronOS was purchased as sterilized 100 mm (long) × 6 mm (thick) rectangular strips. 20 mm (diameter) × 6 mm (thick) disks were punched out from the strips and characterized as a comparison. Data are reported as a mean ± standard deviation for n = 3 with significance level of $p < 0.05$.

MicroCT was used to generate 2D slices and 3D reconstructions of the scaffolds and showed that E1001(1k)-based scaffolds are highly porous with substantial interconnectivity (Fig. 6.4A and B). The microCT data was also used to calculate porosity (Table inset in Fig. 6.4), and revealed that E1001(1k)-based scaffolds and chronOS had porosities of ~40% and 30% respectively, which was significantly lower than that obtained using helium pyconometry. A possible explanation for the underestimation in porosity is that microCT has a limited voxel resolution (20μm), where micropores less than 20 μm could not be detected and were excluded from the porosity measurement. The microCT data was also used to determine the total pore volume and the largest pore volume. It was observed that the largest pore volume was nearly equal to the total pore volume for both E1001(1k)-based scaffolds and chronOS. These data suggest that all scaffolds had a very high degree of interconnectivity, where the microCT recorded all of the interconnected pores as a single, very large pore (Fig. 6.4C). In other words, the percentage of the largest pore volume of the total pore volume was 99.8% or 99.4% for E1001(1k)-based scaffolds and chronOS, respectively, indicating that the majority of the pores were open and and only 0.2% or 0.6% were closed or blind pores.

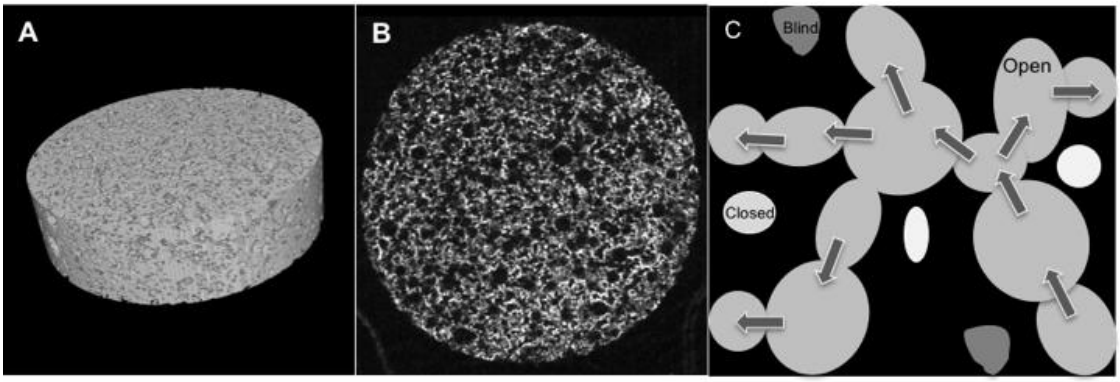

Figure 6.4 MicroCT analyses of scaffolds before implantation: (A) a representative three dimensional (3D) reconstruction image of E1001(1k)-based scaffold, (B) microCT 2D cross-section slice reconstruction, which reveal a highly interconnected porous structure, (C) an illustration of open, blind and closed pores

Table 6.2 Summary of the quantitative 3D morphometric analyses: total scaffold porosity, total pore volume, largest pore volume, percent closed/blind pore and percent open/interconnected pore.

Scaffolds	Total porosity	Total pore volume, mm^3	Largest pore volume, mm^3	% Closed/blind pore	% Open pore
E1001(1k)/β-TCP	40.5 ± 4.3	484 ± 50	483 ± 50	0.2%	99.8%
E1001(1k)/DCPD	40.3 ± 1.5	489 ± 13	488 ± 14	0.2%	99.8%
chronOS	29.8 ± 1.5	359 ± 13	357 ± 12	0.6%	99.6%

6.4.2 Bone regeneration in CSD goat calvaria

MicroCT 2D coronal and transverse images of the calvarial specimens obtained 16 weeks post-treatment are shown in Fig. 6.5A. A qualitative comparison of the defects treated with scaffolds without rhBMP-2 suggests that E1001(1k)/DCPD scaffolds promoted the most new bone formation, where the regenerated bone had grown into the center of the defect and bridged the defect. In contrast, defects treated with chronOS and E1001(1k)/β-TCP scaffolds contained newly formed bone only along the margins of the defect (at the bone-implant interface). Defects treated with E1001(1k)/ β-TCP scaffolds supplemented with 400μg rhBMP-2 had significantly more new bone formation as compared to all treatments without rhBMP-2. These defects were almost completely filled with newly regenerated bone and bridging of the defects was observed. The mean (SD) % BV/TV (Fig. 6.5B) by treatment group was E1001(1k)/DCPD – 23.8 (5.6) E1001(1k)/β-TCP – 17.1 (9.0), chronOS – 15.4 (3.9), and E1001(1k)/β-TCP + rhBMP-2 – 48 (17.1). These results confirm that defects treated with E1001(1k)/β-TCP + rhBMP-2 promoted significantly more new bone formation as compared to all treatments without rhBMP-2. No significant difference was detected among the treatment groups without rhBMP-2.

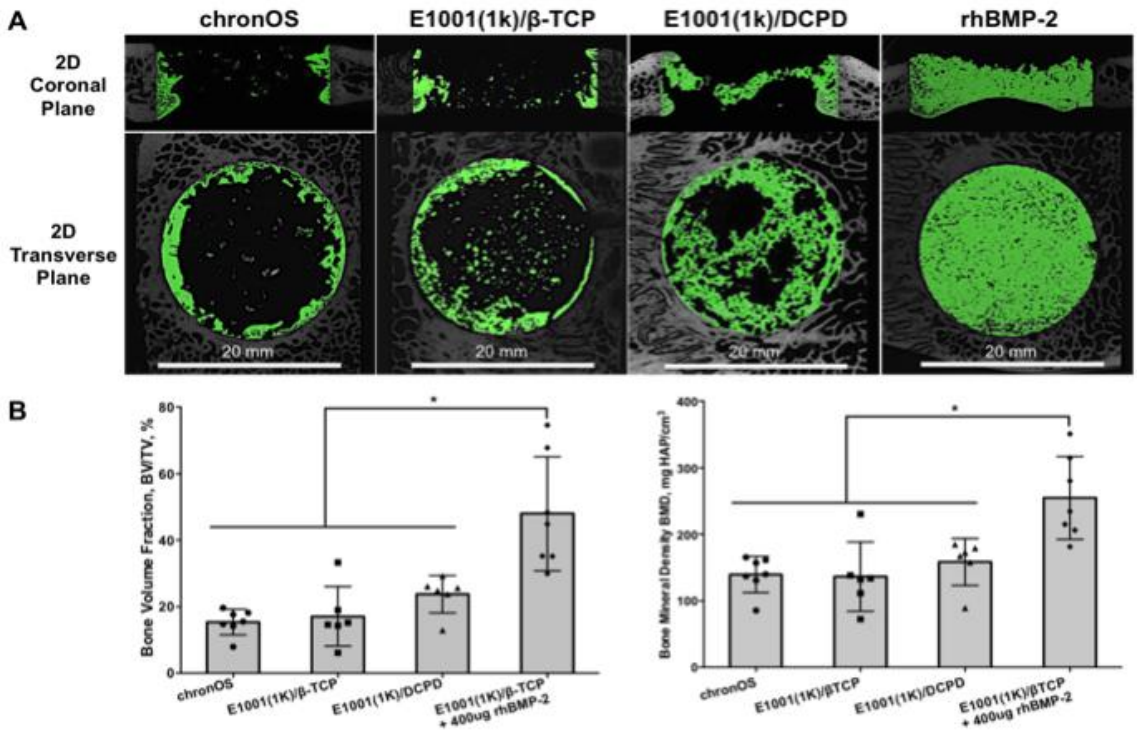

Figure 6.5(A) Representative 2D coronal and transverse microCT images of bone regeneration in the 20 mm goat calvarial defects treated with choronOS, E1001(1k)/ β-TCP and E1001(1k)/DCPD and E1001(1k)/ β-TCP supplemented with 400 μg of rhBMP-2 16 weeks post-implantation. (B) Quantitative analyses of the percentage of trabecular bone volume of the total volume of interest (BV/TV%, left figure) and the bone mineral density (BMD, right figure) as indications of bone regeneration. Data are reported as the mean ± standard deviation for n = 6 – 7. And sign (&) indicates a statistical significance difference with $p < 0.05$.

The histology sections were stained with Stevenel's Blue and counterstained with van Gieson's picrofuchsin (Fig. 6.6A). Normal cellular infiltration and bone healing with no signs of inflammatory response was observed in all defects regardless of treatment group. Of the defects treated with scaffolds without rhBMP-2, substantial bone formation through the center of the defect was observed in those treated with E1001(1k)/DCPD scaffolds. In contrast, marginal bone formation restricted to the implant-native bone interface was noted in defects treated with E1001(1k)/β-TCP scaffolds and chronOS. Defects treated with E1001(1k)/β-TCP scaffolds + rhBMP-2 had the most robust trabecular bone formation. In addition, it appears that bone regeneration originated from the dural side and extended toward the superior side of the defect. Histological examination of the defects also shows that E1001(1k)/DCPD scaffolds were almost completely degraded, whereas substantial fragments of chronOS and E1001(1k)/β-TCP scaffolds (stained black) were still present.

The percent new bone area (Fig. 6.6B) by treatment group was E1001(1k)/DCPD – 23.7 (3.3) E1001(1k)/β-TCP – 12.3 (4.8), chronOS – 16.1 (3.7), and E1001(1k)/β-TCP + rhBMP-2 – 27.8 (7.9). No statistical difference was detected between defects treated with E1001(1k)/DCPD scaffolds without rhBMP and E1001(1k)/β-TCP + rhBMP-2. Further, defects treated with E1001(1k)/DCPD scaffolds had significantly more new bone area that those treated with E1001(1k)/β-TCP scaffolds.

Fig. 6.6C shows that defects treated with E1001(1k)/DCPD scaffolds had significantly higher trabecular bone linear ingrowth than those treated with E1001(1k)/β-TCP and chronOS – 85%, 20%, and 30%, respectively. Further, complete bridging was observed in 3 out of 6 animals treated with E1001(1k)/DCPD scaffolds, and the other 3 animals

had partial bridging. In distinction, defects treated with E1001(1k)/β-TCP + rhBMP-2 treated group had complete bridging in all animals.

The histomorphometric data (BA/TA %) mirrored the microCT data (BV/TV %) in that similar values were obtained for each treatment group, except for E1001(1k)/β-TCP + rhBMP-2. From the histological images (Fig. 6.6A), it is observed that between newly formed trabecula there is residue scaffold materials, while microCT seems to detect them as new bone as seen in 2D microCT images (Fig. 6.5A), probably due to limitation in voxel resolution.

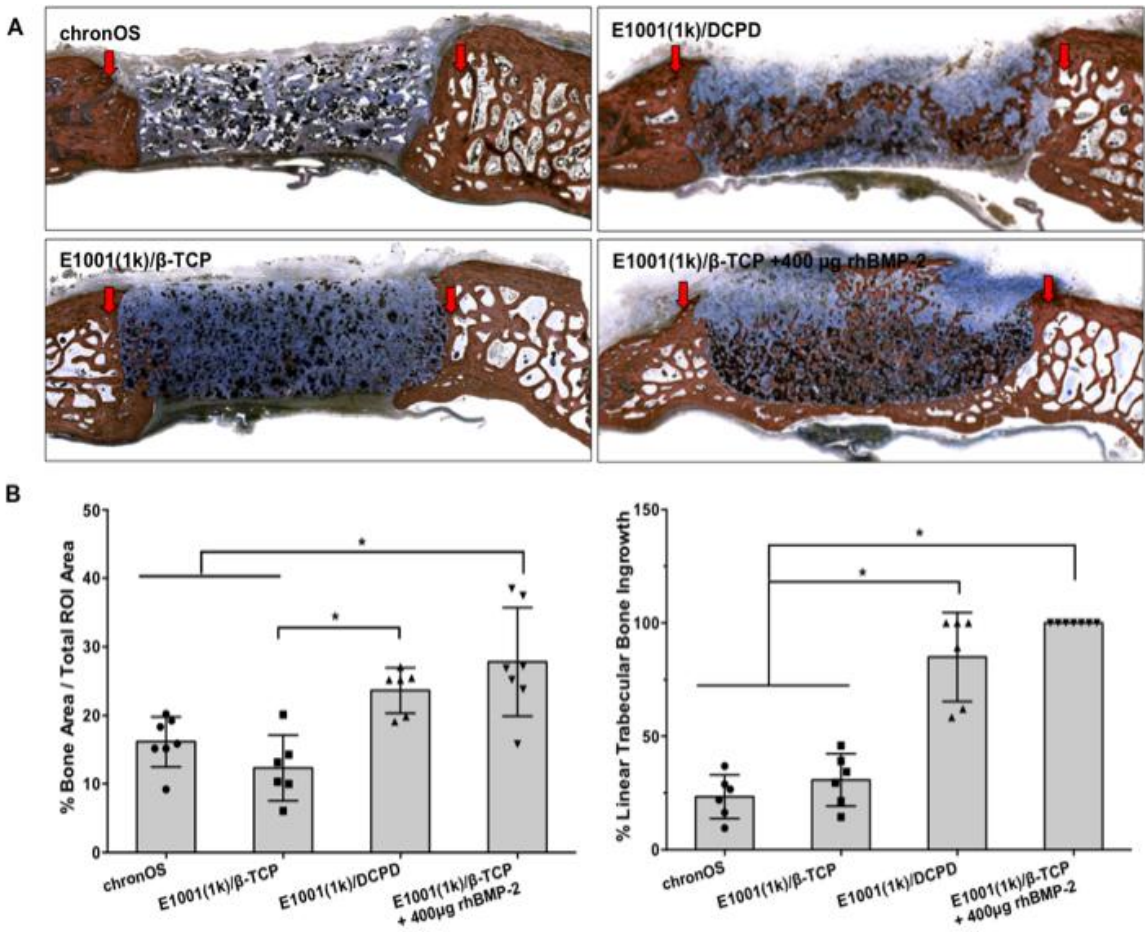

Figure 6.6 (A) Representative histological images of 20 mm goat calvarial defects treated with with choronOS, E1001(1k)/ β-TCP and E1001(1k)/DCPD and E1001(1k)/ β-TCP supplemented with 400 µg of rhBMP-2 16 weeks post-implantation. Red arrows indicate the defect boundary. The un-decalcified sections were stained with Stevenel's Blue and counterstained with van Gieson's Picro Fuchsin, which stains bone red and nonmineralized structure various shades of blue. The residue scaffolds were stained black. (B) Summary of 2D histomorphometric analyses: the percent of bone area of the total area of interest as an indication of the amount of bone formation, and percent linear trabecular bone ingrowth , as an indication of the spatial pattern of bone ingrowth.

6.5 Discussion

In this study, we present a novel E1001(1k)/ DCPD scaffold with osteoconductive porous structure that may be the next-generation synthetic bone graft substrate for large bone defect repair. E1001(1k)/ DCPD scaffold achieved significantly better osteogenic outcome in goat calvarial critical size defects than chronOS, a commercial bone graft substitute and E1001(1k) scaffold mineralized with β-TCP prepared by bulk composite method. In addition, this is a pivotal study in that exceptional bridging of goat calvarial critical size defects was observed for first time in the literature using a novel DCPD mineralized scaffolds without supplemental osteogenic growth factors.

Goats are considered as valuable large animal models for the preclinical testing of bone graft substitutes because they have a metabolic rate and bone remodeling rate similar to humans [23-25]. Goats also have a body weight comparable to humans and a body size suitable for the implantation of large human-sized implants and prostheses [25]. Therefore, the osteogenic results can be used to predict the likely outcomes in clinical conditions. However, only a handful of bone regeneration researches have used large animal models due to the high cost of the studies. In deed, only one paper has been published using the goat calvarial CSD model for the evaluation of a bone regeneration scaffold [26]. This study showed that poly(lactide-co-glycolide) (PLGA)/tricalcium phosphate (TCP) scaffolds prepared by low-temperature rapid prototyping technology failed to regenerate bone at 12 and 24 weeks without the addition of rhBMP-2. In addition, reviewing the existing bone regeneration studies using rats [27], rabbits [7, 28], goats [26, 29], sheeps [30], and dogs [31, 32], no osteoconductive scaffold has demonstrated the ability to complete bridge a critical size defect without the addition of

osteogenic growth factors. Most of these studies showed minimal bone formation limited to the margin of defect, similar to the results we observed for defects treated with E1001(1k)/β-TCP and chronOS.

The performance superiority of E1001(1k)/DCPD scaffolds may be attributed to several factors including polymer chemistry, their porous 3D structure and the excellent osteoconductivity and bone replacement capability of DCPD minerals [33, 34] . First, E1001(1k) scaffolds were designed to have optimal structural properties including porosity, pore size and pore size distribution, surface area and pore interconnectivity to prompt *in vivo* osteogenesis and vascularization. The total porosity of E1001(1k) scaffolds was about 90% (Fig. 6.3A). High scaffold porosity is expected to allow migration and proliferation of osteoprogenitor cells as well as *in vivo* vascularization [33] . The pore size range of 200-400 μm (Fig. 6.2A) are within the well-reported optimal pore size distribution for bone regeneration scaffolds and has been previously shown to support osteoconduction [33]. In addition to macroporosity, the walls of the macropores are decorated with a substantial amount of micropores (< 20 μm) that significantly contributed to the high surface area of E1001(1k) scaffolds (5 times higher) compared to the predicate device (Fig 6.3.B). Studies have reported that the presence of micropores and high surface area of scaffolds benefit angiogenesis and osteoconduction by enhancing endogenous protein adsorption, nutrition and osteogenic factors transportation, as well as to ion exchange and bone-like apatite formation by dissolution and precipitation [33, 35, 36] . Furthermore, Mastrogiacomo M. et al. reported that pore interconnectivity is an equally important scaffold characteristic as an incomplete pore interconnection could represent a constraint of overall biological system, limiting blood

vessel invasion and cell migration [37, 38]. MicroCT analysis of E1001(1k) scaffolds revealed a highly interconnected porous structure with 99.8% open pores (Fig. 6.4B).

A second reason for the superior performance of E1001(1k)/DCPD scaffold may attributed to the high solubility of DCPD [13, 14]. It has been suggested that high concentration of Ca^{2+} ions released from CaP materials may mimic bone resorption microenvironment, thus stimulate osteoblast proliferation and differentiation by directly activating intracellular mechanisms through Ca-sensing receptors in osteoblastic cells, and encourage bone mineralization and bone regeneration.[39, 40]. For example, Ana Barradas et al. reported that hMSCs cultured *in vitro* on β-TCP scaffolds expressed more osteogenic genes, including osteopontin (OP), osteocalcin (OC), bone sialoprotein (BSP) and BMP-2 than HA scaffolds [41, 42]. Since they designed the scaffolds to have the same 3D structure, they attributed the finding to the likely variable: high solubility of β-TCP as compared to HA. A similar finding was observed in our *in vitro* study where hMSCs cultured on E1001(1k)/DCPD scaffolds expressed significant higher alkaline phosphatase (ALP) than E1001(1k)/β-TCP scaffolds, likely due to the higher solubility of DCPD as compared to β-TCP. The high local calcium ion concentration is also expected *in vivo* because the extracellular fluid is undersaturated with respect to DCPD.

A stringent comparison between solubility of calcium phosphates and their bioactivity at molecular level remain as a challenge because CaPs vary in terms of chemical composition, crystallinity, macro-and micro- structure, and surface topography. Nonetheless, a fundamental understanding of calcium phosphate solubility that drives specific molecular and cellular responses might improve the design of CaP materials.

A third reason is the method of scaffold preparation. It is well known that CaP-containing scaffolds adsorb proteins and other macromolecules, leading to a biological layer that favors cell attachment, proliferation and osteogenic differentiation by resembling a bone-like mineral matrix [15, 43-45]. Despite this, most of these scaffolds are prepared as composites using blending techniques, where the CaP are embedded as fillers within the polymer matrix. It is suspected that this method of fabrication generally results in the formation of a polymer skin covering the inorganic particles, which may shadow the osteconductivity of the CaPs [15, 17, 46]. In our study, DCPD was precipitated onto pre-formed E1001(1k) scaffolds, which likely provided increased contact between CaP and cells and attributed to its increased osteoconductivity compared to E1001(1k)/β-TCP scaffolds and chronOS which were prepared as bulk composites. A direct comparison between the effectiveness of DCPD and β-TCP as CaP additives should not be made because each was incorporated into the E1001(1k) scaffold using a different fabrication process (coated vs. composite), since it was not possible to coat with β-TCP. Moreover, many other factors including surface roughness, calcium phosphate crystallinity, particles size and phase composition, and microstructure collectively influence the outcome of an implant [34].

Our previous work has shown that E1001(1k)/β-TCP scaffolds have been well-optimized for bone regeneration using a lower than recommended dose of rhBMP-2 to repair rabbit calvarial critical size defect (15 mm in diameter). Base on this dosage, 400 μg rhBMP-2 was calculated as an equivalent dose for the goat calvarial CSD, combined with E1001(1k)/β-TCP scaffold and used as a positive control in this study. All defects treated with 400 μg rhBMP-2 achieved complete bridging in 16 weeks, which is

significantly less than the recommended dosage used in the literature for large animal models. Studies have reported rhBMP-2 dosing up to 1mg per defect site delivered with PLGA/TCP 3D scaffolds in goat CSD calvarial model [26] and 1.4 mg per defect site delivered with collagen sponge in Rheesus monkey calvaria defects [47]. It is likely that even less rhBMP-2 may be required for E1001(1k)/DCPD scaffold because it demonstrated higher osteoconductivity than E1001(1k)/β-TCP scaffolds. In addition, the histomorphometric analysis showed comparable bone area for defects treated with E1001(1k)/DCPD without rhBMP-2 and E1001(1k)/β-TCP + rhBMP-2. Furthermore, studies have reported that osteoinductive efficacy of rhBMP-2 can be enhanced when incorporated with calcium phosphate coating [48, 49]. Nonetheless, future studies are required to determine if the use of E1001(1k)/DCPD scaffolds as carriers for rhBMP-2 delivery offer an additional advantage to lower the dose.

6.6 Conclusions

In this study, we showed that treatment with E1001(1k)/DCPD scaffolds provided complete bridging of critical size defects in a goat calvarial model without supplemental osteogenic growth factors for the first time in the literature. On the other hand, defects treated with E1001(1k)/β-TCP scaffolds and chronOS, a commercially available predicate, regenerated bone along the margins of the defect only. These results suggest that E1001(1k)/DCPD scaffolds have great potential to be the next-generation synthetic bone graft substrate for large bone defect repair.

References

[1] De Long WG, Jr., Einhorn TA, Koval K, McKee M, Smith W, Sanders R, et al. Bone grafts and bone graft substitutes in orthopaedic trauma surgery. A critical analysis. J Bone Joint Surg Am 2007;89:649-58.

[2] Amini AR, Laurencin CT, Nukavarapu SP. Bone tissue engineering: recent advances and challenges. Crit Rev Biomed Eng 2012;40:363-408.

[3] Gazdag A, Lane J, Glaser D, Forster R. Alternatives to Autogenous Bone Graft: Efficacy and Indications. Journal of the American Academy of Orthopaedic Surgeons 1995;3:1-8.

[4] Nandi S, Roy S, Mukherjee P, Kundu B, De D, Basu D. Orthopaedic applications of bone graft & graft substitutes : a review2010.

[5] Ogose A, Hotta T, Kawashima H, Kondo N, Gu W, Kamura T, et al. Comparison of hydroxyapatite and beta tricalcium phosphate as bone substitutes after excision of bone tumors. J Biomed Mater Res B Appl Biomater 2005;72:94-101.

[6] Cao H, Kuboyama N. A biodegradable porous composite scaffold of PGA/β-TCP for bone tissue engineering. Bone 2010;46:386-95.

[7] Kim J, Magno MH, Waters H, Doll BA, McBride S, Alvarez P, et al. Bone regeneration in a rabbit critical-sized calvarial model using tyrosine-derived polycarbonate scaffolds. Tissue Eng Part A 2012;18:1132-9.

[8] LeGeros R. Preparation of octacalcium phosphate (OCP): A direct fast method. Calcif Tissue Int 1985;37:194-7.

[9] Johnsson MS, Nancollas GH. The role of brushite and octacalcium phosphate in apatite formation. Crit Rev Oral Biol Med 1992;3:61-82.

[10] Kanzaki N, Onuma K, Treboux G, Ito A. Dissolution kinetics of dicalcium phosphate dihydrate under pseudophysiological conditions. Journal of Crystal Growth 2002;235:465-70.

[11] LeGeros RZ. Properties of osteoconductive biomaterials: calcium phosphates. Clin Orthop Relat Res 2002;395:81-98.

[12] Bohner M. Calcium orthophosphates in medicine: from ceramics to calcium phosphate cements. Injury 2000;31, Supplement 4:D37-D47.

[13] Apelt D, Theiss F, El-Warrak AO, Zlinszky K, Bettschart-Wolfisberger R, Bohner M, et al. In vivo behavior of three different injectable hydraulic calcium phosphate cements. Biomaterials 2004;25:1439-51.

[14] Theiss F, Apelt D, Brand B, Kutter A, Zlinszky K, Bohner M, et al. Biocompatibility and resorption of a brushite calcium phosphate cement. Biomaterials 2005;26:4383-94.

[15] Seyedjafari E, Soleimani M, Ghaemi N, Shabani I. Nanohydroxyapatite-Coated Electrospun Poly(l-lactide) Nanofibers Enhance Osteogenic Differentiation of Stem Cells and Induce Ectopic Bone Formation. Biomacromolecules 2010;11:3118-25.

[16] Nandakumar A, Yang L, Habibovic P, van Blitterswijk C. Calcium Phosphate Coated Electrospun Fiber Matrices as Scaffolds for Bone Tissue Engineering. Langmuir 2010;26:7380-7.

[17] Vaquette C, Ivanovski S, Hamlet SM, Hutmacher DW. Effect of culture conditions and calcium phosphate coating on ectopic bone formation. Biomaterials 2013;34:5538-51.

[18] Kim HJ, Kim U-J, Kim HS, Li C, Wada M, Leisk GG, et al. Bone tissue engineering with premineralized silk scaffolds. Bone 2008;42:1226-34.

[19] Zhao J, Zhang Z, Wang S, Sun X, Zhang X, Chen J, et al. Apatite-coated silk fibroin scaffolds to healing mandibular border defects in canines. Bone 2009;45:517-27.

[20] Surmenev RA, Surmeneva MA, Ivanova AA. Significance of calcium phosphate coatings for the enhancement of new bone osteogenesis – A review. Acta Biomaterialia 2014;10:557-79.

[21] Magno MHR, Kim J, Srinivasan A, McBride S, Bolikal D, Darr A, et al. Synthesis, degradation and biocompatibility of tyrosine-derived polycarbonate scaffolds. Journal of Materials Chemistry 2010;20:8885-93.

[22] Kim J, Magno MH, Alvarez P, Darr A, Kohn J, Hollinger JO. Osteogenic differentiation of pre-osteoblasts on biomimetic tyrosine-derived polycarbonate scaffolds. Biomacromolecules 2011;12:3520-7.

[23] Reichert JC, Saifzadeh S, Wullschleger ME, Epari DR, Schutz MA, Duda GN, et al. The challenge of establishing preclinical models for segmental bone defect research. Biomaterials 2009;30:2149-63.

[24] Pearce AI, Richards RG, Milz S, Schneider E, Pearce SG. Animal models for implant biomaterial research in bone: a review. Eur Cell Mater 2007;13:1-10.

[25] Li Y, Chen S-K, Li L, Qin L, Wang X-L, Lai Y-X. Bone defect animal models for testing efficacy of bone substitute biomaterials. Journal of Orthopaedic Translation 2015;3:95-104.

[26] Yu D, Li Q, Mu X, Chang T, Xiong Z. Bone regeneration of critical calvarial defect in goat model by PLGA/TCP/rhBMP-2 scaffolds prepared by low-temperature rapid-prototyping technology. Int J Oral Maxillofac Surg 2008;37:929-34.

[27] Yoon E, Dhar S, Chun DE, Gharibjanian NA, Evans GR. In vivo osteogenic potential of human adipose-derived stem cells/poly lactide-co-glycolic acid constructs for bone regeneration in a rat critical-sized calvarial defect model. Tissue Eng 2007;13:619-27.

[28] Kim J, Magno MHR, Ortiz O, McBride S, Darr A, Kohn J, et al. Next-generation resorbable polymer scaffolds with surface-precipitated calcium phosphate coatings2015.

[29] Nienhuijs ME, Walboomers XF, Briest A, Merkx MA, Stoelinga PJ, Jansen JA. Healing of bone defects in the goat mandible, using COLLOSS E and beta-tricalciumphosphate. J Biomed Mater Res B Appl Biomater 2010;92:517-24.

[30] Gugala Z, Gogolewski S. Regeneration of segmental diaphyseal defects in sheep tibiae using resorbable polymeric membranes: a preliminary study. J Orthop Trauma 1999;13:187-95.

[31] Itoh T, Mochizuki M, Nishimura R, Matsunaga S, Kadosawa T, Kokubo S, et al. Repair of ulnar segmental defect by recombinant human bone morphogenetic protein-2 in dogs. J Vet Med Sci 1998;60:451-8.

[32] Sciadini MF, Johnson KD. Evaluation of recombinant human bone morphogenetic protein-2 as a bone-graft substitute in a canine segmental defect model. J Orthop Res 2000;18:289-302.

[33] Karageorgiou V, Kaplan D. Porosity of 3D biomaterial scaffolds and osteogenesis. Biomaterials 2005;26:5474-91.

[34] Barrere F, van Blitterswijk CA, de Groot K. Bone regeneration: molecular and cellular interactions with calcium phosphate ceramics. Int J Nanomedicine 2006;1:317-32.

[35] Wei J, Jia J, Wu F, Wei S, Zhou H, Zhang H, et al. Hierarchically microporous/macroporous scaffold of magnesium-calcium phosphate for bone tissue regeneration. Biomaterials 2010;31:1260-9.

[36] Lan Levengood SK, Polak SJ, Wheeler MB, Maki AJ, Clark SG, Jamison RD, et al. Multiscale osteointegration as a new paradigm for the design of calcium phosphate scaffolds for bone regeneration. Biomaterials 2010;31:3552-63.

[37] Mastrogiacomo M, Scaglione S, Martinetti R, Dolcini L, Beltrame F, Cancedda R, et al. Role of scaffold internal structure on in vivo bone formation in macroporous calcium phosphate bioceramics. Biomaterials 2006;27:3230-7.

[38] Lemon G, Reinwald Y, White LJ, Howdle SM, Shakesheff KM, King JR. Interconnectivity analysis of supercritical CO2-foamed scaffolds. Computer Methods and Programs in Biomedicine 2012;106:139-49.

[39] Marie PJ. The calcium-sensing receptor in bone cells: a potential therapeutic target in osteoporosis. Bone 2010;46:571-6.

[40] Hoppe A, Güldal NS, Boccaccini AR. A review of the biological response to ionic dissolution products from bioactive glasses and glass-ceramics. Biomaterials 2011;32:2757-74.

[41] Barradas AM, Fernandes HA, Groen N, Chai YC, Schrooten J, van de Peppel J, et al. A calcium-induced signaling cascade leading to osteogenic differentiation of human bone marrow-derived mesenchymal stromal cells. Biomaterials 2012;33:3205-15.

[42] Barradas AM, Monticone V, Hulsman M, Danoux C, Fernandes H, Tahmasebi Birgani Z, et al. Molecular mechanisms of biomaterial-driven osteogenic differentiation in human mesenchymal stromal cells. Integr Biol 2013;5:920-31.

[43] Vaquette C, Ivanovski S, Hamlet SM, Hutmacher DW. Effect of culture conditions and calcium phosphate coating on ectopic bone formation. Biomaterials 2013;34:5538-51.

[44] Mavis B, Demirtaş TT, Gümüşderelioğlu M, Gündüz G, Çolak Ü. Synthesis, characterization and osteoblastic activity of polycaprolactone nanofibers coated with biomimetic calcium phosphate. Acta Biomaterialia 2009;5:3098-111.

[45] Jiang X, Zhao J, Wang S, Sun X, Zhang X, Chen J, et al. Mandibular repair in rats with premineralized silk scaffolds and BMP-2-modified bMSCs. Biomaterials 2009;30:4522-32.

[46] He C, Xiao G, Jin X, Sun C, Ma PX. Electrodeposition on Nanofibrous Polymer Scaffolds: Rapid Mineralization, Tunable Calcium Phosphate Composition and Topography. Advanced Functional Materials 2010;20:3568-76.

[47] Sheehan JP, Sheehan JM, Seeherman H, Quigg M, Helm GA. The safety and utility of recombinant human bone morphogenetic protein-2 for cranial procedures in a nonhuman primate model. J Neurosurg 2003;98:125-30.

[48] Dadsetan M, Guda T, Runge MB, Mijares D, LeGeros RZ, LeGeros JP, et al. Effect of calcium phosphate coating and rhBMP-2 on bone regeneration in rabbit calvaria using poly(propylene fumarate) scaffolds. Acta Biomaterialia.

[49] Lee JS, Suarez-Gonzalez D, Murphy WL. Tissue Engineering: Mineral Coatings for Temporally Controlled Delivery of Multiple Proteins (Adv. Mater. 37/2011). Advanced Materials 2011;23:4278-.

7

Conclusion

The goal of this doctoral research was to develop bone graft substitutes based on E1001(1k) and calcium phosphates for large bone defect repair. The current bone graft substitutes are often fabricated from simple laboratory processes that are never optimized or scaled-up and thus inconsistent bone regeneration results are often observed. Most scaffolds are only evaluated *in vitro*. If they are evaluated *in vivo*, small animal models such as rats and rabbits are used, which have very different bone remolding rate as human. Thus, the bone regeneration results are not likely translated into clinical outcome. This dissertation provided effective and innovative solution to the problems by describing a systemic approach of process development, optimization and preclinical evaluation of the E1001(1k)-CaP scaffolds progressively in small animal models and then in a clinically relevant large animal model. The results showed that E1001(1k)-CaP scaffolds performed significantly better than chronOS, a commercial bone graft substitute. The work shown in this dissertation demonstrate that E1001(1k)-CaP scaffolds are promising substrates for large bone defect regeneration.

The composite scaffolds combined the processability and flexibility of E1001(1k) polymer with bioactive calcium phosphates that facilitated faster bone remodeling by resembling the composition as well as the structure of human bone. The fabrication process was optimized and controlled to produce scaffolds with uniform structure. In addition, the process was scaled-up to produce large human-sized scaffolds for translational research. The process is ready for transfer to a third party contractor under

Good Manufacturing Practice (GMP). The 3D structure of the scaffolds was optimized including unique bimodal pore size distribution (macropores 200 – 400 μm and micropores < 20 μm), high porosity (90%) and surface area to enhance protein adsorption and nutrient transportation. Moreover, the pores were highly interconnected, allowed rapid infiltration and migration of cells and blood vessels into the 3D structure after implantation. The scaffold materials as well as the optimized 3D structure had a significant effect on cellular response and drove *in vivo* bone regeneration.

The systemic *in vitro* biological evaluation using human mesenchymal stem cells revealed that E1001(1k)-CaP scaffolds supported cell attachment, proliferation and osteogenic differentiation. *In vivo* evaluation of scaffolds in the small animal models demonstrated excellent biocompatibility and osteoconductivity. In addition, osteoinductive property was observed for the CaP coated E1001(1k) scaffolds as indicated by ectopic bone tissue formation after rat subcutaneous implantation. This result is of significant importance, which suggests that the coating may provide signal or surface topography that induces progenitor cells recruitment and their subsequent differentiation into bone forming cells lineage. Moreover, a synergistic effect between CaP coating and rhBMP-2 was observed, as CaP coated scaffolds induced significantly more ectopic bone formation than uncoated scaffolds or scaffolds prepared by blending method when the same amount of rhBMP-2 was delivered. The CaP coating provided exposed surface sites, which may facilitate rhBMP-2 binding and retention and thus osteoinductivity. Furthermore, the preclinical evaluation in large animal model, goat calvarial critical size defect model, revealed performance superiority of E1001(1k)-based scaffolds, especially DCPD coated scaffolds over chronOS, a commercial bone graft

substitute. Treatment with DCPD coated scaffolds provided complete bridging of 2 cm human-sized defects without supplemental osteogenic growth factor. This is of significant importance that has never been reported in the literature. The results suggest that E1001(1k)-CaP scaffold could be the next-generation synthetic bone graft substitute for large bone defect repair.